NASA-S-66-6852 JUN

SPECIFIC LUNAR MISSION REQUIREMENTS

- ALLOW EXPLORATIONS OF THE LUNAR SURFACE FOR DISTANCES OF AT LEAST 0.5 NM FROM THE LM
- PROVIDE FOR 4 HOURS OF CONTINUOUS SEPARATION FROM THE SPACECRAFT FOR EACH EXCURSION & A TOTAL OF 24 HOURS
- PERMIT TWO CREWMEN TO BE EXTRAVEHICULAR AT THE SAME TIME
- PERMIT RECHARGE OF THE EMU WITHIN AN HOUR

FIGURE 3

NASA-S-66-6851 JUN

PORTABLE LIFE SUPPORT SYSTEM (PLSS) DESIGN REQUIREMENTS

• THERMAL CAPACITY	
• METABOLIC	4800 BTU'S TOTAL 1200-1600 BTU/HR AVERAGE RATES 2000 BTU/HR PEAKS
• EXTERNAL LEAKAGE	250 BTU/HR IN 350 BTU/HR OUT
• PRESSURE	3.8 PSIA NOMINAL 3.2 PSIA MINIMUM (EMERGENCY)
• CARBON DIOXIDE	7.5 MM Hg NOMINAL 15 MM Hg MAXIMUM (CONTINGENCY)
• COMMUNICATIONS - TELEMETRY	REDUNDANT 2 WAY SIMULTANEUOUS VOICE 7 CHANNELS OF TELEMETRY

FIGURE 4

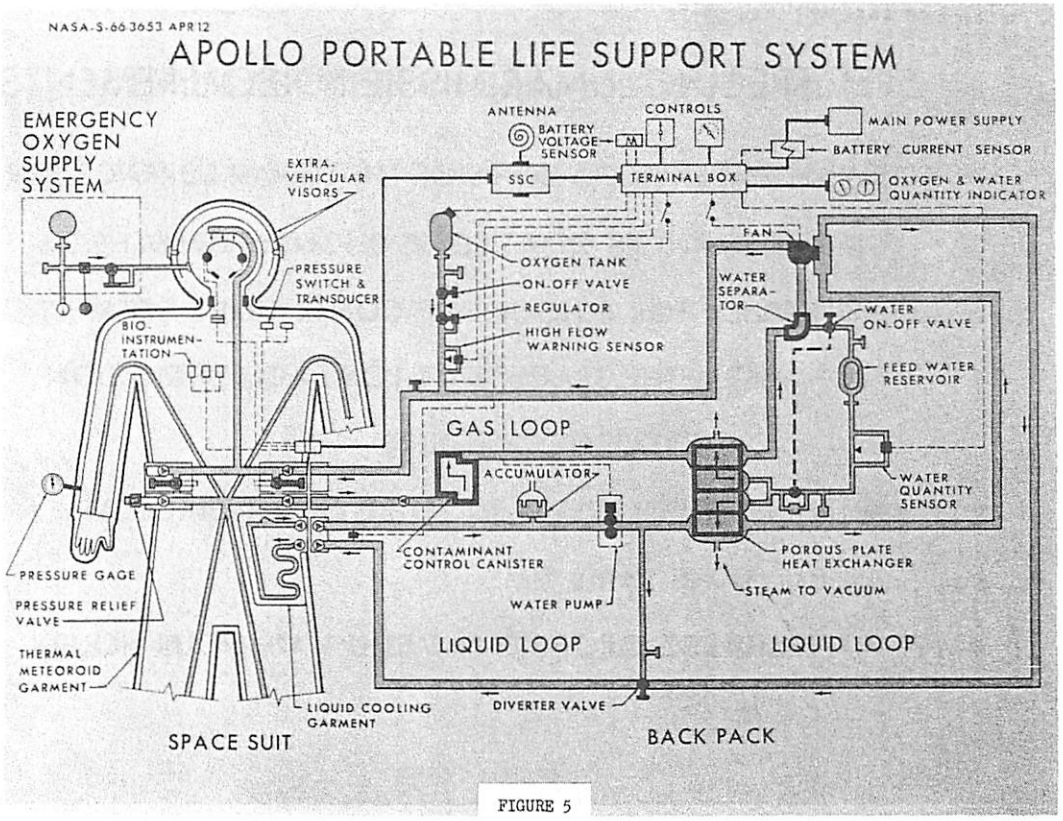

FIGURE 5

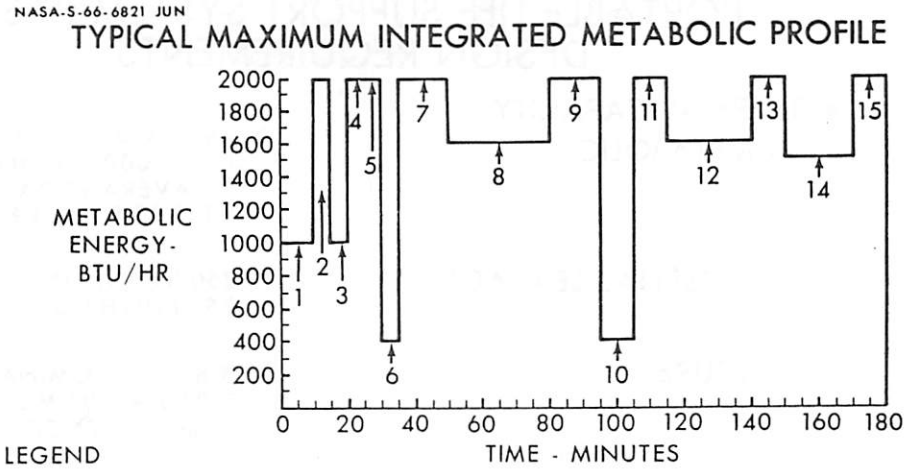

LEGEND

1 SSA CHECKOUT
2 EGRESS
3 SSA CHECKOUT (LUNAR SURFACE)
4 ERECTION OF SHIELDED STORAGE AREA
5 TRANSFER EQUIPMENT
6 REST
7 WALK TO OBJECTIVE NO. 1
8 SET-UP AND PERFORM EXPERIMENT NO.1
9 RETURN TO LM FOR EQUIPMENT
10 REST
11 WALK TO OBJECTIVE NO. 2
12 SET-UP AND PERFORM EXPERIMENT NO. 2
13 RETURN TO LM
14 PROCESS SPECIMENS
15 INGRESS

FIGURE 6

NASA-S-66-6866 JUN

EMU INSTRUMENTATION

TELEMETERED

- SUIT PRESSURE
- WATER QUANTITY
- OXYGEN QUANTITY
- BATTERY CURRENT
- LIQUID COOLED GARMENT ΔT (INLET-OUTLET)
- SUIT INLET TEMPERATURE
- EKG

SELF MONITORED

- SUIT PRESSURE
- OXYGEN QUANTITY
- WATER QUANTITY
- HIGH OXYGEN FLOW (AUDIBLE WARNING)
- LOW SUIT PRESSURE (AUDIBLE WARNING)

FIGURE 7

NASA-S-66-6815 JUN

PLSS CONTROL ACTUATION

FIGURE 8

NASA-S-65-2965

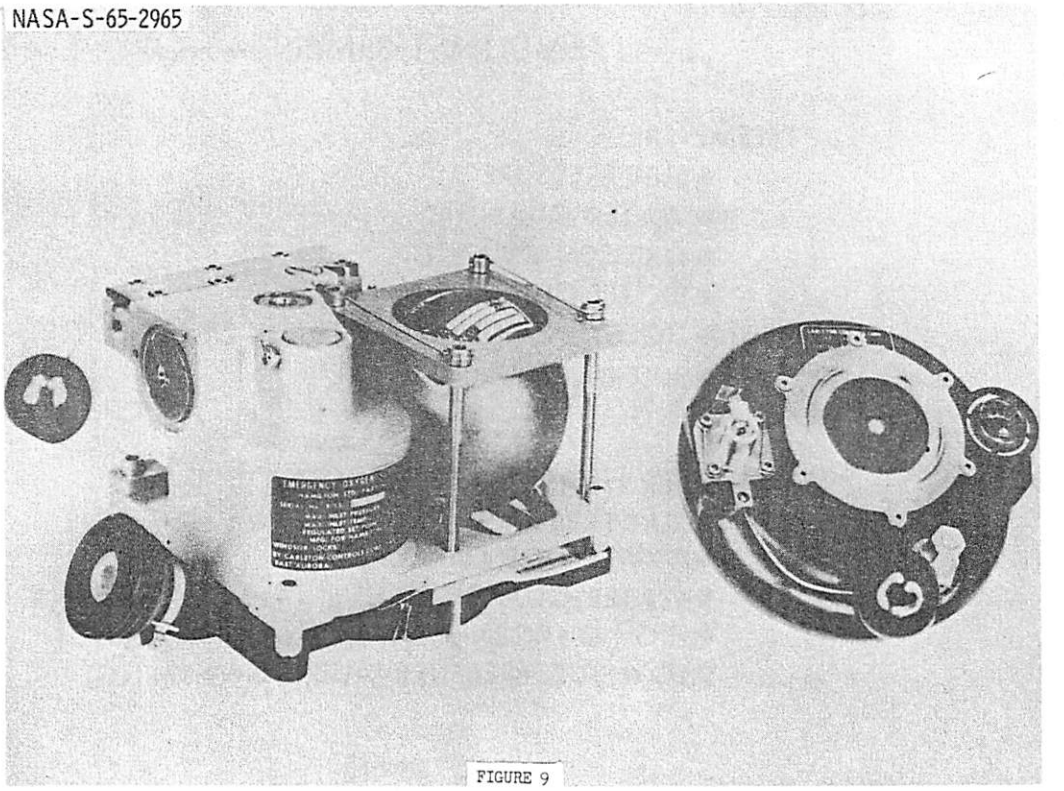

FIGURE 9

NASA-S-66-6853 JUN

PRESSURE GARMENT ASSEMBLY (PGA) DESIGN REQUIREMENTS

- PRESSURE PROTECTION, WITH MINIMUM LEAKAGE
- MOBILITY TO ACCOMPLISH LUNAR EXPLORATION
- STORAGE FOR BODY WASTES
- VENTILATION DISTRIBUTION
- VISIBILITY & EYE PROTECTION
- COMMUNICATIONS
- TOLERABLE FOR CONTINUOUS PRESSURIZED WEAR FOR UP TO 115 HOURS

FIGURE 10

FIGURE 11

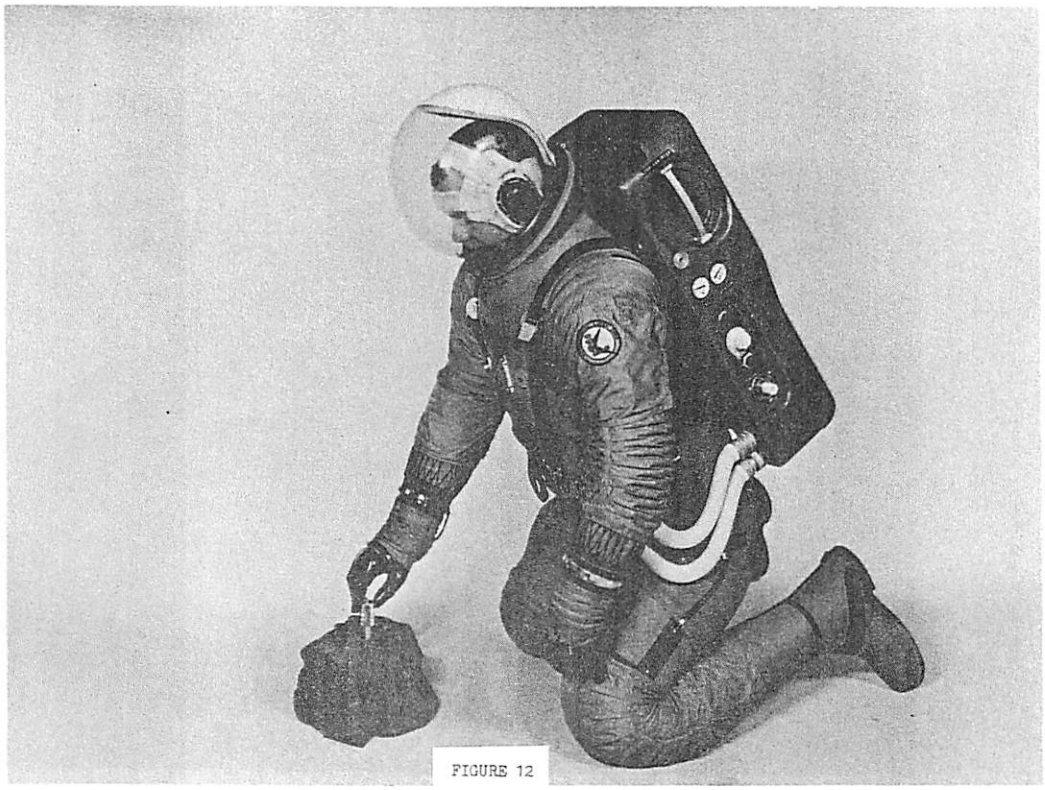

FIGURE 12

FIGURE 13

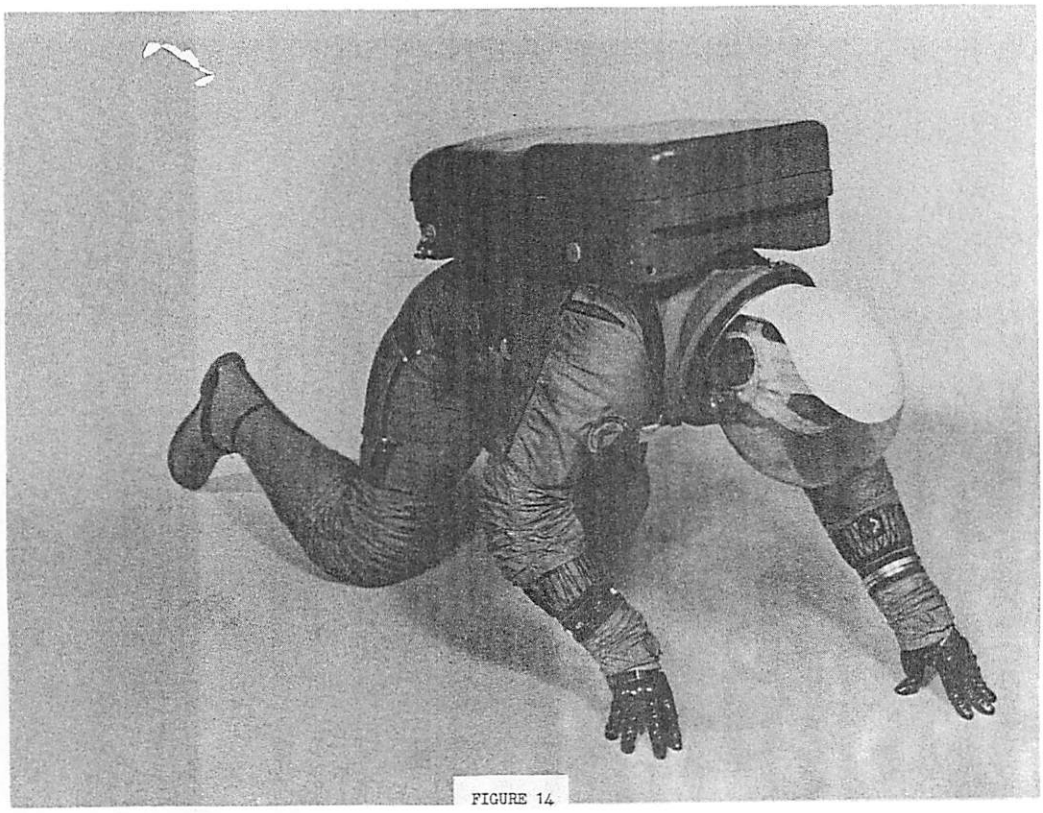

FIGURE 14

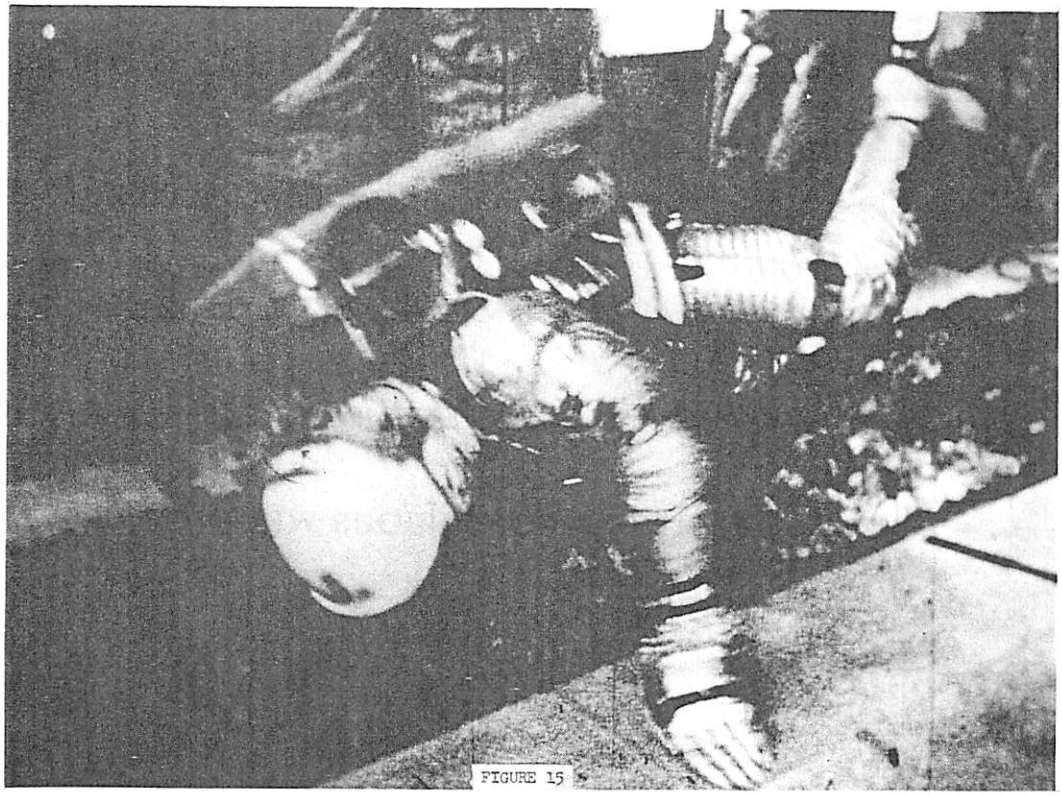

FIGURE 15

WATER COOLED GARMET

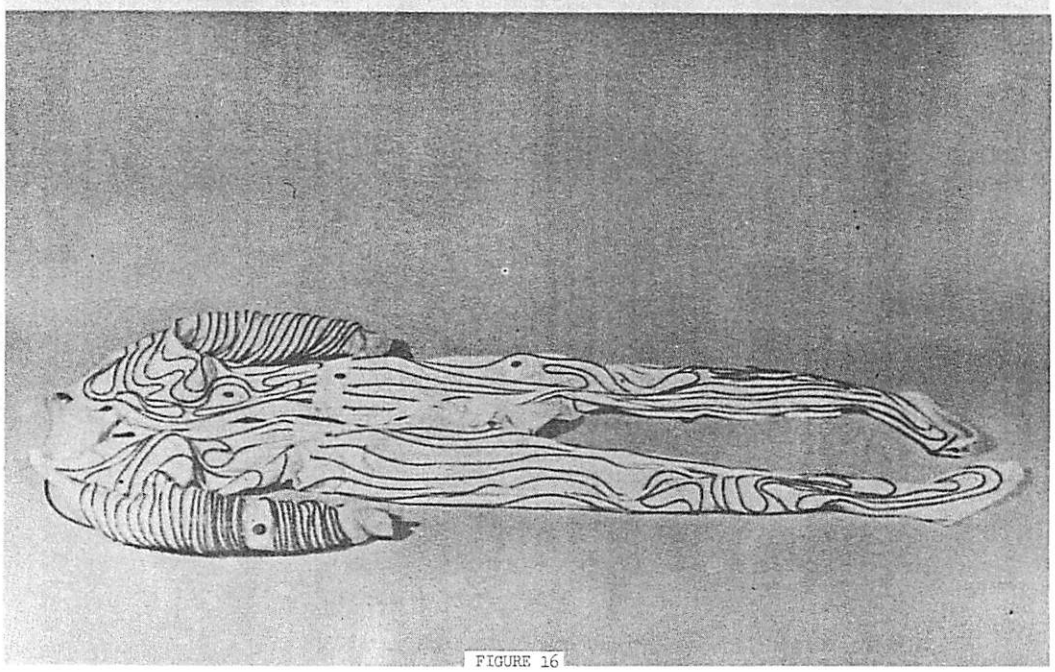

FIGURE 16

NASA-S-66-6850 JUN

LIQUID COOLED GARMENT (LCG) DESIGN REQUIREMENTS

- LIMIT PERSPIRATION TO 130 GM/HR AT 2000 BTU/HR
- LIMIT LOCAL SKIN TEMPERATURE TO 105° F MAXIMUM
- LIMIT LOCAL SKIN TEMPERATURE TO 50° F MINIMUM
- TOLERABLE FOR CONTINUOUS WEAR FOR UP TO 115 HOURS

FIGURE 17

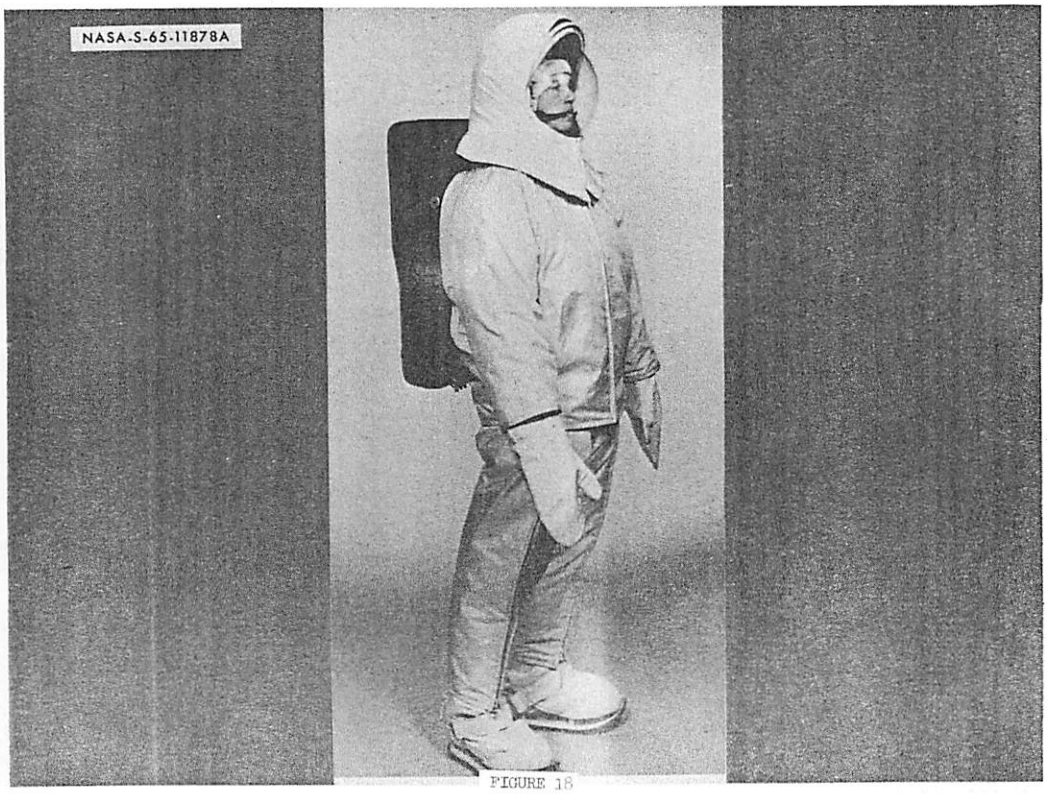

FIGURE 18

NASA-S-66-6849 JUN

THERMAL METEOROID GARMENT (TMG) DESIGN REQUIREMENTS

- ABRASION PROTECTION
- METEOROID PROTECTION
- PASSIVE THERMAL PROTECTION

  ELIMINATE "HOT SPOTS"
  250 BTU/HR IN
  350 BTU/HR OUT

- DON-DOFF CAPABILITY TO PREVENT CONTAMINATION

FIGURE 19

NASA-S-66-6814 JUN

PROTOTYPE APOLLO EXTRA VEHICULAR GLOVE TEST

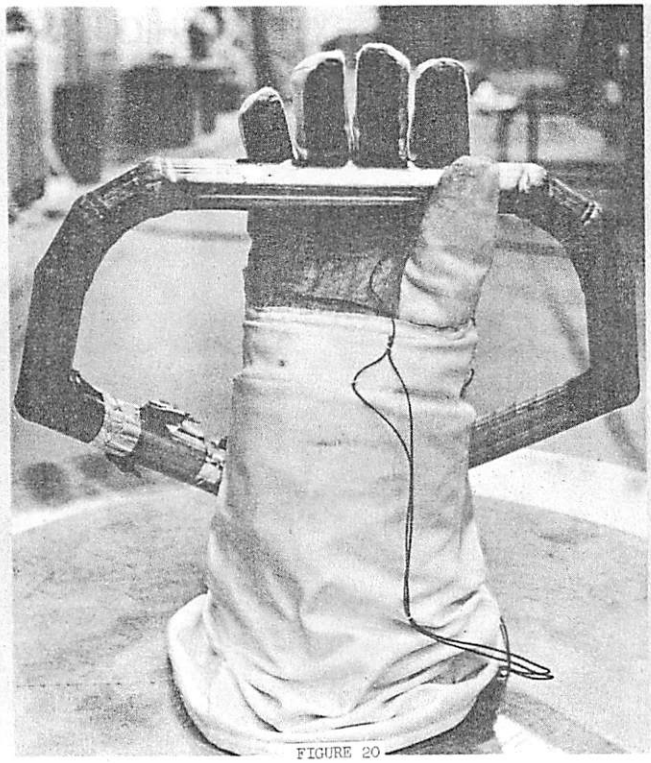

FIGURE 20

PROTOTYPE APOLLO LUNAR BOOTS

FIGURE 21

PROTOTYPE APOLLO EXTRA VEHICULAR VISOR ASSEMBLY

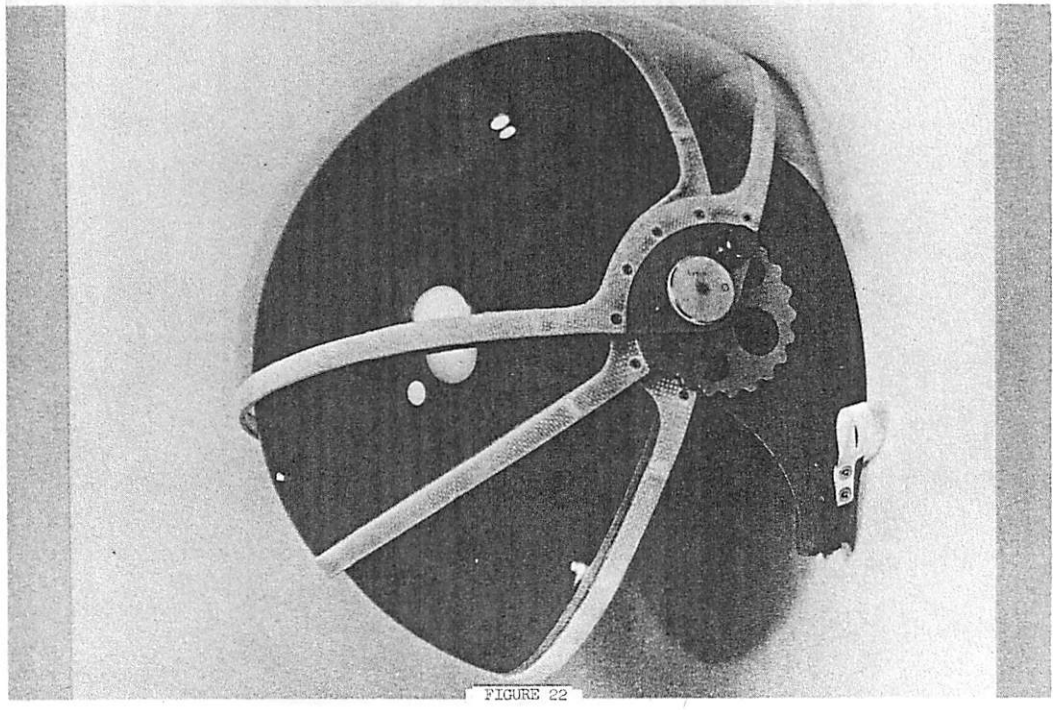

FIGURE 22

APOLLO EMU THERMAL TEST

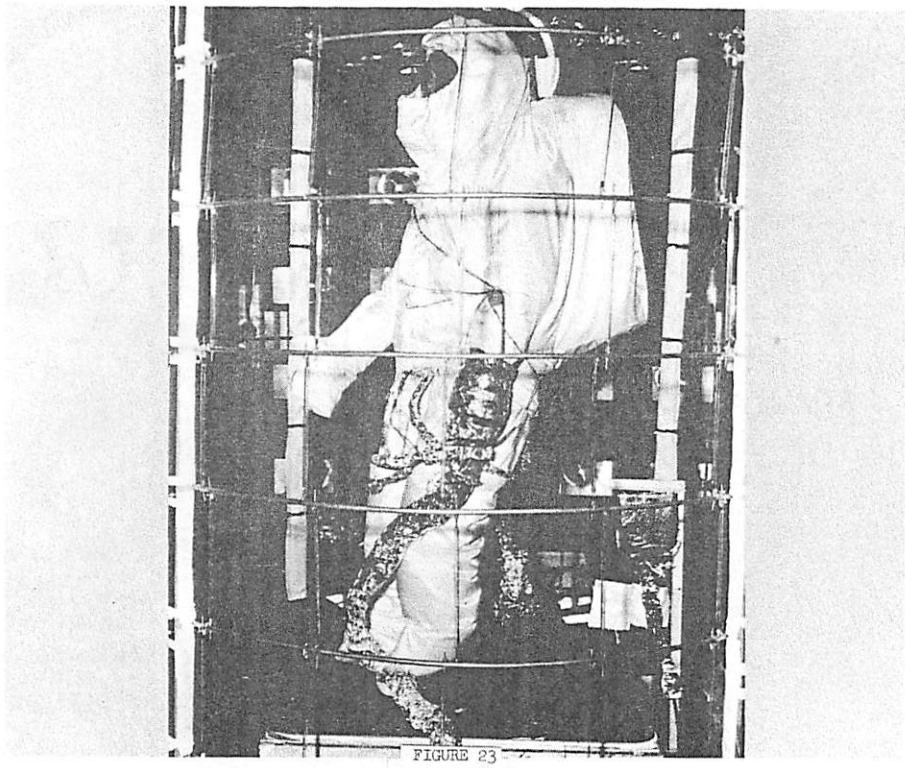

FIGURE 23

NASA-S-66-2157 MAR 3

METABOLIC RATE COMPARISON

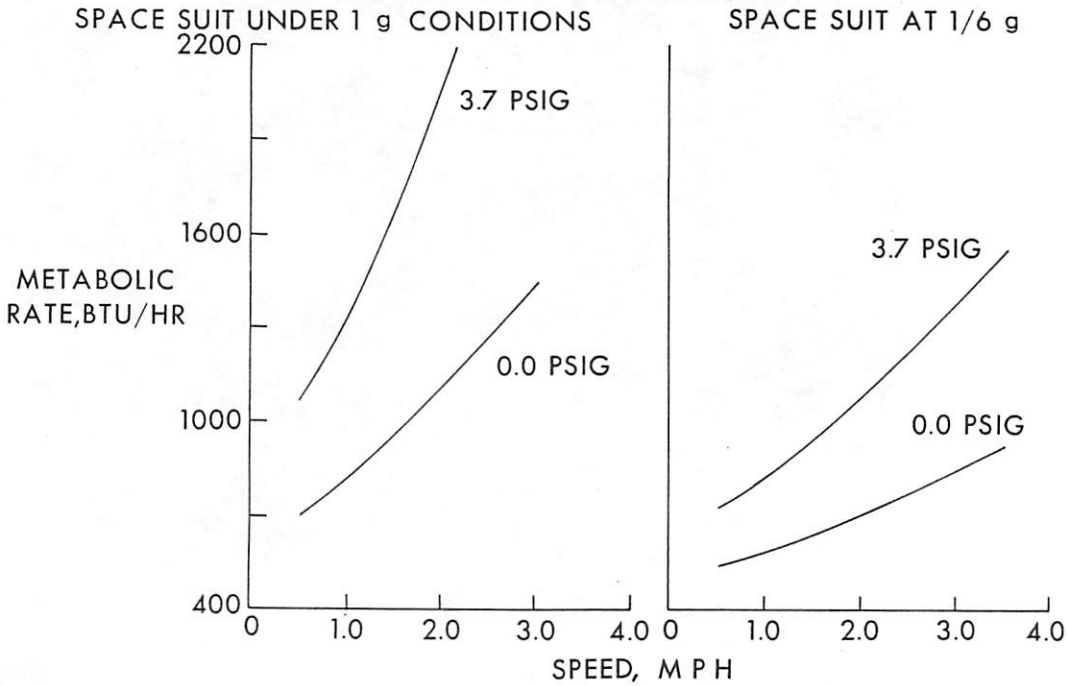

FIGURE 24

NASA-S-66-2163 MAR 3

FIGURE 25

NASA-S-66-6816 JUN

EMU 1/6 GRAVITY - LUNAR SURFACE TESTING

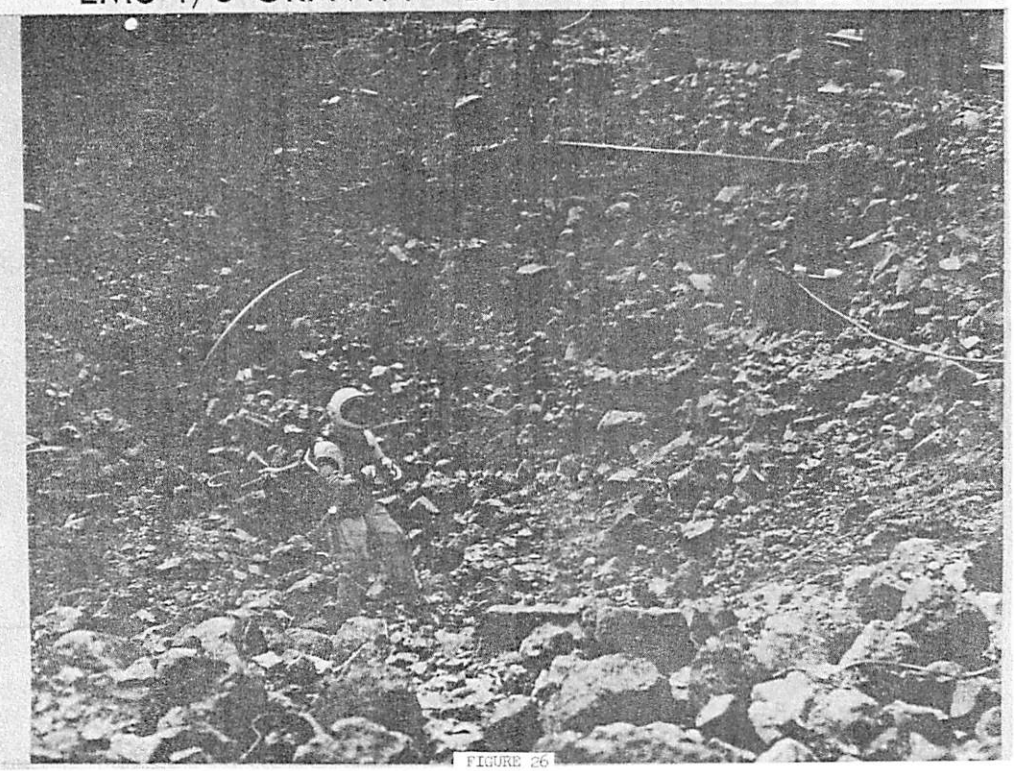

FIGURE 26

NASA S-65-1866

SUITED ASTRONAUT USING JACOBS' STAFF TO ASSIST IN WALKING ON SIMULATED LUNAR SURFACE

FIGURE 27

NASA S-65-1862

ASTRONAUT WEARING COMPLETE EMU DURING SIMULATED LUNAR SURFACE TESTS (BEND, ORE)

FIGURE 28

NASA-S-66-6828 JUN

RANGE LIMITATION RESULTING FROM THE OXYGEN AVAILABLE FOR EMERGENCY USE

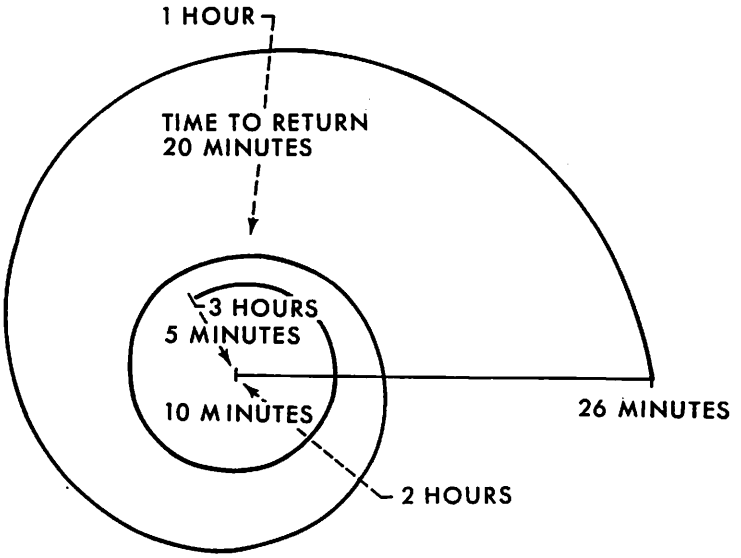

FIGURE 29

LM TOUCHDOWN DYNAMICS

by

Hugh M. Scott

LEM LANDING DYNAMICS

1.0 INTRODUCTION

The landing simulation studies accomplished at MSC define the vehicle state at touchdown. The purpose of this presentation is to give a description of the landing system and to discuss the dynamics of the LEM following the initial landing impact, including the analysis work accomplished and planned to predict vehicle landing performance.

The lunar landing must obviously avoid toppling instability of the LEM, within the flying qualities of vehicle control system, for the range of lunar surface parameters selected for design.

2.0 DEFINITION OF LANDING GEAR DESIGN CRITERIA

Landing gear design was initiated on the LEM before current lunar data, such as Ranger and Surveyor flights, were available. A criteria was chosen for the contractor to design the LEM gear and is summarized in Figure 1. In addition to the geometric characteristics of the design lunar model of 6° general slope with 24-inch depressions or 24-inch protuberances under the foot pads at impact giving a maximum effective slope of approximately 12°, the surface material was considered to be infinitely rigid for shock absorber design. Foot pad size was based on a minimum surface dynamic bearing strength of 12 psi. Shearing or sliding resistance as a friction coefficient was considered to vary from 0.4 to 1.0 in addition to partial or full constraint of the foot pad.

The vehicle velocity, attitudes and rates were established from the 3σ control system capabilities given in the preceding discussion. These criteria are a vertical velocity of 10 ft/sec with a horizontal velocity of 0 ft/sec; a vertical velocity of 7 ft/sec and horizontal of 4 ft/sec. The attitude criteria is $\pm 6^{\circ}$ with a maximum attitude rate of 2°/sec. The control system will be active during landing dynamics, but was not considered so for original gear design and performance analysis. Gear design also considered the possible de-stabilizing moment generated during some landing conditions from crushing of the descent engine skirt extension, and the crush load characteristics used were included as a specification requirement on the engine design. The design landing weights were selected based upon minimum and maximum usage of expendables in the descent from lunar orbit. The maximum landing weight is, in general, critical for the

energy absorption requirements while the minimum landing weight, which also has the highest center of gravity position, is critical for the stability requirements.

3.0 DESCRIPTION OF LANDING GEAR

The landing gear design that evolved from this set of requirements is referred to as the "Cantilever" gear. As shown in Figure 2, each of the four gear assemblies consists of a primary strut and two secondary struts. The primary strut consists of an inner cylinder with a foot pad at its lower end, and an outer cylinder connected through a type of universal joint at its upper end to the outrigger support truss. A dual crush level honeycomb cartridge shown at the top of Figure 2 acts in compression to absorb energy at the indicated load-stroke values. Each secondary strut consists of an outer cylinder connected through a ball joint to the primary strut, an inner cylinder connected through the deployment truss to the base of the descent stage, and an arrangement of honeycomb cartridges that can absorb energy, at the load-stroke values shown in the bottom of Figure 2, while the secondary strut is extending or compressing. The 36-inch diameter foot pad has sufficient area and strength to provide flotation and minimal impact penetration on low bearing strength surfaces. The center of each foot pad is 167.57 inches from the LEM centerline.

4.0 LANDING - PERFORMANCE TO DESIGN CRITERIA

To predict landing performance on the lunar surface, considerable effort has been and continues to be expended in extensive landing dynamic analysis. Of prime concern during the development of the analysis was the realistic treatment of the non-linear geometry and loading of the articulating landing gear. Since the properties of the landing surface were not well known, special attention was given to allow the analysis to accommodate a wide variety of conditions. Other significant effects treated in the analysis include the influence of crushing the descent engine skirt extension, fuel slosh, reaction control and engine thrust forces, and the logic required to account for the initiation of engine shutdown and thrust-decay characteristics. Since purely symmetric landings appear unlikely, it became desirable to determine the effect of introducing asymmetric parameters into the initial conditions, (e.g., variations in the flight path with respect to the lunar slope, and vehicle yaw angle with respect to the flight path).

Results of a landing simulation include time histories of all pertinent data (e.g., center of gravity velocities and accelerations, strut loads, strokes, and foot pad position). Another

form of the simulation output is a movie describing stroking of the struts, crushing of the engine skirt and vehicle motions resulting from the dynamics. The vehicle is assumed unstable if the LEM center of gravity falls outside a vertical plane passing through any two adjacent foot pads. In a stable run, the minimum distance between the LEM center of gravity and any of these vertical planes is recorded as a measure of stability. Results of such an analysis with various initial conditions, within the criteria, give us performance boundaries indicated by Figure 3. These boundaries then indicate that the present gear design is optimized to a high degreee to meet the original design criteria for worst case energy absorption and stability critical landing conditions.

5.0 LEM STATE AT TOUCHDOWN

Factors affecting the vehicle state at touchdown include probes mounted on the LEM foot pad used to sense the landing surface and to provide a signal for engine thrust termination (See Figure 4). A landing surface bearing strength of about 3 psi acting on the probe tip is sufficient to activate the cutoff signal. Upon receipt of the sensing probe signal, the astronaut manually terminates the thrust.

Terminating thrust before touchdown causes the spacecraft velocity to increase at touchdown. The earlier the thrust is terminated, the higher the touchdown velocity. If the astronaut delays too long in terminating thrust, the engine will be firing at touchdown. Thus, two possible problem areas exist: landing with velocities in excess of design velocity and landing with the engine on.

Figure 5 shows the predicted 99% probability touchdown velocities together with the touchdown velocity envelope. The predicted touchdown velocity includes the effect of astronaut reaction time and system delays. The figure shows that the predicted touchdown velocities fall well within design values. Therefore, no problem is anticipated in this area.

To avoid possible undesirable failure modes of the engine skirt and increased pressure and temperatures on the base heat shield, it is desirable to terminate thrust by the time the footpads contact the surface. At this point, the engine skirt is approximately 19 inches above the surface. The engine may be thrusting at touchdown if the descent velocity is too high or if the astronaut delays too long in initiating engine cutoff. Figure 6 shows the probability of a given vertical velocity occurring at probe surface contact when the nominal descent velocity of 3.5 fps is desired. The figure also shows the probability of a given crew reaction time for initiating engine cutoff. These data were generated during the landing simulator studies mentioned above.

Referring to the figure, there is a 97% probability that the descent velocity at probe contact will be less than 5 fps. For this descent velocity, the astronaut reaction time must be in one-half second before it is physically possible for the engine to be thrusting at touchdown. The probability of the astronaut reaction time exceeding one-half second is about 2%. Combining the two probabilities results in a probability of about 99.94% that the engine will be off at touchdown.

The minimum engine operation height above the surface of 19 inches used at this time is from preliminary plume analysis. To better define the engine/surface interaction limits, MSC has initiated contracts to develop two different analytical models of the engine plume/surface interaction as well as an experimental program.

One analytical approach will develop a free plume program for an ideal nozzle (parallel flow at exit). An initial investigation of a plume impinging on a surface will also be made to obtain approximate surface pressures. The other analytical program will develop a free plume program for a Rao nozzle, assuming no strong shocks and omitting that portion of the flow where a lip shock occurs. An experimental program, using the Langley Research Center 41 foot high altitude facility, will be performed incorporating the Apollo 100-pound thrust Reaction Control System engine (a 1/10-scale LEM descent engine). These tests will correlate the above analytical programs and aid in evaluating the descent engine flow under various conditions. (See Figure 7)

Phase II of this effort will select the more descriptive computer program, and continue using the selected program for engine flow near the surface to evaluate surface interaction. This study will consider both normal and off-normal orientation of the engine plume to the surface. The initial analytical and experimental programs should be completed by September 1966. The more detailed Phase II completion is estimated for February 1967.

6.0 IMPLICATIONS OF LUNAR ENVIRONMENT ON LANDING PERFORMANCE

As noted earlier, the landing performance of the LEM is satisfactory for the design lunar surface model. We now turn our attention to the landing performance on surfaces that are less rigid than the design surface.

Determination of landing performance on soft surfaces relies heavily on a knowledge of the interaction of the landing gear foot pad with the soft surface as the pad penetrates the surface.

The interaction forces and moments depend on the soil dynamics and the foot pad size and shape.

Since soil dynamics in a lunar environment is a relatively unexplored field, a considerable amount of experimental and theoretical work has been initiated in this area. This work is aimed at determining the foot-pad/soil interaction for several soil types that have a high probability of occuring on the lunar surface. The necessary data should start becoming available within the next six months.

In the meantime, some landing performance bounds can be established through the use of simplified theoretical soil/foot-pad interaction models. Experimental and theoretical interaction force models that have been developed to date usually are of the form expressed by the equation in Figure 8.

The first two terms in the equation are associated with the static penetration resistance, while the last two terms are associated with the dynamic penetration resistance of the soil. This equation has been programmed into MSC's digital computer simulation of the LEM lunar touchdown dynamics. Work is underway to determine the lunar landing performance based on this theoretical foot-pad/soil interaction model. The next several figures summarize the results of our work to date. As experimental data becomes available, the results shown here will be updated as necessary.

The ground rules being used to determine soft surface landing performance are listed in Figure 9. Lateral motion of the foot pad was <u>not</u> allowed to get conservative answers for the vertical penetration.

The procedure for determining landing performance is outlined in Figure 10.

Figure 11 is an example of how "bad" stability cases are determined. The stability performance was computed for each set of initial conditions and plotted vs stability margin. Stability margin is the minimum distance between the LEM c.g. and a vertical plane passing through any two adjacent foot pads as shown in Figure 12.

The worst case is the point of least stability. Similar curves are being generated for a range of slopes, velocities, yaw angles, and interaction models.

The next step in landing performance evaluation is to determine foot pad penetrations.

Figure 13 shows foot pad penetrations for soil where penetration increases linearly with depth. Foot pad penetration is not too dependent on landing slope for these soil models. One of the study ground rules is that the spacecraft heat shield shall not contact the surface. Heat shield contact occurs when the foot pad penetration exceeds approximately 44 inches. Figure 13 shows that the surface strength should be greater than about 5 psi/ft to avoid penetrations greater than 44 inches.

Also shown on Figure 13 is the effect of adding a small amount of dynamic penetration resistance to the 5 psi/ft soil. As could be expected, the penetration decreases considerably when the dynamic terms are included. It will be shown later that stability also tends to improve as the dynamic penetration resistance increases.

Figure 14 shows foot pad penetration for a soil whose penetration resistance is constant with depth. A soil strength of about 8 psi is required to prevent foot pad penetration beyond 44 inches in this type of soil.

The results of the previous figures have been plotted together on Figure 15 to obtain a preliminary landing performance envelope.

The horizontal lines represent stability boundaries for the different soil models considered. It is important to note that soils that are acceptable from a penetration standpoint provide good landing areas from a stability standpoint. In fact, the stability performance on these soils is practically the same as the rigid surface performance.

Based on this preliminary data, it appears that the LEM can land safely on a surface slope of about 7 degrees plus 2-foot depressions, provided the soil strength is greater than 5 psi/ft or 8 psi depending on the type of soil.

This simplified theoretical soil/foot pad interaction model is also useful to approximate landing performance on particular landing areas as more information becomes available, e.g., the recent Surveyor 1 site. The limited penetration of the Surveyor foot pads into the lunar surface leaves the soil properties open

to interpretation, but as far as LEM landing acceptability, it may be bounded using the findings presented in the preliminary report of the Surface Mechanical Properties working group. This report suggests that the bearing strength of the material in the area of the Surveyor foot pads photographed is approximately 5 psi. If we assume this to be a material that bearing strength varies linearly with depth, then the 5 psi at 2 inches could be represented by a 30 psi/ft interaction model which would result in LEM landing performance similar to that shown for a rigid surface.

If we assume the conservative interaction model of 5 psi constant, then the computed penetration of the LEM for a 10-fps straight down landing would be approximately 8 inches for all four foot pads. By introducing horizontal velocity component and vehicle maximum attitude and attitude rates, the greatest foot pad penetration is approximately 1.7 feet; therefore, for landing performance considerations, the LEM would land safely on a landing area similar to the Surveyor 1 site.

7.0 CONCLUSIONS

LEM landing performance meets the original specification design criteria.

The probe surface sensor allows manual engine cut-off consistent with design touchdown velocities and minimum engine operation height above the surface.

Study is continuing to determine minimum engine operating height above the surface that is required to establish maximum descent velocity and range of reaction times consistent with design touchdown velocities.

LEM landing performance on soft surfaces relies heavily on footpad/soil interaction forces.

Experimental work to determine interaction forces for several soil types is underway.

Preliminary data based on theoretical interaction forces indicate that the LEM can land safely on a slope of about 7 degrees plus 2-foot depressions if the soil strength is 5 psi/ft or 8 psi constant.

LEM landing would be successful on a lunar surface similar to the one indicated by the Surveyor 1 spacecraft.

Questions and Answers

TOUCHDOWN DYNAMICS

Speaker: Hugh Scott

1. Is it possible for LM to come to rest on three of the four foot pads?

   ANSWER - Yes. Simulation tests show that if the center of gravity is forward of the mid gears the LM will come to rest with one of the pads off the surface.

2. Assuming 7 ft/sec. vertical velocity, 4 ft/sec. horizontal velocity, and a 12 degree effective slope, then what coefficient of friction is required to overturn the vehicle?

   ANSWER - The performance boundaries shown in the presentation used infinite coefficient of friction, and the vehicle did not turn over.

NASA-S-66-5131 JUNE 7

LM LANDING CONDITIONS

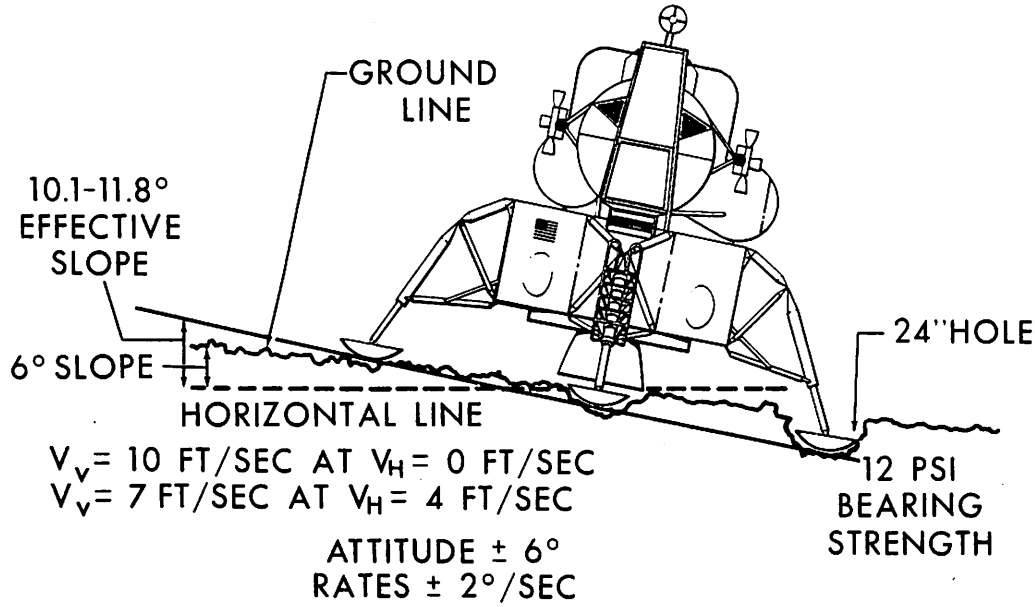

Figure 1

NASA-S-66-5128 JUNE 7

LANDING CONDITIONS - LOAD STROKE

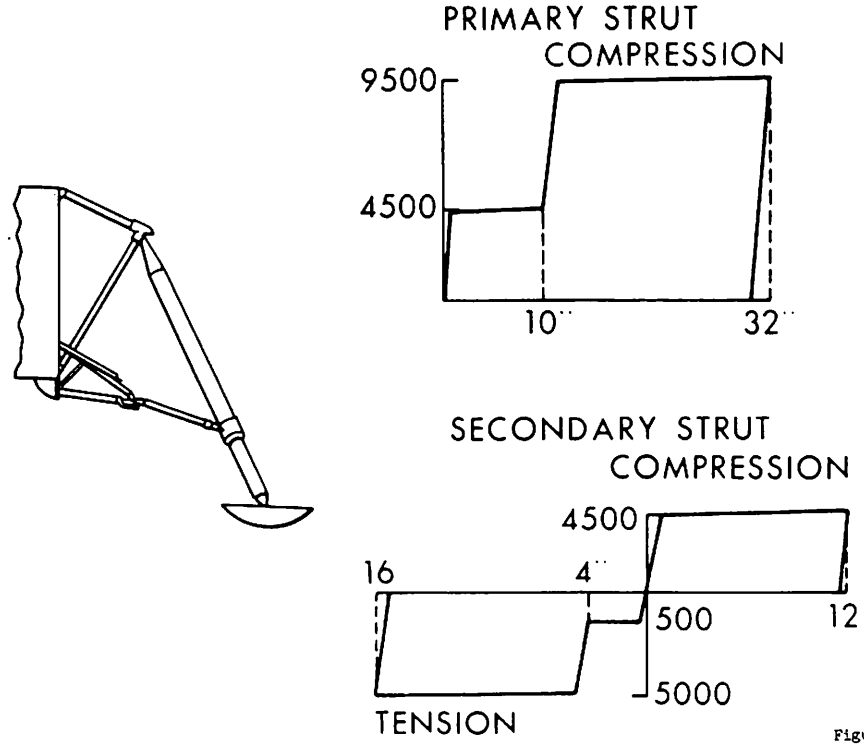

Figure 2

NASA-S-66-5130 JUNE 7

LANDING PERFORMANCE

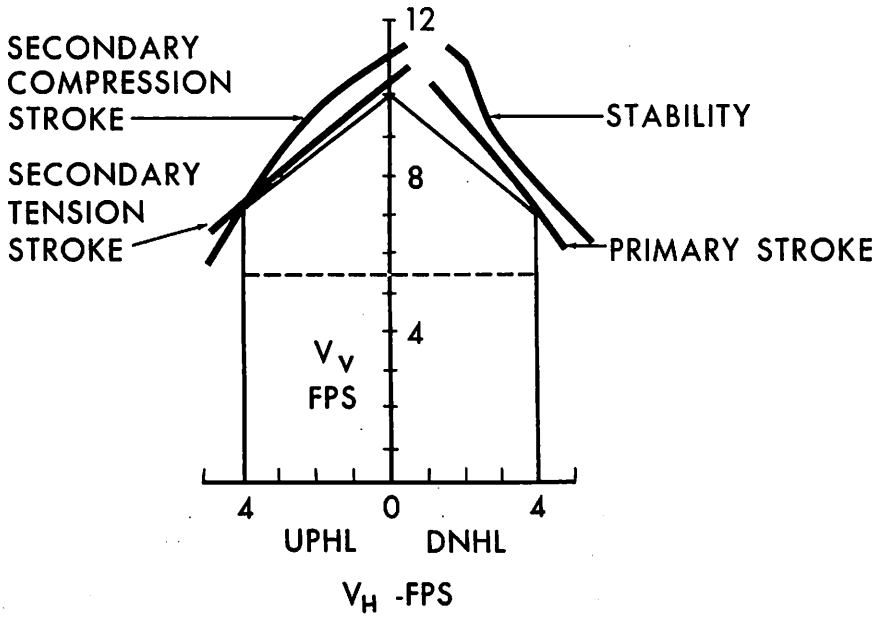

Figure 3

NASA-S-66-5129 JUNE

PROBE SENSOR

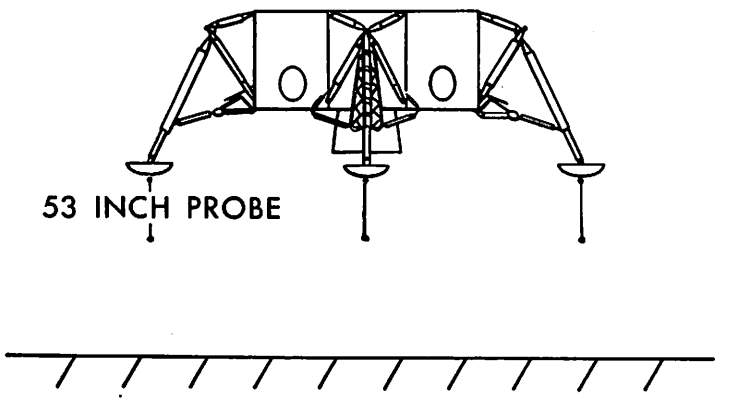

Figure 4

NASA-S-66-6581 JUN

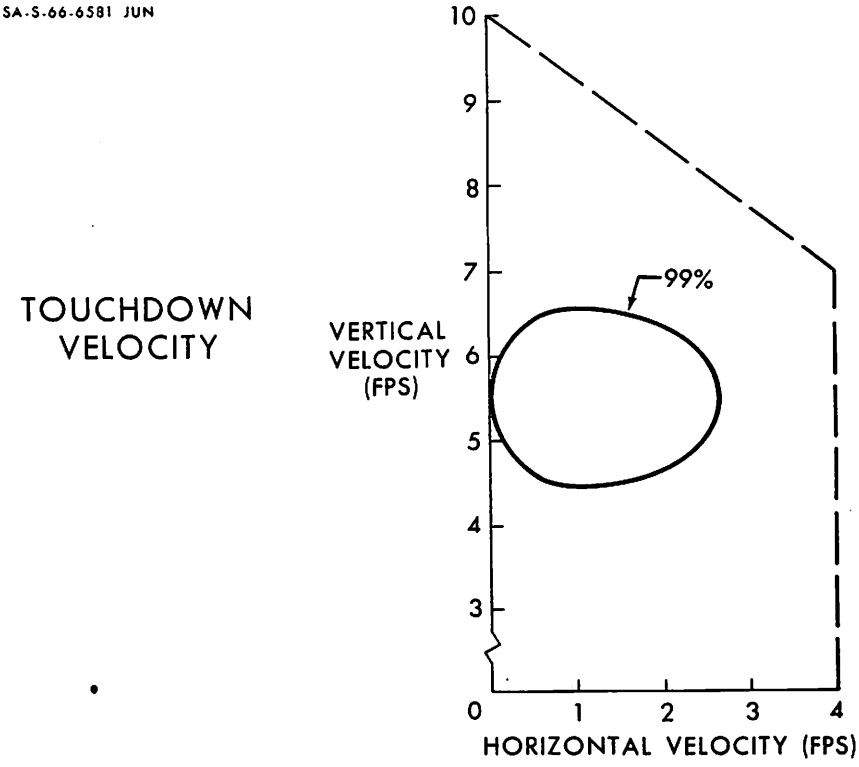

Figure 5

NASA-S-66-6580 JUN

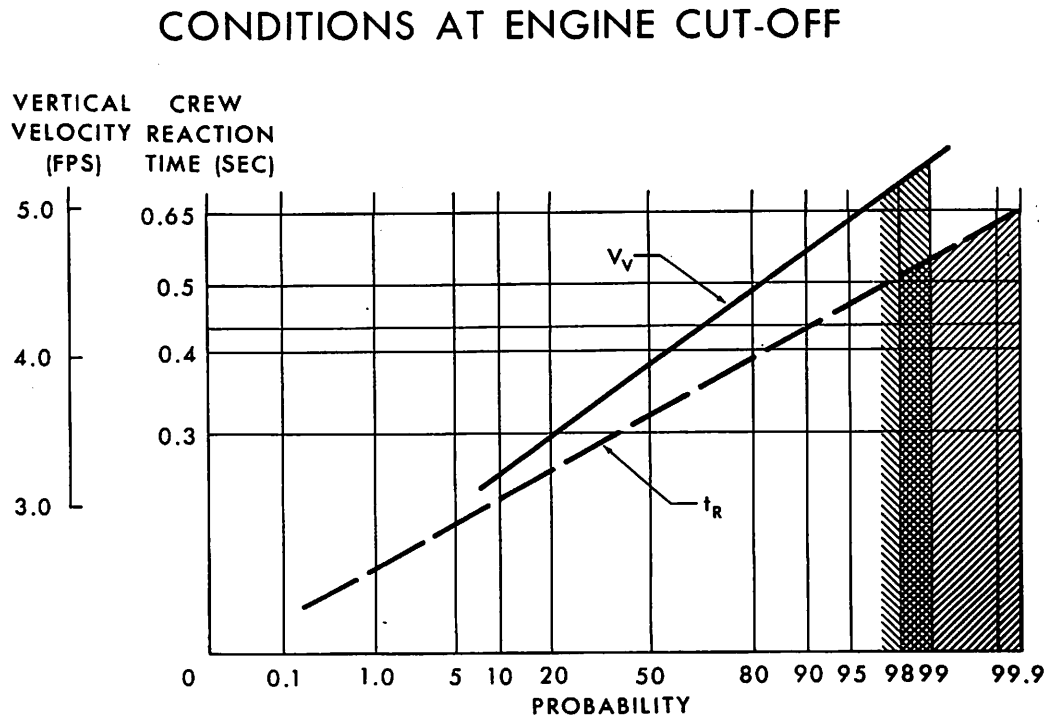

Figure 6

NASA-S-66-6862-JUN

PLUME-SURFACE INTERACTION TEST IN LRC VACCUM CHAMBER

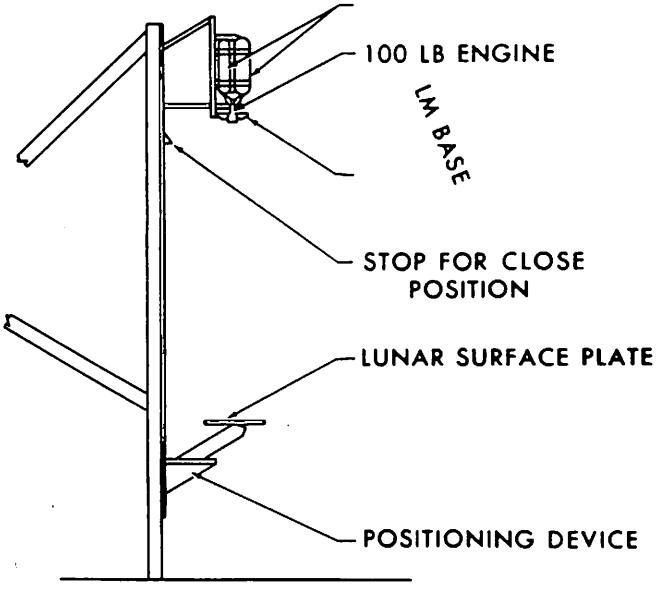

Figure 7

NASA-S-66-5161 JUN

SOIL MODEL

$$F = (K_1 + K_2X + K_3\dot{X} + K_4\dot{X}^2)\ A_P$$

Figure 8

NASA-S-66-5162 JUN

GROUND RULES

- DESCENT STAGE HEAT SHIELD SHALL NOT CONTACT LANDING SURFACE
- 4-JET CONTROL SYSTEM ACTIVE
- NO LATERAL FOOTPAD MOTION
- SURFACE PROTUBERANCES & DEPRESSIONS $\leq$ 2 FT
- TOUCHDOWN STATE VECTOR-SAME AS DESIGN CRITERIA

Figure 9

NASA-S-66-6079 JUN

PERFORMANCE EVALUATION PROCEDURE

1) CHOOSE INTERACTION MODEL, E. G., $F = K_2X(A_p)$

2) DETERMINE "BAD" STABILITY & PENETRATION LANDINGS BY SIMULATING SERIES OF LANDINGS WHILE PARAMETICALLY VARYING TOUCHDOWN CONDITION & SLOPE

3) DETERMINE MAXIMUM FOOTPAD PENETRATION VS SLOPE

4) DETERMINE TOUCHDOWN STABILITY VS SLOPE

Figure 10

NASA-S-66-6081 JUN

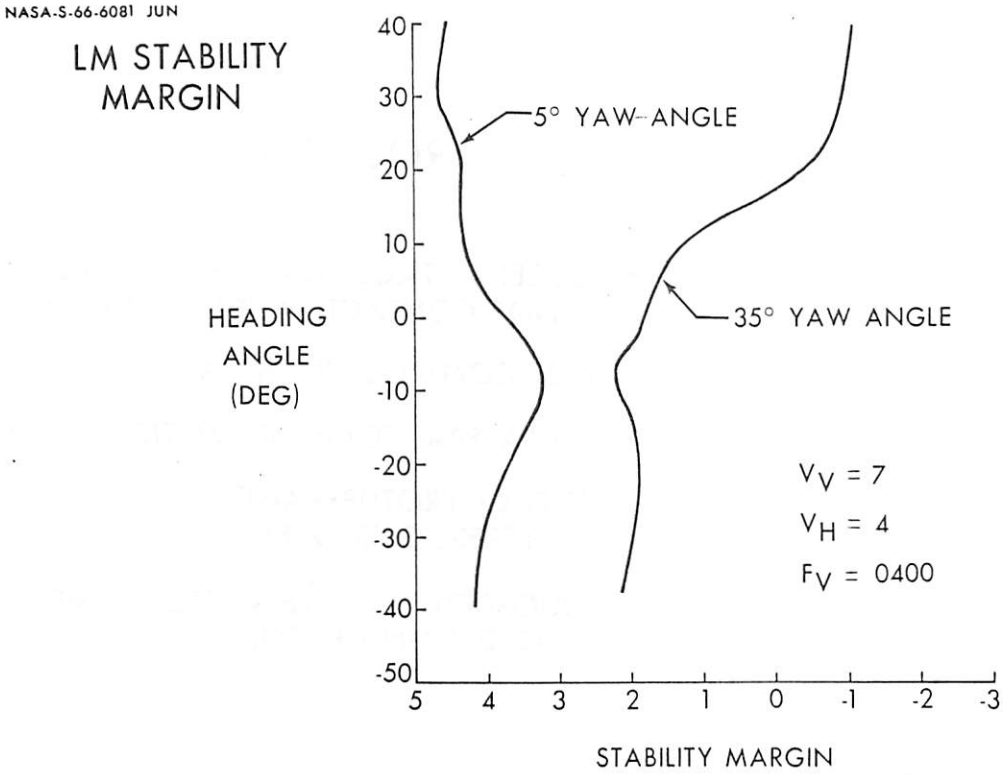

Figure 11

NASA-S-66-6857 JUN

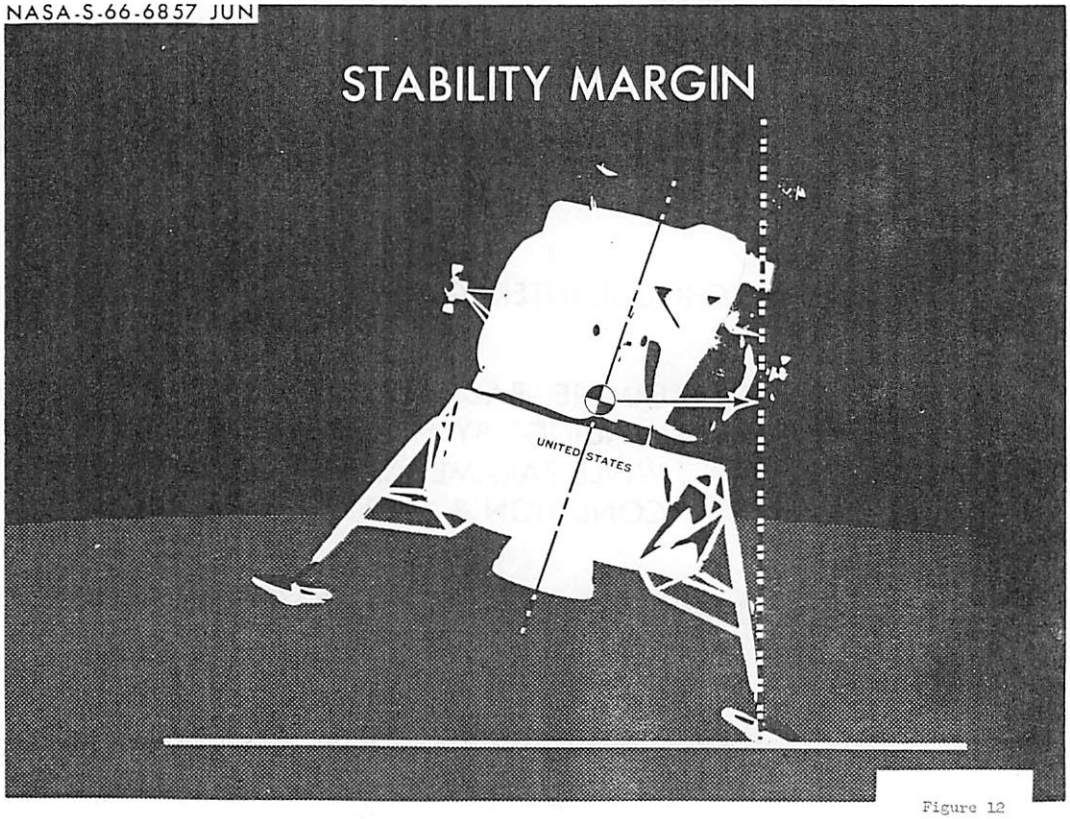

Figure 12

NASA-S-66-6082 JUN

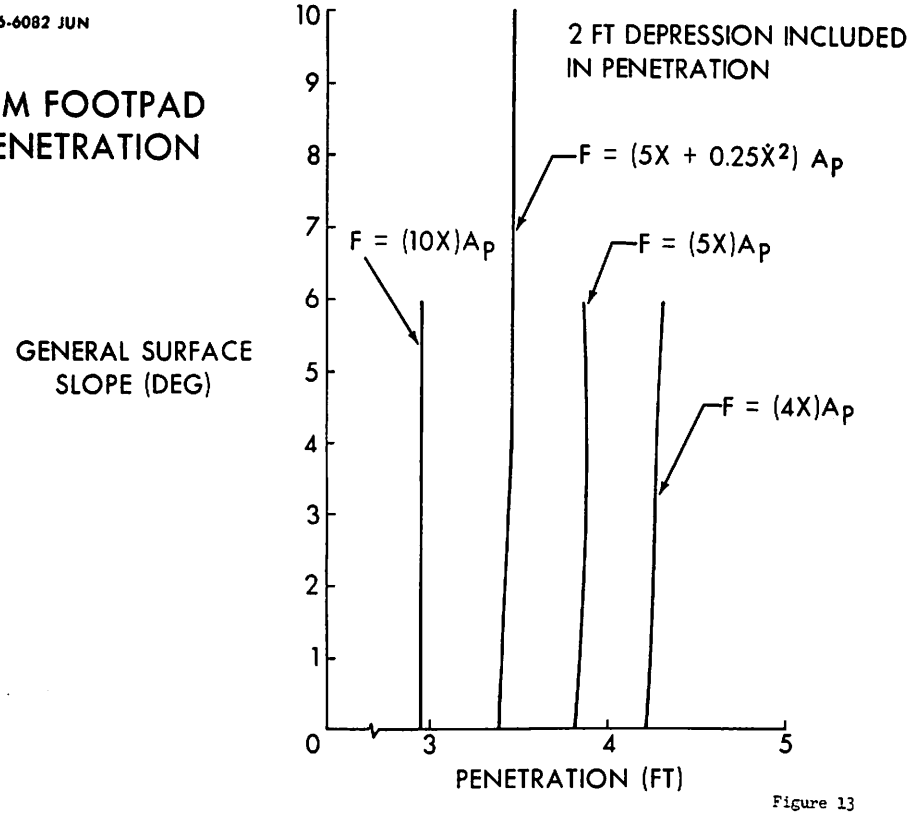

Figure 13

NASA-S-66-6083 JUN

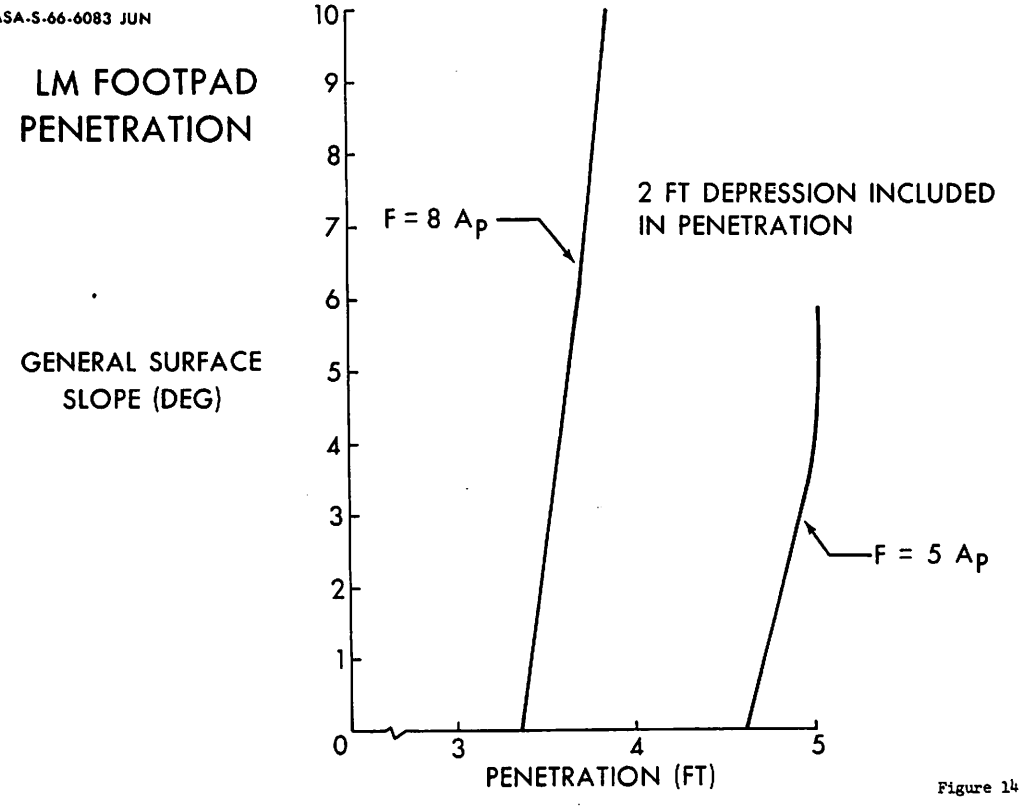

Figure 14

NASA-S-66-6080 JUN

PRELIMINARY LANDING PERFORMANCE ENVELOPE

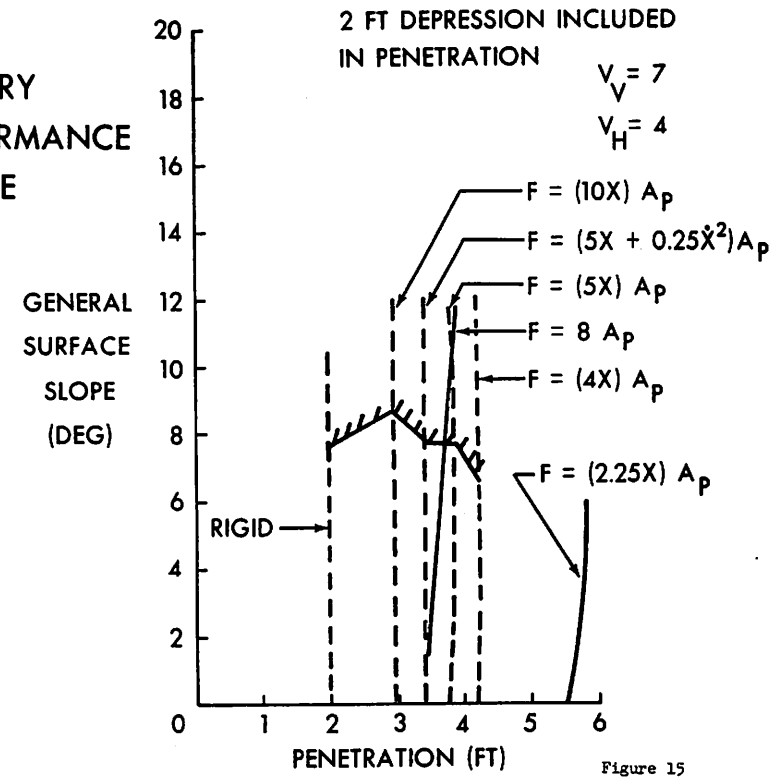

Figure 15

LANDING SITE SELECTION CRITERIA

by

A. V. Bernard, Jr.

LANDING SITE SELECTION CRITERIA

1.0 INTRODUCTION

The presentation on Site Selection is given in two parts: Site Selection Criteria and Site Selection Data Sources and Interpretation (Fig. 1). This document presents the Site Selection Criteria portion of the presentation and the associated charts.

The objectives of the site selection activities as shown on Fig. 2 are:

- To develop site selection criteria that will maximize the probability of successful LM landing
- To develop methods of ranking candidate sites
- To utilize lunar surface data in ranking candidate sites
- To select the landing sites

The site selection process must be completed not later than six months prior to launch to satisfy targeting requirements.

The capabilities and constraints of LM and its associated subsystems have been developed in previous papers. Similarly, the operational problems that must be considered have been developed in previous papers. It is these various considerations that constitute the site selection criteria. This criteria used in conjunction with the available lunar surface data provides the mechanism for candidate site selection as noted on Fig. 3.

The various considerations used to establish the site selection criteria have been divided into two categories: Operational considerations and spacecraft/surface interactions. These two categories will be discussed in subsequent sections.

2.0 OPERATIONAL CONSIDERATIONS

The operational considerations consist of lunar lighting, visibility and CSM performance as noted on Fig. 4. Lunar lighting and visibility will be discussed in some detail followed by a shorter discussion on the implications of lighting and CSM performance on the accessible lunar area and the required landing site spacing.

NASA-S-66-6117 JUN

LUNAR LANDING SITE SELECTION

- SITE SELECTION CRITERIA
- SITE SELECTION DATA SOURCES AND INTERPRETATION

Fig. 1

NASA-S-66-6112 JUN

OBJECTIVES

- DEVELOP CRITERIA TO SELECT SITES THAT WILL MAXIMIZE PROBABILITY OF SUCCESSFUL LM LANDING
- DEVELOP METHODS OF RANKING CANDIDATE SITES
- UTILIZE LUNAR SURFACE DATA IN RANKING CANDIDATE SITES
- SELECT LANDING SITES
- TARGETING REQUIRES SITE SELECTION NO LATER THAN SIX MONTHS PRIOR TO LAUNCH

Fig. 2

NASA-S-66-5399 MAY 31

BASIS FOR SITE SELECTION

- LIGHTING REQUIREMENTS
- CSM PERFORMANCE
- GN&C REQUIREMENTS
- LM LANDING REQUIREMENTS

} SITE SELECTION CRITERIA

- EARTH-BASED OBSERVATIONAL DATA
- RANGER DATA
- LUNAR ORBITER DATA
- SURVEYOR DATA

} LUNAR SURFACE DATA

} CANDIDATE SITE SELECTION

Fig. 3

NASA-S-66-6116 JUN

OPERATIONAL CONSIDERATIONS

- LIGHTING CONSIDERATIONS
- CSM PERFORMANCE

Fig. 4

2.1 LUNAR LIGHTING AND VISIBILITY

An important crew task during LM descent is visual inspection of the lunar surface. This requirement for visual evaluation of the surface will affect site selection by the imposition of constraints on acceptable sun angles. The range of sun angles, in turn, influences the spacing of lunar sites and launch dates. In this section, the basis for the current choice of minimum and maximum sun angles is developed.

The visibility of obstacles is strongly dependent on the solar and viewing elevation angles. In general, above some minimum value of sun angle, visibility decreases as sun angle increases. Thus, for a given viewing angle, it is necessary to select a maximum sun angle which permits both acceptable visibility and allows sufficient operational flexibility.

The viewing angle to the nominal landing site is fixed by the descent trajectory and varies during the LM descent. The maximum acceptable sun angle for a given trajectory will, thus, depend on the point during descent at which visual interrogation of the surface is necessary.

In spite of the face that this point is not yet firmly determined it is possible to establish preliminary criteria for the minimum and maximum sun angles based on several sources of data. As indicated on Fig. 5, these are:

- Lunar reflectance characteristics.
- Detection range estimates.
- The effects of glare for forward sun angles.
- The need for shadowing to enhance site evaluation and detection.
- The amount of shadowing at low sun angles.

Correlation of these results with the viewing angle history resulted in the range of sun angles and lighting conditions currently used for site selection. Each set of results will now be described.

2.1.1 LUNAR REFLECTANCE PROPERTIES

Fig. 6 presents the variation in luminance of the horizontal lunar surface as it is viewed over a 180° range for three sun

NASA-S-66-6810 JUN

LUNAR LIGHTING & VISIBILITY

DATA SOURCES

- REFLECTANCE PROPERTIES
- ANALYTICAL STUDIES OF DETECTION
- EFFECTS OF GLARE
- SHADOWING REQUIREMENT FOR RECOGNITION
- SHADOWING AT LOW SUN ANGLES

DETERMINATION OF SUN ANGLE LIMITS

- CORRELATION WITH VIEW ANGLE

Fig. 5

NASA-S-66-3878 JUN

LUNAR REFLECTANCE

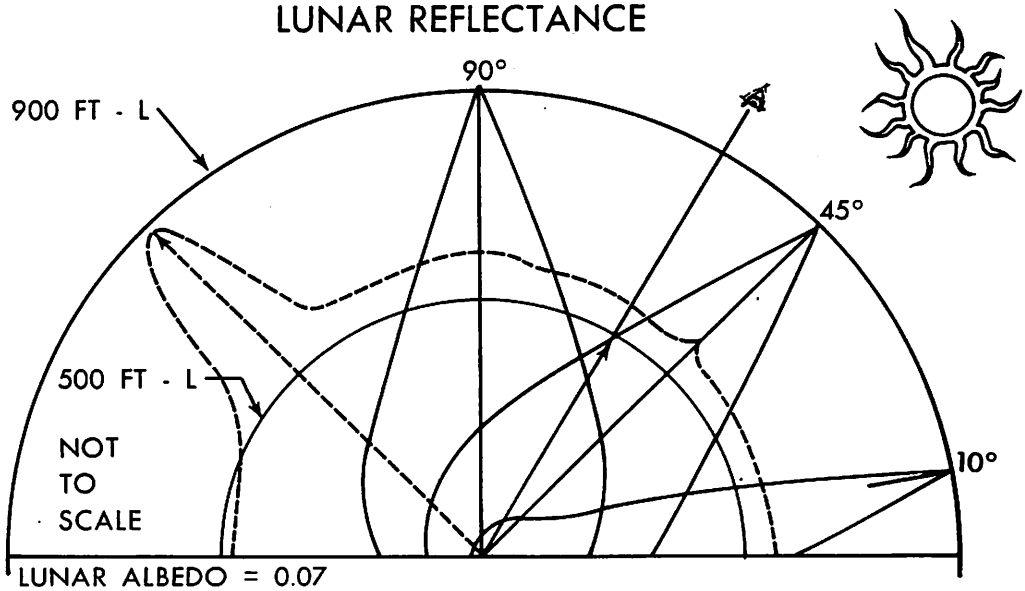

LUNAR ALBEDO = 0.07
SOLAR ILLUMINATION = 13,000 LUMENS/FT^2
--- SEMI-SPECULAR EARTH MATERIAL
—— RETRO REFLECTIVE LUNAR SURFACE

REF: JPL TR NO. 32-664

Fig. 6

angles; 10°. 45°. and 90°. Two luminance contours are shown, 500 ft.-Lamberts and 900 ft.-Lamberts. Shown also, but not to scale, is a reflectance curve for a semi-specular material as an example of typical Earth terrain.

The important lunar reflectance characteristics are summarized on Fig. 6. These lunar reflectance properties were derived by JPL from Earth-based telescopic observations for use in the Ranger and Surveyor Programs (JPL TY 32-664, "The Lunar Reflectivity Model for Ranger Block III Analyses", by D. Willingham, November 1964). Although the telescopic data are of low resolution, the Ranger pictures have provided some confirmation at higher resolutions. Furthermore, studies of lunar surface models indicate that the surface structure responsible for such reflectance characteristics can be in the mm region. The possibility of deviations on the small scale from the currently used reflectance standard must be considered and it is hoped that analysis of the Surveyor pictures will provide additional information on this point.

The data presented on Figures 6 and 7 indicate that the lunar surface acts as a retroreflector; i.e., most of the incident illumination is reflected back along the direction of incidence. This is quite unlike typical Earth terrain for which peak reflectance occurs at a viewing angle opposite and equal to the incident angle and for which the reflectance is relatively uniform at other viewing angles. The lunar surface luminance reaches a maximum when the viewing angle equals the solar angle, that is, when the sun is directly behind the viewer. A rapid dropoff of luminance occurs on either side of this zero phase angle. For example, when the sun is at an angle of 45 degrees, the data in Fig. 6 indicates that luminance decreases from 900 ft.-Lamberts to 500 ft.-Lamberts when the viewing angle is increased 15 degrees beyond the zero phase angle. The luminance value at zero phase is equal for all sun angles. At that point, a variation in sun angle is equivalent to a variation in surface slope in terms of the amount of light reflected. Thus, a variation in luminance will not occur as slope is varied for this condition and the scene will appear homogeneous and "washed out". Except at the washout area, surface slope is the main contributor to visual contrast since the lunar albedo variation is small. However, for zero phase, even surface slope is ineffective. This is the reverse of the Earth situation in which albedo and color variations are most important and slope variations are of relatively minor significance. In addition to slope variations, shadows provide contrast areas and are the dominant visual features for low sun angles.

2.1.2 DETECTION RANGE ESTIMATES

Analytical studies of obstacle detection ranges have been conducted by MSC and by contractors under MSC direction. These studies are based on the lunar reflectance characteristics just described and on standard visual threshold data.

The principal results of such studies are parametric analyses of obstacle detection ranges as a function of solar angle and viewing angle. These results indicate the regions of optimal visibility and the relative degradation for deviations from the optimal. Less confidence can be attached to the absolute values of estimated detection range than can be given to the form of the functions; however, experimental studies are in progress to more firmly establish absolute values.

Typical results are shown in the next three figures. Fig. 8 presents detection range as a function of solar angle for model craters and protuberances. Two viewing angles are shown, 14° and 38°. Both obstacles were assumed to have depth (or height) to diameter ratios of 1:10 and to be 20 feet in diameter.

Note that the detection range for craters and protuberances decreases rapidly as sun angle increases. Protuberances show a greater detection range than craters at low sun angles, due to their large shadows. Note also that an increase in viewing angle results in an increase in detection range and that detection ranges approach zero for sun angles greater than the view angle. The loss of detection range is due to a severe decrease of contrast related to slope variations for sun angles higher than the viewing angle and to the loss of shadows.

Fig. 9 shows the effect of an azimuthal difference between the viewing angle and incidence angle. For low viewing angles, an azimuthal change is beneficial; however, for high viewing angles, an azimuthal change is somewhat detremental. Thus, objects will be more detectable when the viewing angle is low, if one looks to the side of a zero phase washout area.

With regard to the possibility of the sun being in front of the viewer, these data were extended for a complete range of sun angles. Results for a 14° viewing angle are shown is Fig. 10 for sun angles from 5° to 175°. The analysis carried out indicates that the detection range does not reach an appreciable magnitude, after the initial decrease to zero, until an angle of about 150° is reached; i.e., 30° above the horizon in front of LM. However, the values shown for the sun in front do not include the effect of glare, which seriously degrades visibility.

NASA-S-66-6119 JUN

LUNAR REFLECTANCE PROPERTIES

- LUNAR SURFACE ACTS AS A RETRO-REFLECTOR
  - SURFACE BRIGHTNESS DEPENDS ON VIEW & SUN ANGLES
  - LUMINANCE REACHES MAXIMUM AT SUN ANGLE
  - WASHOUT PHENOMENA OCCURS AT ZERO PHASE ANGLE
- ALBEDO VARIATION IS SMALL
  - FROM 0.065 (MARIA) TO 0.13 (BRIGHTEST RAYS)
- CONTRAST DEPENDS ON LOCAL SLOPE VARIATIONS AND SHADOWS
- MEASUREMENTS OF REFLECTANCE PROPERTIES ARE EARTH-BASED AND OF LOW RESOLUTION

Fig. 7

NASA-S-66-6125 JUN

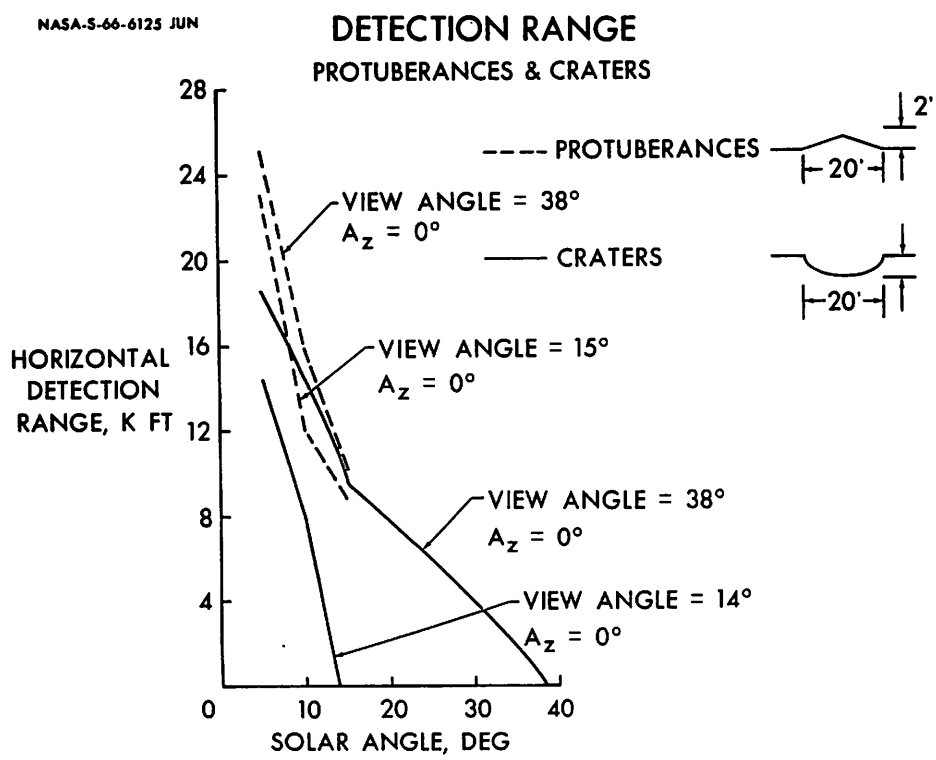

Fig. 8

2.1.3 GLARE AT FORWARD SUN ANGLES

When the sun shines directly in the LM window, a veiling luminance results which obscures the lunar surface (Fig. 11). The main component of the veiling luminance is the scattering at the window due to deposits from the adjacent RCS motor. A smaller component results from scattering in the eye. As can be seen from Fig. 12, the veiling luminance may be five to six times as great as the lunar background luminance. This results in a large reduction in scene contrast and precludes consideration of low forward sun angles.

2.1.4 SHADOWING AND RECOGNITION

Shadows are desirable for the enchancement of object recognition, as well as for detection. The maximum sun angle for shadowing is shown in Fig. 13 for typical crater configurations. The 10:1 diameter to depth ratio configuration is the most typical observed and corresponds to sun angles of 22° or less for shadowing. Sun angles of 22° or less would result in shadowing from at least 60% of the craters.

2.1.5 SHADOWING AT LOW SUN ANGLES

For very low sun angles, a substantial portion of each crater is covered by its shadow and a general decrease in luminance occurs. Acceptable landing areas with a slope of a few degrees could be completely contained within a shadow when the sun is at a low angle. Hence, a lower limit must be placed on the sun angle. This limit is presently set at 7° (Fig. 14).

2.1.6 VISIBILITY RESULTS

The results of the visibility studies insofar as they affect the relationship between the viewing angles and the sun angles are shown in Fig. 15.

2.2 SELECTION OF MAXIMUM SUN ANGLES

The visibility results have established the relationships between viewing angles and sun angles. The results must be related to the LM viewing angle history to arrive at a maximum and minimum sun angle. Fig. 16 shows viewing angle histories as a function of range from the landing site for the lunar descent trajectory developed in an earlier presentation.

The maximum view angle possible is defined by the lower window limit, this angle varies from 25° at high gate to approximately 50° in the vicinity of the landing site. The view angles to the landing site itself are seen to vary from 14° at high gate to approximately 38° in the vicinity of the landing site.

NASA-S-66-6122 JUN

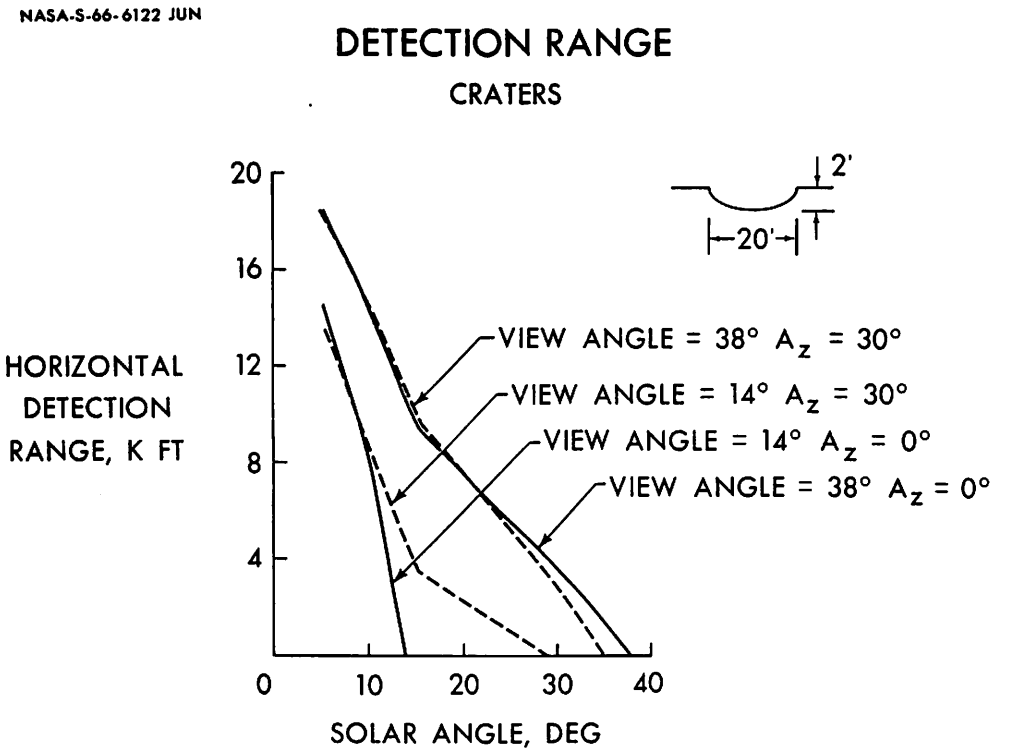

Fig. 9

NASA-S-66-3879 JUN

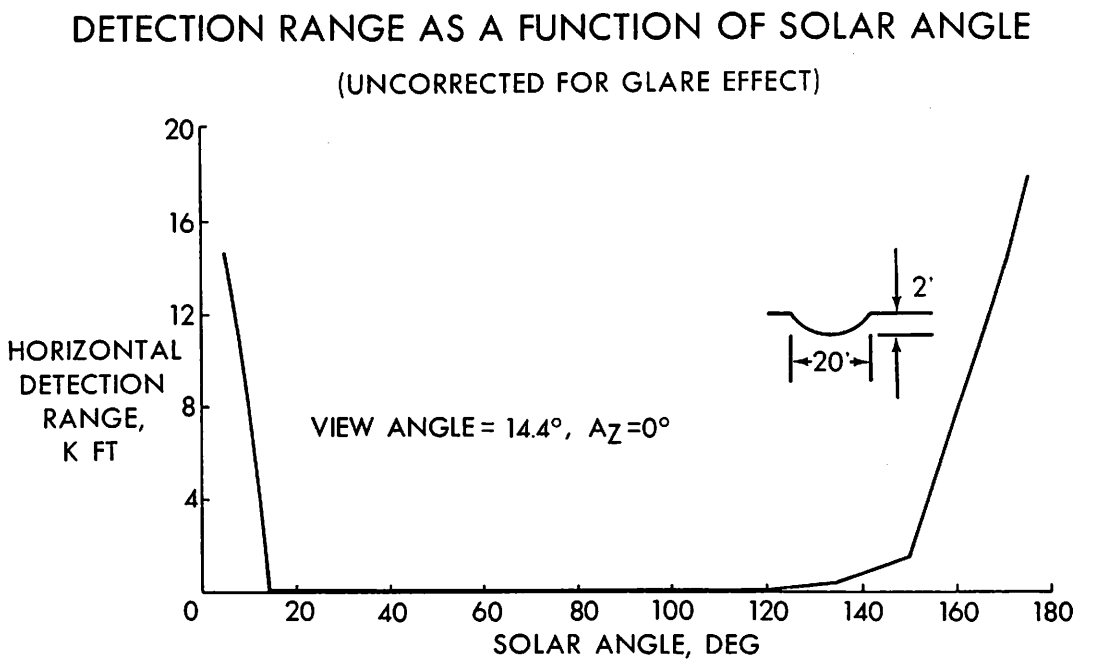

Fig. 10

NASA-S-66-5946 JUL 1

SOURCES OF VEILING LUMINANCE

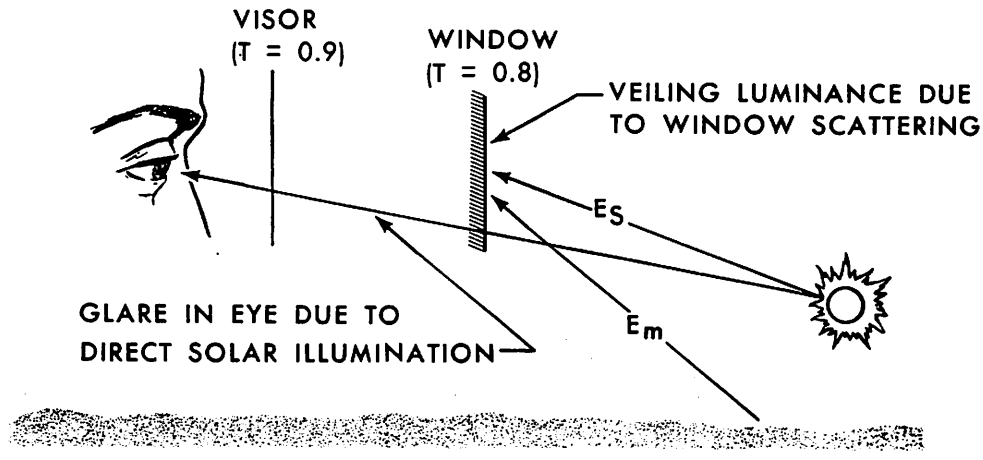

E_S = SOLAR ILLUMINATION ON LM WINDOW
E_m = LUNAR ILLUMINATION ON LM WINDOW

Fig. 11

NASA-S-66-3882 JUN

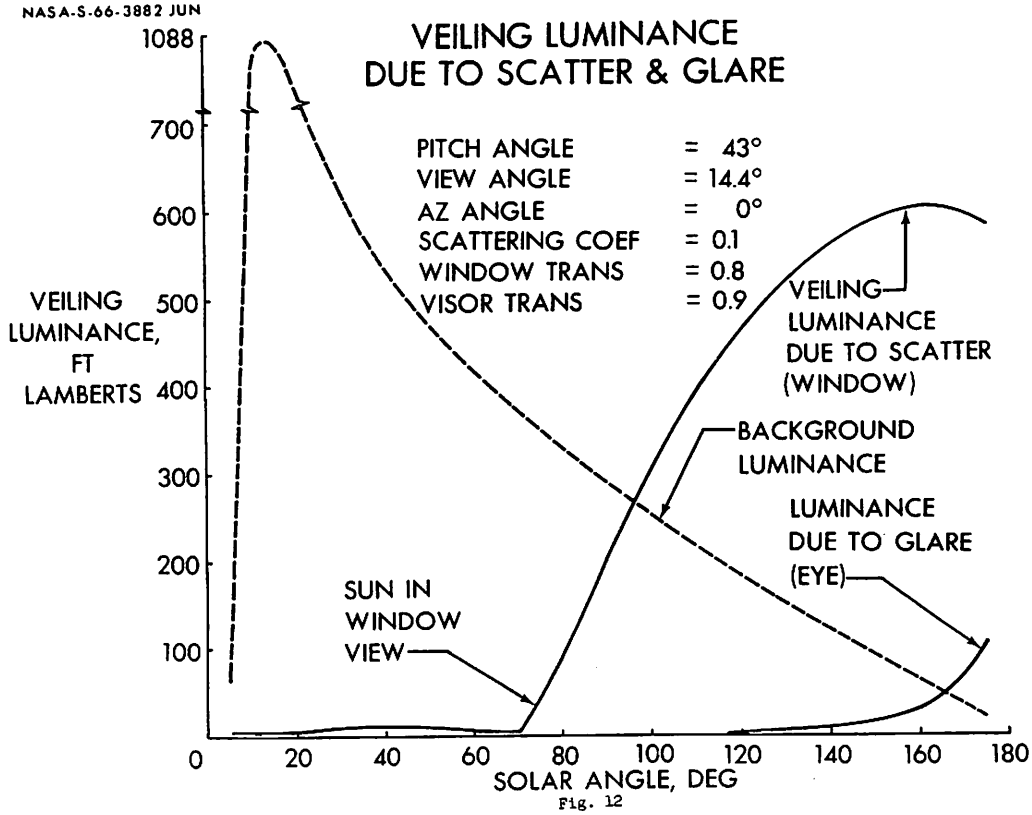

Fig. 12

NASA-S-66-5417 MAY 31

CRATERS

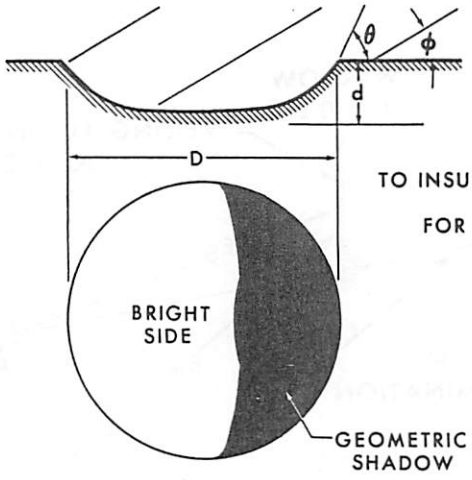

TO INSURE SHADOWS (SPHERICAL SEGMENTS)

FOR $\frac{D}{d} = \frac{12}{1}$, $\theta_{MAX} \approx 18.5° \geq \phi_{MAX} \leq 18.5°$

$\frac{D}{d} = \frac{10}{1}$, $\theta_{MAX} \approx 22.6° \geq \phi_{MAX} \leq 22.6°$

$\frac{D}{d} = \frac{8}{1}$, $\theta_{MAX} \approx 28.6° \geq \phi_{MAX} \leq 28.6°$

ϕ = SUN ANGLE
θ = CRATER SLOPE ANGLE

Fig. 13

NASA-S-66- 6812 JUN

MINIMUM SUN ANGLES

- EXTREME SHADOWING & LOW BRIGHTNESS OCCUR AT SUN ANGLES LESS THAN 5 - 7°
- VARIATIONS FROM EXPECTED SLOPE & TERRAIN MAY RESULT IN ENTIRE AREA COVERED BY SHADOWS

Fig. 14

NASA-S-66-6120 JUN

VISIBILITY RESULTS

- DETECTION RANGE DECREASES RAPIDLY AS SUN ANGLE INCREASES
- AT ZERO AZIMUTH, VIEW ANGLE MUST BE ABOVE SUN ANGLE FOR NON-ZERO DETECTION RANGE
- AZIMUTH CHANGE ON THE ORDER OF 30° IS BENEFICIAL ONLY FOR SUN ANGLES GREATER THAN THE VIEWING ANGLE
- FOR A FIXED SUN ANGLE, AN INCREASE IN VIEW ANGLE IS BENEFICIAL
- GLARE AT LOW SUN ANGLES IN FRONT OF THE LM PRECLUDES THAT CONDITION
- WASHOUT AT ZERO PHASE ANGLE RESULTS IN A DEAD BAND ABOUT THE VIEWING ANGLE

Fig. 15

NASA-S-66-6510 JUN

VIEW ANGLES
VISIBILITY PHASE

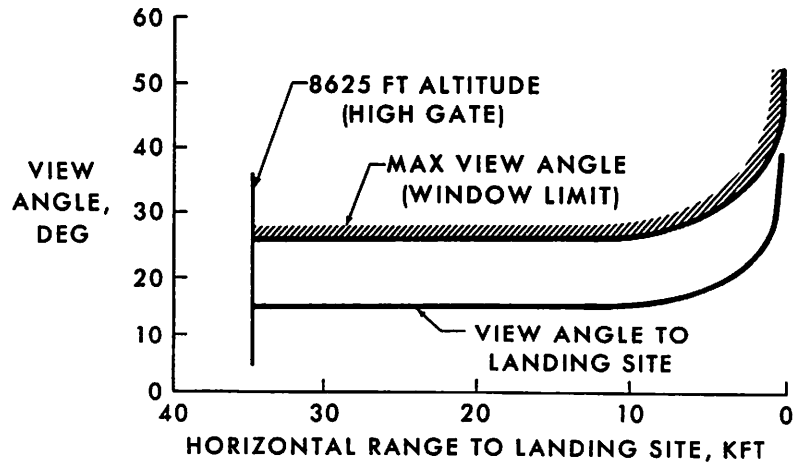

Fig. 16

NASA-S-66-6533 JUN

MAXIMUM SUN ANGLES

VISIBILITY PHASE

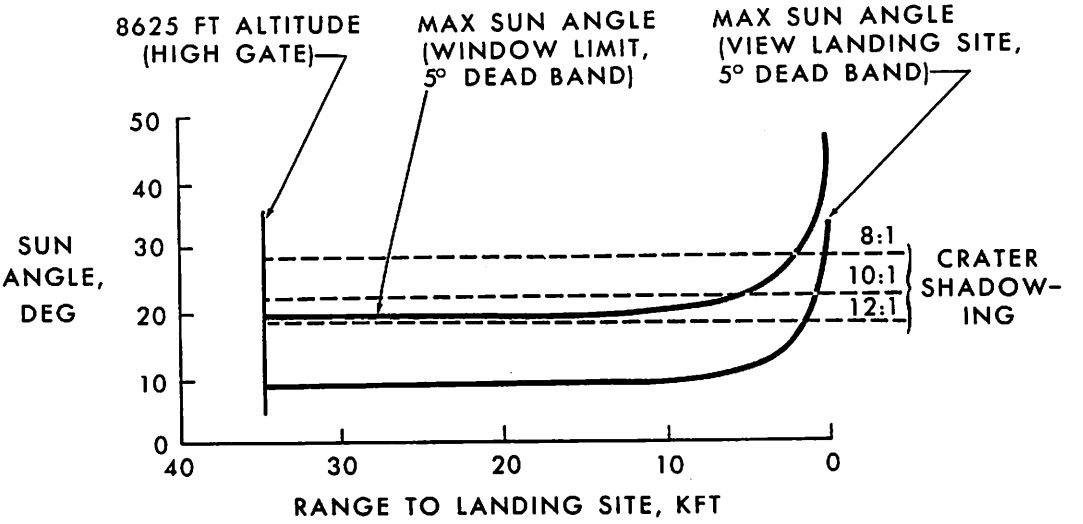

Fig. 17

As discussed earlier, the sun angle must be less than the viewing angle and also when the sun angle and the viewing angle are within a few degrees of being coincident, washout occurs. Thus, the maximum sun angles are taken to be 5° less than the viewing angle to accommodate the detection requirements and to accommodate an assumed 5° washout deadband.

Fig. 17 presents the sun angle histories corresponding to the maximum viewing angles and the view angles to the landing site. Also presented are the maximum sun angles for initiation of crater shadowing. Note that a maximum sun angle of 20° allows continuous viewing of the lunar surface from high gate, with favorable viewing conditions of:

1. View angle at least 5° greater than sun angle.

2. Crater shadows for most craters.

Also, the 20° maximum sun angle provides a view of the landing site under these favorable viewing conditions from a range of at least 1,000 ft., and at the phase in the landing trajectory of greatest importance; i.e., immediately prior to landing. Lower sun angles would increase the range of favorable viewing conditions even more.

For these reasons, a maximum value for the sun angle has been set at 20° and the minimum value set at 7° for the lunar landing site selection criteria. These values will change if newer information so indicate. The study program on which these data are based is not complete. Analysis of simulation studies on detection and recognition and of Surveyor and Orbiter photographs will assist in the evaluation of the current choice of lighting conditions.

2.3 CSM PERFORMANCE

2.3.1 ACCESSIBLE LUNAR REGION

The sun angle range of 7° to 20° will now be considered in conjunction with the CSM performance to establish the accessible lunar region and hence, establish the region which will be considered in the site selection process. The details relating to the CSM performance have been developed in a previous paper.

Fig. 18 shows the accessible lunar landing area when lighting conditions are correct for a typical month (February 1968). The accessible lunar area for the year of 1968 is shown on Fig. 19. Based on these typical data, the latitude boundaries for the lunar area of interest for site selection have been taken to be $\pm 5^{\circ}$.

The longitude boundaries are extablished by tracking and communications considerations. The Eastern boundary is set at 45° longitude to satisfy powered descent requirements. The Western boundary is set -45° longitude to satisfy ascent requirements.

2.3.2 LANDING SITE SPACING

The sun angle range of 7° to 20° results in a one day launch opportunity for a given sity as noted on Fig. 20. This implies that the landing sites must be spaced in a manner which is dependent on the launch philosophy.

A consecutive day launch window will require, for example, separate sites which are spaced in longitude 10 $\pm 2^{\circ}$. For an every-other-day launch philosophy, the sites must be spaced approximately 23 $\pm 3^{\circ}$ in longitude, and so on.

2.4 SUMMARY OF OPERATIONAL CONSIDERATIONS

The operational considerations which make up part of the site selection criteria are summarized in Fig. 21. The key items are the definition of the lunar region which will be considered in the site selection process, the fact that the sun angle range of 7° to 20° results in only a one day launch opportunity per landing site, and that landing sites must be spaced in longitude in a manner which is dependent on the launch philosophy.

3.0 SPACECRAFT/SURFACE INTERACTIONS

The second category of considerations which is included in the site selection criteria is the interaction between LM and the lunar surface. As noted in Fig. 22, the spacecraft/surface interactions apply to the landing approach and the landing.

3.1 LANDING APPROACH CONSIDERATIONS

The landing approach considerations relate to the interactions of the landing radar with the lunar surface. The portion of the descent trajectory where this interaction takes place is discussed below.

3.1.1 LM DESCENT TRAJECTORY

The portion of the descent trajectory where the landing radar interacts with the lunar surface is from initiation of landing radar altitude update to landing. As noted on Figures 23 and 24, this phase of the flight begins when the LM is 30 n.m. uprange of the landing site and at an altitude of approximately 25,000 feet.

NASA-S-66-5179 JUN 13

ACCESSIBLE LUNAR LANDING AREA IN FEB 1968 WHEN THE LIGHTING CONDITIONS ARE CORRECT

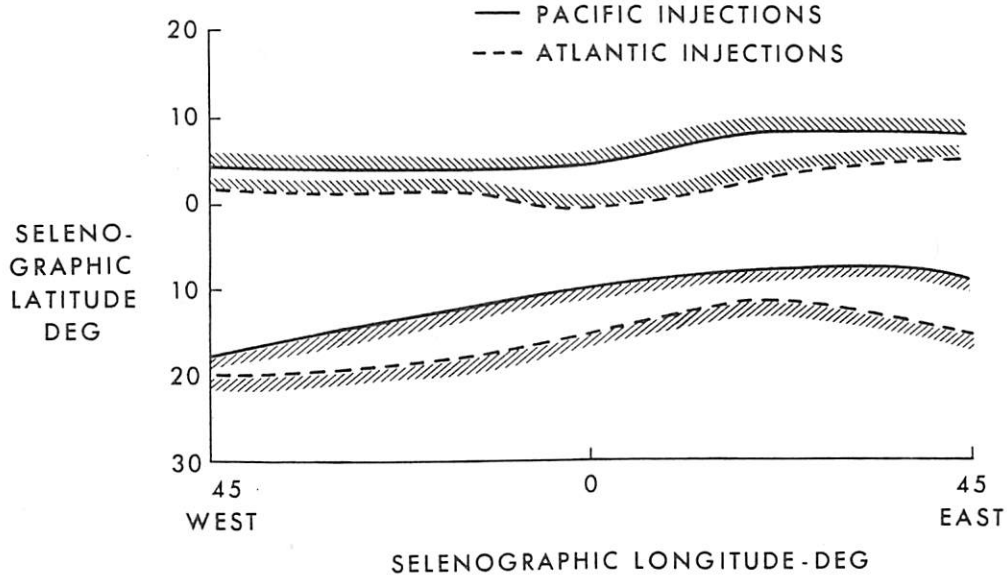

Fig. 18

NASA-S-66-5182 JUN

100% LUNAR SURFACE ACCESSIBILITY FOR 1968

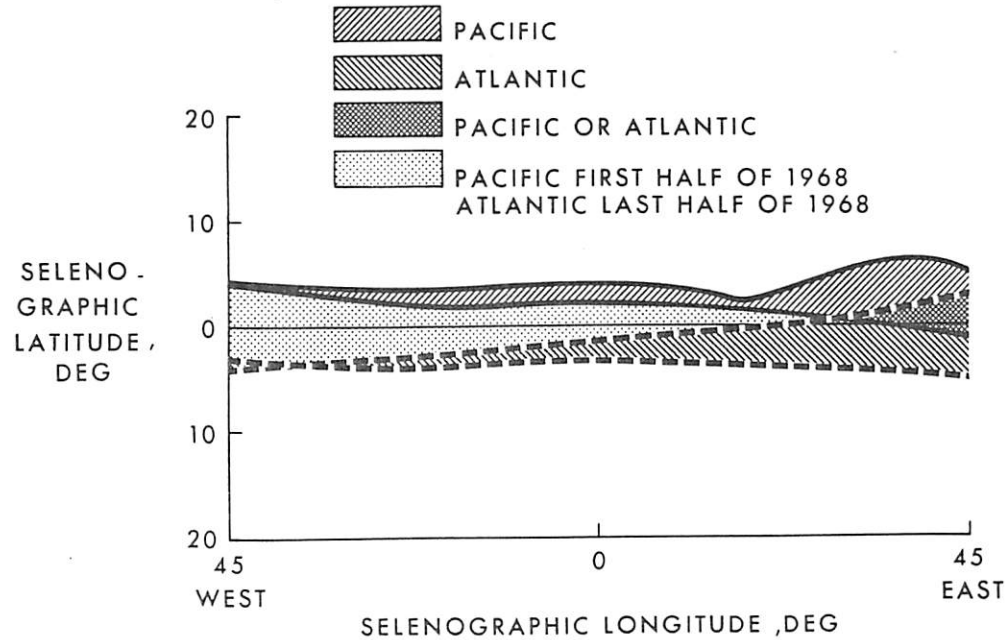

Fig. 19

NASA-S-66-5021 MAY 31

LUNAR LANDING OPPORTUNITIES

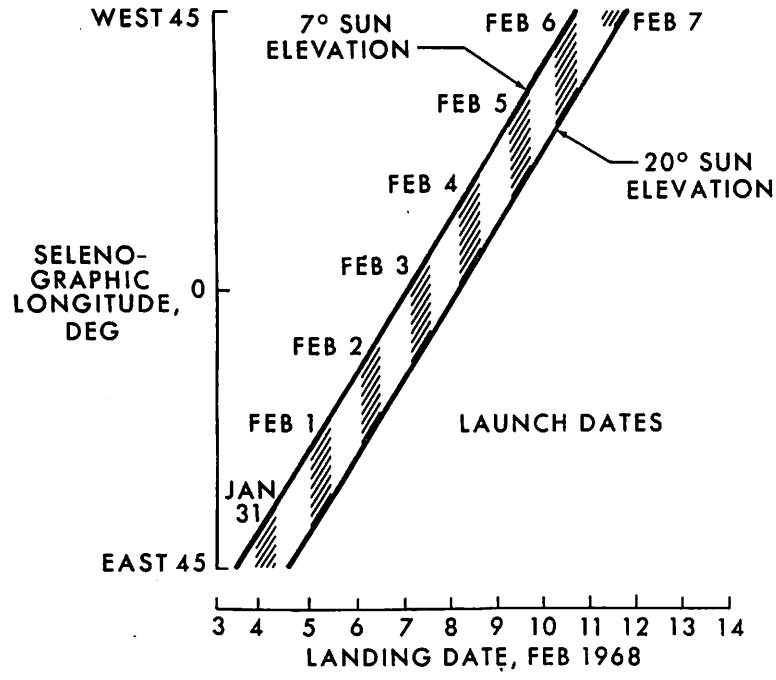

Fig. 20

NASA-S-66-5053 JUNE

SLIDE 21

SUMMARY OF OPERATIONAL CONSIDERATIONS

- DEFINITION OF ACCESSIBLE AREA
  - LONGITUDE: 45° W TO 45° E
  - LATITUDE: 5° N TO 5° S
  - LANDING SITES IN CLUSTERS WITH INDIVIDUAL SITES DISTRIBUTED LONGITUDINALLY WITH A 10° ± 2° OR 23° ± 3° INTERVAL BETWEEN SITES
- LIGHTING CONSIDERATIONS
  - SUN ANGLE IN THE RANGE 7° TO 20°
  - VIEW ANGLE GREATER THAN SUN ANGLE AT RANGE WHERE OBJECT DETECTION AND RECOGNITION CAPABILITY IS REQUIRED

Fig. 21

The use of the landing radar during the last 30 n.m. results in certain restrictions being imposed on the lunar surface in this region. These restrictions are discussed below.

3.1.2 TOPOGRAPHIC RESTRICTIONS IMPOSED BY LANDING RADAR

The restrictions imposed by the landing radar on the approach topography of the lunar surface are presented in Fig. 25. The restrictions are that the mean slope not exceed $\pm 2^{\circ}$ over the last 30 n.m. to touchdown. In addition, the deviation due to local surface effects about the mean slope must be less than or equal to $\pm 5\%$ of the nominal LM attitude. These topographic restrictions must be satisfied throughout an approach path ray which is 30 n.m. long and varies in width from 16,000 feet at the landing site to approximately 8.6 n.m. at a distance of 30 n.m. from the landing site. If the topography of the landing approach ray exceeds the restrictions described, then the commanded attitudes and commanded throttle ratios of LM can become excessive. This can result in excessive LM attitude excursions which would cause the landing radar to loose lock.

The inclination of the landing radar approach ray varies as a function of lunar latitude and longitude in such a manner that the angles η_1 and η_2 noted on the chart, possess the following properties:

$$\eta_1 + \eta_2 = 20^{\circ}$$

$$4^{\circ} \leq \eta_1 \leq 16^{\circ}$$

$$4^{\circ} \leq \eta_2 \leq 16^{\circ}$$

This variation is due to the change in spacecraft orbital inclination as a function of landing site position.

3.2 LANDING CONSIDERATIONS

The landing considerations relate to the size of the landing area and the requirements imposed on the lunar topography and the soil characteristics within the landing area. The requirements on topography and soil characteristics are defined by LM landing dynamics and stability considerations.

3.2.1 LANDING SITE SIZE

The landing area, for site selection purposes, corresponds to the 3-sigma dispersion ellipse of the LM at landing. The

NASA-S-66-6118 JUN

SPACECRAFT/SURFACE INTERACTION

- APPROACH CONSIDERATIONS
- LANDING CONSIDERATIONS

Fig. 22

NASA-S-66-5418 MAY 31

LM POWERED DESCENT

ENGINE IGNITION
h=50,000 FT
θ=86°
T=0 SEC
V=5500 FT/SEC
γ=0°

MAXIMUM THROTTLE
h=50,000 FT
θ=88°
T=28 SEC
V=5564 FT/SEC
γ=−.2°

TARGET SWITCHOVER
h=43,000 FT
θ=80°
T=228 SEC
V=3385
γ=−1.4°

LR ALTITUDE UPDATE
h=25,000 FT
θ=71°
T=328 SEC
V=2164 FT/SEC
γ=−4.0°

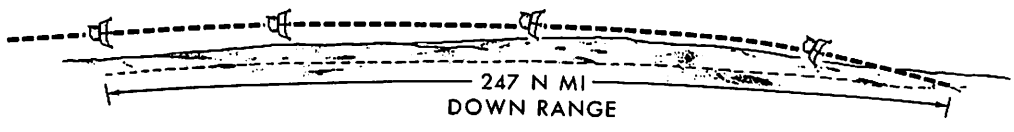

Fig. 23

NASA-S-66-5414 MAY 31

LM POWERED DESCENT (CONT)

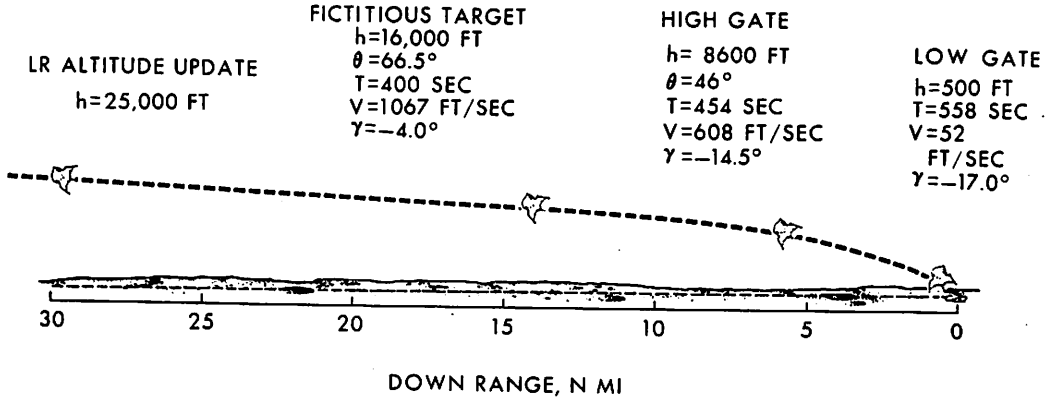

Fig. 24

NASA-S-66-5233 JUN

LM APPROACH RAY

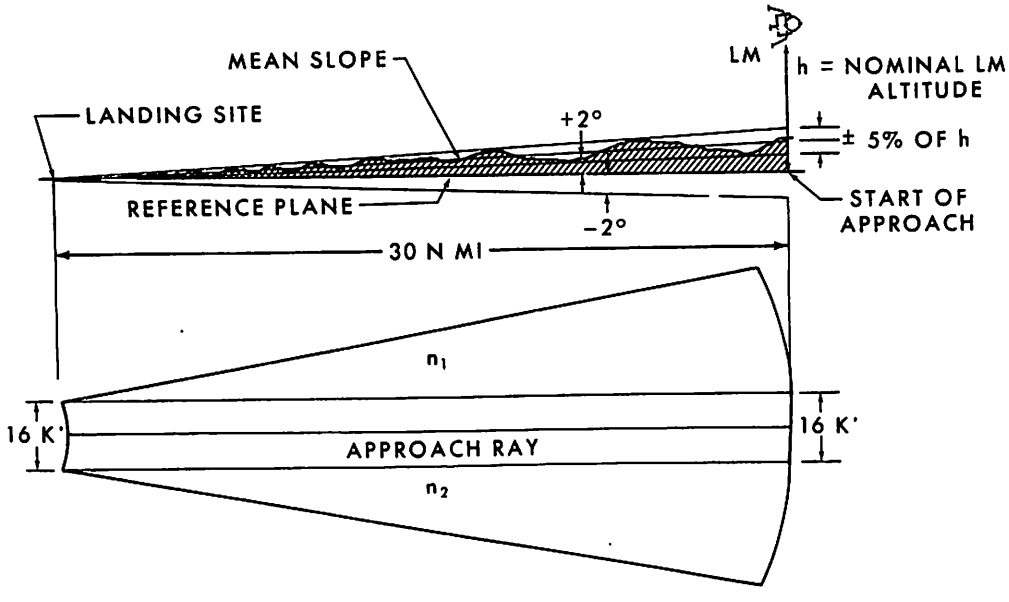

Fig. 25

dimensions of the landing dispersion ellipse were developed in a previous paper and are repeated on Fig. 26. As noted, the landing area has a major axis of 52,000 feet and a minor axis of 10,800 feet.

This landing dispersion ellipse is based on MSFN tracking for three orbits and does not include site location uncertainties. This ellipse corresponds to the guidance philosophy which allows range to be a free parameter.

3.2.2 LANDING SITE RESTRICTIONS IMPOSED BY LANDING DYNAMICS/STABILITY CONSIDERATIONS

The characteristics of the lunar topography and the soil within the landing area (3-sigma dispersion ellipse) are defined by landing dynamics and landing stability considerations. A previous paper described the studies carried out by MSC in this area and established surface requirements.

The results of the analysis previously described indicated that the maximum allowable penetration of the lunar surface by LM is approximately 44 inches. Based upon this value, it has been determined that for a surface with 24 inch deep holes the surface slope must not exceed 7°. The corresponding static bearing stress must be greater than 8 psi or equivalently, the bearing stress must be greater than 5 psi per foot of penetration. For a surface devoid of holes, the surface slope must not exceed 13 degrees and the bearing stress must be greater than 4 psi. In addition, the soil coefficient of friction must be ≤ 0.4 to prevent excessive sliding.

Fig. 27 summarizes these slope and soil requirements.

4.0 SITE SELECTION CRITERIA

The site selection criteria is summarized on Figures 28 and 29. This criteria consists of all the operational considerations and spacecraft/surface considerations discussed herein. This criteria represents the most realistic requirements as presently understood and will be updated as the requirements change.

As stated in the Introduction, the site selection criteria will be used in conjunction with the available lunar surface data to provide the mechanism for selecting candidate landing sites.

The next discussion entitled, "Site Selection Data Sources and Interpretation" will elaborate on the lunar surface data and how it will be used for selecting candidate landing sites.

NASA-S-66-5945 JUL

LANDING SITE SIZE

3-SIGMA LANDING DISPERSION ELLIPSE

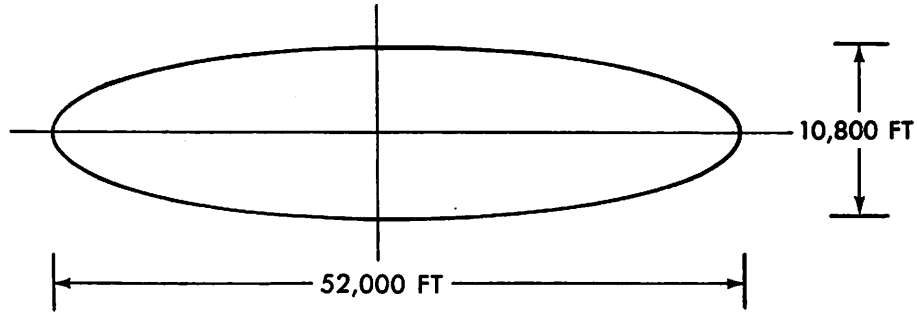

- RANGE FREE
- MSFN ONLY - 3 ORBITS
- NO SITE UNCERTAINTIES

Fig. 26

NASA-S-66-6864 JUNE

LANDING DYNAMICS/STABILITY CONSIDERATIONS

TO PRECLUDE EXCEEDING MAXIMUM ALLOWABLE SURFACE PENETRATION OF 44 INCHES

- FOR SURFACE WITH 24 INCH DEEP HOLES
  - SURFACE SLOPE MUST BE ≤ 7 DEGREES
  - SOIL BEARING STRESS MUST BE:
    1. ≥ 8 PSI (CONSTANT) OR
    2. ≥ 5 PSI PER FOOT OF PENETRATION
- FOR SURFACE DEVOID OF HOLES
  - SURFACE SLOPE MUST BE ≤ 13 DEGREES
  - SOIL BEARING STRESS MUST BE ≥ 4 PSI (CONSTANT)

TO PREVENT EXCESSIVE SLIDING, SOIL COEFFICIENT OF FRICTION MUST BE ≥ 0.4

Fig. 27

NASA-S-66-6811 JUN

SITE SELECTION CRITERIA

DEFINITION OF ACCESSIBLE AREA

- LONGITUDE: 45° W TO 45° E
- LATITUDE: 5° N TO 5° S
- LANDING SITES IN CLUSTERS WITH INDIVIDUAL SITES DISTRIBUTED LONGITUDINALLY WITH A 10° ± 2° OR 23° ± 3° INTERVAL BETWEEN SITES

LIGHTING CONSIDERATIONS

- SUN ANGLE IN THE RANGE 7° TO 20°
- VIEW ANGLE GREATER THAN SUN ANGLE AT RANGE WHERE OBJECT DETECTION & RECOGNITION CAPABILITY IS REQUIRED

Fig. 28

NASA-S-66-5404 MAY 31

SITE SELECTION CRITERIA (CONT)

TOPOGRAPHY

- LANDING RADAR AND GUIDANCE CONSIDERATIONS
  - MEAN SLOPE OF ≤ ±2° OVER LAST 30 N MI
  - LOCAL TERRAIN DEVIATIONS (ABOUT MEAN SLOPE) ≤ ±5% OF NOMINAL LM ALTITUDE
  - APPROACH RAY: 16,000 FT WIDE AND INCLINATION VARIES AS A FUNCTION OF LONGITUDE AND LATITUDE
- LANDING ELLIPSE GEOMETRY
  - BASED ON MSFN WITH NO SIGHTINGS, THE 3σ DISPERSION ELLIPSE DIMENSIONS ARE: 52 K FT BY 10.8 K FT WITH RANGE FREE
- LM STABILITY
  - WITH HIGH CONFIDENCE, 95% OF THE POSSIBLE RANDOM LM LANDINGS ON THE TOPOGRAPHIC SURFACE WITHIN THE 3σ DISPERSION ELLIPSE CAUSE THE LM TO TILT ≤7° WITH RESPECT TO THE LOCAL VERTICAL. THE REGION SHALL ALLOW AVOIDANCE OF BOTTOMING HAZARDS DUE TO PROTUBERANCES > 24'' IN HEIGHT

SOIL MECHANICS

- COEFFICIENT OF FRICTION: ≥0.4
- SOIL BEARING STRENGTH ≥8 PSI TO PRECLUDE LM SINKAGE OF >44 INCHES

Fig. 29

Questions and Comments

SITE SELECTION CRITERIA

Speaker: A. V. Bernard

1. Comment by Mr. Milwitzky - Although the photometric function (as reviewed in this presentation) indicates that a certain range of sun angle is highly desirable (and the Surveyor data generally confirm this), the Surveyor data have shown that the degradation of visibility is not as bad at the higher sun angles as was indicated in the presentation. Further study will be made on this subject; however, there is no question that the low sun angle is best.

2. Dr. Shoemaker - What were the main contributors to scattering, the window or the helmet? How were the scattering data established?

   ANSWER - Only the window scattering was considered, not the helmet. A rather pessimistic scattering coefficient was used, assuming that the RCS had left deposits on the LM window. The scattering coefficient assumed was 0.1.

3. E. Stern - Why does the landing radar limit the acceptable slope to 2 degrees?

   ANSWER - The consideration is one of excursions in LM attitude. As the slope and the local deviations exceed those presented in the criteria, it would probably result in excessive attitude rates or excursions from the nominal attitude.

4. How did the assumption for the window degradation compare with the experience in Gemini?

   ANSWER - The GT-9 flight crew observed that particles from the RCS from the other vehicle came back and impacted the windows like raindrops. The actual numerical value for the degradation is not known at this time.

5. Comment by Dr. Von Braun - The shadow of the LM with the sun behind it could be used as an aid to the crew in surface contour identification, for general observations, and for use as an altimeter during the final landing phase.

   ANSWER (O. Maynard) - Mr. Loftus has been looking into the potential value of the shadow as an aid to the crew. A cursory review of the analysis to date indicates that the shadow is not of much use to the pilot for assessment of the terrain contour or altitude until the last portion of the descent at which time there are some useful altitude cues. The study will be available early in August. We do plan to perform flight tests which seem promising and use the phenomenon if appropriate.

LUNAR LANDING SITE DATA SOURCES AND ANALYSIS

by

John E. Dornbach

LUNAR LANDING SITE DATA SOURCES AND ANALYSIS

1.0 INTRODUCTION

Information from earth-based studies and from Surveyor and Luna spacecraft indicates that Apollo landing sites can be found within areas to be photographed by Lunar Orbiter. Analysis of lunar data in relation to Apollo Spacecraft and operational constraints has shown that favorable sites can be located, so as to provide for maximum mission flexibility. The favorable areas are generally clustered around 30° East longitude, near 0°, and 35° West longitude.

This portion of the program will concentrate on lunar surface data as gathered from Earth or from unmanned spacecraft and how it is being used in the Apollo landing site analysis program at MSC.

2.0 EARTH-BASED STUDIES

FIGURE 1 - LAC 1:1,000,000 SCALE COVERAGE

At the present time most of the visible face of the Moon has been mapped for the NASA by the U.S. Air Force Aeronautical Chart and Information Center. These charts at sixteen miles to the inch are about the same scale as the best you could get today for covering parts of Antarctica, Australia, and Africa. By carefully measuring on observatory photographs, the lengths of shadows cast by craters at low sun angles, we are able to estimate one thousand foot contours on the lunar surface. This slide illustrates that at this scale charts of the lunar equitorial region, or the region of interest for early Apollo missions, have already been completed. The area covered by one of these charts is shown by the outline of the Kepler chart.

FIGURE 2 - USGS PHOTOGEOLOGICAL MAP

At the present time professional geologists of the U.S. Geological Survey are using the Air Force charts as base maps on which they are plotting terrain and stratigraphic relationships. These geologists headquartered at the USGS Center of Astrogeology in Flagstaff, Arizona, spend many hours at the telescope to provide such maps as this one of the region surrounding the crater, Kepler. The various colors indicate materials such as mare, ray, impact ejecta, and volcanic. The Apollo area of interest has already been geologically mapped at this scale.

FIGURE 3 - AIC 1:500,000 SCALE COVERAGE

Within the past year, the Air Force Chart Center has also been asked by the NASA to produce charts at a scale of eight miles to the inch concentrating on the equatorial area of immediate Apollo interest. These charts carry the maximum amount of information that can be gained visually or photographically through the finest earth-based observatory telescopes. They are concentrating their viewing efforts in detailing the flatter mare areas, where landing sites may most probably be found. These charts are keyed to the 1:1,000,000 scale series as may be seen on the Kepler sheet.

FIGURE 4 - THERMAL ANOMALIES

The cartographers and geologists have mapped from Earth, how the Moon varies from place to place in the visible spectrum. As the wavelength of instrumental observation is increased into the infrared, we see that around 10 microns wavelength, the Moon begins to demonstrate anomalous characteristics. This slide by Shorthill and Saari illustrates that during an eclipse, as the source of energy - the sun - is quickly removed, certain portions of the lunar surface retain heat longer than others. From this we might infer that the areas retaining heat are rocky or covered by more dense material, whereas those which quickly cool could be covered with a less dense or highly insulating material.

FIGURE 5 - RADAR MAPPING

The NASA is also conducting studies with the Lincoln Laboratories of Massachusetts Institute of Technology in another portion of the spectrum. By examining the Moon in the centimeter and meter radar wavelength regions it should also be possible to infer differences from place to place as small as several square miles. From an analysis of the returned signals, scientists expect to learn something of the density of materials making up the upper lunar matle and the average roughness of the surface from place to place. By combining all data gathered from Earth with knowledge gained from discrete samples from Surveyor and Luna, we feel confident that satisfactory landing sites can be located on the Orbiter photography.

FIGURE 6 - APOLLO ZONE OF INTEREST

The Apollo Area of interest has been defined as forty-five degrees East to forty-five degrees West longitude and from five

degrees North to five degrees South latitude. NASA has already photographically explored part of this region as a result of the Ranger Project and soon the unmanned Orbiter A spacecraft will supply detailed photographic information for Apollo landing site selection. The surface has been photographed at two locations - by Surveyor I and Luna IX, but only Surveyor was in the Apollo Zone of Interest. Data from Surveyor has indicated that the soil bearing strength would be acceptable for the Lunar Module in this area. Future Surveyors will sample some of the other areas indicated by circles on this chart.

3.0 RANGER DATA ANALYSIS

FIGURES 7 AND 8 - RANGER IX AND LUNAR SLOPES AT LM SCALE

The highest resolution photographs taken during the Ranger flights came from Ranger IX. The last few P frames as seen on this figure provided surface resolution less than one foot. MSC has conducted a computer analysis of photometrically derived slopes on these photographs. Data from these programs indicates that more than 90 percent of the slopes within the area of the last few photographs were less than 10°. It was only on those photographs where the large two hundred foot crater was located, that a cumulative slope frequency diagram would indicate a potential problem in landing. With the astronauts performing the lunar landing, a crater such as this could easily be avoided.

FIGURES 9 AND 10 - RANGER VIII APOLLO SITE ANALYSIS AND LM LANDABILITY

These two slides illustrate how our computer analysis of lunar photography is being used to determine Lunar Module topographic landability. The Jet Propulsion Laboratory has provided a magnetic tape containing the digital information as received from Ranger VIII and a computer program to remove extraneous noise from the photography and to rectify each image. On this figure, the photo on the left illustrates a composite map of slope and protuberance values derived from the photograph.

The graphs on figure 10 were computed from the Ranger VIII photography and illustrate numerically that which is shown on the map on the previous figure. We can see that from our analysis of this photograph, the Lunar Module would have encountered slopes of more than six degrees over only twenty-five percent of the area and protuberances of more than two feet over less than five percent of the area.

FIGURES 11 AND 12 - RANGER IX PHOTOGRAPH OF FLOOR OF ALPHONSUS AND GEOLOGICAL MAP

This photograph and map cover an area of about 20 x 30 km (about 240 sq. miles) on the north-east floor of the crater Alphonsus. Very evident on the photograph are geologic features such as young craters, old or worn-down craters, rilles, chain craters, and others. As our knowledge of the lunar surface improves, we will be able to draw much more detailed maps. The geological map was prepared by the USGS and is included in the JPL report on Rangers VIII and IX. We anticipate that as a result of Surveyor and Orbiter, much more detailed and precise geologic maps will be prepared for use in Apollo landing site analysis. Large scale geologic maps will also aid in mission planning and in lunar surface exploration.

FIGURE 13 - KUIPER BEARING STRENGTH ANALYSIS

By formulating concepts for the evolution and morphology of features seen on the Ranger photographs, it is possible to estimate some physical properties. Dr. Gerard Kuiper of the University of Arizona and Principal Investigator for Ranger photography established several basic assumptions and from them, estimated the bearing strength of the cratered surface. He examined many protuberances, indicated on this Ranger IX photograph by small arrows, and surmised that they were materials ejected from the 150 ft. primary crater at the top of the photo. The materials measured at the 10° sun angle appeared to be about 3 feet across and about a foot high. Assuming they were ejected from the primary crater to where they are found and that their bulk density was about 2, he concluded that most of the protuberances were probably half squashed and half buried. From this he concluded the bearing strength to be over 14 pounds per square inch averaged for the upper one to two feet of this part of the lunar surface.

4.0 LUNAR SURFACE DATA

A. LUNA IX

FIGURES 14 AND 15 - LUNA IX PANORAMIC SKETCH AND ANALYSIS OF CLOSE-UP PHOTOGRAPHY

The soft landing on the lunar surface by Luna IX provided the first substantive information that a man-made vehicle could

land, transmit information to Earth, and not slowly sink into a morass of dust. In fact, the spacecraft and optical surfaces showed a remarkable absence of fine particles or dust. This sketch is a composite of much of the information which has been interpreted from analysis of the photography. By locating conjugate images on two mirrors and a direct photo image, we were able to determine the distance to the materials photographed. From this distance we could determine that the size of particles 3 to 5 feet from the spacecraft were about 2/10" in size. The larger objects are 10" - 12". The crater on the left horizon is approximately 50 feet in diameter.

I have included this figure to illustrate some of the problems we encounter when working with photography taken close to the surface. We assume the Luna IX spacecraft camera to have been only about 22 inches or less above the lunar surface. Due to the small mirror base of about 12", reliable measurements are limited to a distance between about 3 to 20 feet.

The Surveyor TV camera provided photographs from about five and a half feet above the lunar surface. Also, a more precise knowledge of the Surveyor spacecraft, landing dynamics, camera calibration, and orientation, should provide much more quantative information than Luna IX.

In this Luna photograph we have indicated the location of the mirror images and some of the scaling measurements we have made.

B. SURVEYOR I

FIGURES 16 AND 17 - SURVEYOR I SPACECRAFT SHADOW

The mosaic figure illustrates lunar lighting conditions with a 10° sun angle looking toward the 0° phase angle point (directly along the sun line, away from the sun). The spacecraft shadow is about 35' long. The detailed texture of the lunar surface is evident below the camera shadow and to each side.

The side-angle view of the camera shadow taken at about the same sun angle covers a 25° field of view. It may be noted that even from the Surveyor camera height of about 5.5 feet above the lunar surface, there is a very strong back-scattering of light above and around 5° below and on either side of the camera shadow. As discussed by previous speakers, this factor is being considered in the mission planning for Apollo by utilizing sun angles below the viewing angle. This would be the region covered by the spacecraft below the top of the camera.

FIGURE 18 - SURVEYOR I FOOT-PAD PHOTOGRAPH

This is the computer enhanced photograph of Footpad 2 released by JPL at the June 16 press conference in Washington, D.C. It clearly shows the honeycomb structure of the pad and lunar surface materials in the millimeter size range (.04 inches). On the basis of photographs such as this and other touchdown dynamics measurements, JPL scientists and investigators have estimated that the upper surface materials have a static bearing strength of 5 pounds per square inch at a penetration depth of one inch.

FIGURES 19 AND 20 - SURVEYOR I PANORAMAS - 20° AND 10° SUN ANGLES

These two panoramas are looking to the south of the Surveyor spacecraft as the sun was setting in the West. Figure 19 was made with the sun approximately 20° above the horizon. On figure 20, the sun was about 10° or less than twenty-four hours before sunset. These panoramas illustrate dramatically how visible detail on the lunar surface is directly related to the sun angle.

The large crater just beyond the rock in the left foreground is about 35 feet from the spacecraft, and has been estimated to be about ten feet in diameter and 1 to 2 feet deep. Even at the 20° sun angle, it is difficult to locate this crater. At higher sun angles it would become even more difficult.

The 10° sun angle mosiac shows a pock-marked surface composed of fragmented materials, with the majority being much less than one-sixteenth inch in size. This type of surface has been postulated by many scientists working on NASA programs. In investigating surface and sub-surface explosions on Earth, scientists of the USGS and Ames Research Center found a direct relationship to the cohesion of the material and the type of crater formed. In cohesive material such as basalt they would expect a rocky ejecta with no apparent lip or rim. In loosely cohesive material they would expect little apparent ejecta, but a well-formed and raised lip. JPL investigators have surmised that the 10 foot crater was in loosely cohesive material, whereas the much larger crater in the center of the mosaic is deep enough to have reached a more cohesive or rocky layer.

MOVIE - MARE CARBORUNDUM (AMES RESEARCH CENTER)

Researchers at the NASA Ames Research Center and USGS - Menlo Park have studied high and low velocity impacts in their laboratory through use of special light gas guns and other devices. By relating their results to primary and secondary craters formed by atomic and explosive projectile explosions at various test grounds; Gault, Moore, and others have deduced that the principal small-scale crater forming process on the Ranger photographs resulted from primary and secondary cratering in loosely cohesive materials. The following short movie called Mare Carborundum by Don Gault illustrates how much of the surface layer of the lunar landscape could have been formed by low velocity secondary impacts in loosely cohesive material such as dry sand.

Other than the possibility of using a wider range of projectile sizes, Gault believes this simulation to be characteristic of the major process responsible for the particulate material making up the upper few feet of surface as seen on the Surveyor photographs.

5.0 ORBITER MISSIONS AND DATA ANALYSIS PROCEDURES

FIGURE 21 - ORBITER MISSION A AND B

From an altitude of about 30 miles, the Orbiter will photograph areas about 22 x 56 miles in 8 meter resolution and 10 x 38 miles in 1 meter resolution on each photographic orbit. The A mission has ten photographic sites and the B mission has eleven. On the A mission Sites 2, 4, and 6 are in upland areas and the remaining in mare terrain. On the B mission, Sites 4 and 5 are in upland areas, Sites 7 and 9 are mixed, and the remainder generally in mare terrain. The low resolution photos will provide for stereoscopic analysis. Monoscopic or photometric slope analysis will be performed on the high resolution photos.

It may be noted that two consecutive passes will be used on Mission A in order to insure that the area in which Surveyor landed will be included in the photographs. Langley Research Center, Lunar Orbiter Project Office, has stated that the two consecutive passes may provide side-lap stereo on the high resolution photography of the landed Surveyor I.

FIGURE 22 - DETERMINATION OF POTENTIAL AREAS OF LANDING INTEREST

Due to the large amount of photographs to be returned from each Orbiter mission (about 2,000, 9" x 14" photos) it will be necessary to concentrate the search for acceptable landing sites in areas most accessible according to operational mission and spacecraft constraints. We have initiated a program to analyze each Orbiter Site utilizing as much data as we have available at this time. This chart shows that based on application of current landing site selection criteria certain portions of the Orbiter areas may not be available for use, regardless of the detailed topographic or geologic data obtained from the Orbiter photography.

FIGURE 23 - ORBITER A MISSION - SITE NO.5 AND SLOPES AND CRATERS

This site near the center of the visible side of the Moon will be used as a sample to illustrate some of our current data analysis procedures. The base map illustrates all of the surface topographic detail which can be seen through telescopic observation from Earth. The areas shaded on the base chart illustrate those slopes too steep to be acceptable for landing or those craters several thousand feet or more across which would not be acceptable as a touchdown point.

FIGURE 24 - ORBITER A MISSION - SITE NO.5 - ACCEPTABLE AREA FOR

LANDING ELLIPSE

This figure shows areas rejected on the previous figure and the area remaining which could be reached when using a 30 mile radar approach path which did not exceed the site selection criteria by passing over a large crater or steep slope. We have also concluded that to provide the best slope data along the landing radar descent path, the entire approach should be included within the area of low resolution Orbiter photography.

In using the 5.3 x 18.5 kilometer (3 x 11 mile) 3δ landing dispersion ellipse, it is evident that only one landing area can be found in which there are only topographic features below the resolution which can be seen from Earth. If we were to use a 20 mile approach path, there would be five available ellipses of this size and with a ten mile approach path the number increases to eight. If the landing ellipse size were reduced to 3 x 7 kilometers (2 x 4 miles) there would be 24 available landing sites

with a ten mile radar approach path in Orbiter Site 5.

FIGURE 25 - ORBITER A MISSION - SITE NO.5 TERRAIN FEATURES

This figure illustrates geologic data prepared by the USGS for the Orbiter Sites. Most of the area is covered by what is considered "undifferentiated mare". This is similar to the type of terrain in which Surveyor I landed. In our analysis of areas available for LM landings, we did not attempt to classify areas topographically or geologically at the scale of the LM landing gear. This information can only be supplied after receipt of the Orbiter photos and after the USGS extrapolates geological information from Surveyor on to the Orbiter photography at the scale of the LM landing gear.

If at this time we consider the ridges, domes, rilles, and escarpments (indicated by the Roman Numeral IV) to be unacceptable within the landing ellipse, it would be necessary to reduce the radar approach path to 10 or 20 miles to get within the large IA (undifferentiated Mare) areas between 0° and 2° W. longitude.

FIGURES 26 AND 27 - PARAMETRIC ANALYSIS OF ORBITER A AND B SITES

These figures illustrate that on the basis of today's knowledge of the Orbiter sites, favorable Apollo landing sites may be found on most of the mare locations, even by taking the most conservative operational approach.

If the lunar surface proves to be exceedingly rough or very heterogeneous insofar as physical properties are concerned, it may be necessary to alter operational plans to reduce the size of the landing ellipse or the length of the radar approach path. Many more sites are available for analysis by utilizing the small landing ellipse and the ten mile radar approach path.

FIGURES 28 AND 29 - RANKING OF MORE FAVORABLE ORBITER SITES AND

CLUSTERED LOCATION IN APOLLO ZONE OF INTEREST

These figures illustrate the Orbiter Sites from Missions A and B which possess favorable areas for Apollo landing site analysis. As a result of application of operational site selection criteria and the changes resulting from month to month due simply to celestial motions, it is fortuitous that by selecting alternate days for three launch opportunities, favorably clustered sites are

located at about 30° East longitude, near the 0° meridian, and about 35° West longitude.

6.0 SOURCES OF DATA FOR LANDING SITE SELECTION

FIGURE 30

Other NASA Centers, the USGS, DoD Mapping Agencies, JPL and Surveyor Scientific Evaluation Teams, and MSC will participate in providing data for the selection of candidate Apollo landing sites for the first and subsequent lunar missions. The final selection of the lunar sites to be used for each Apollo mission will be made by the Associate Administrator for Manned Space Flight from the recommendations of the Apollo Site Selection Board, chaired by Major General Samuel Phillips, Office of Manned Spaceflight.

Questions and Answers

SITE SELECTION DATA SOURCES AND INTERPRETATION

Speaker: John E. Dornbach

1. Why was site A5 used in the discussion?

   ANSWER - It was purely an example.

2. Comment from Audience: The Orbiter sidelap percentages are quite small, and it would be difficult to include a Surveyor site in stereo coverage.

   Comment from Mr. Dornbach: It is our understanding that Orbiter will have a larger sidelap than the normal 5%. This could be done by tilting the spacecraft; however, the actual method to be used is not known.

3. Were there filters on the Surveyor and could the details [of the surface features] be increased by the use of these filters?

   ANSWER - There were filters, but their purpose was for colorimetry. Since the lunar surface is basically grey, the filters had little effect on the imagery received.

4. Has any consideration been given to observing the LM landing by another spacecraft in orbit, such as Lunar Orbiter?

   ANSWER (Dr. Shea) - The answer is basically "no", primarily because it would represent an extra constraint [to get into phase with some other spacecraft which was already in lunar orbit] out of which one would expect to get very little additional real value to the program.

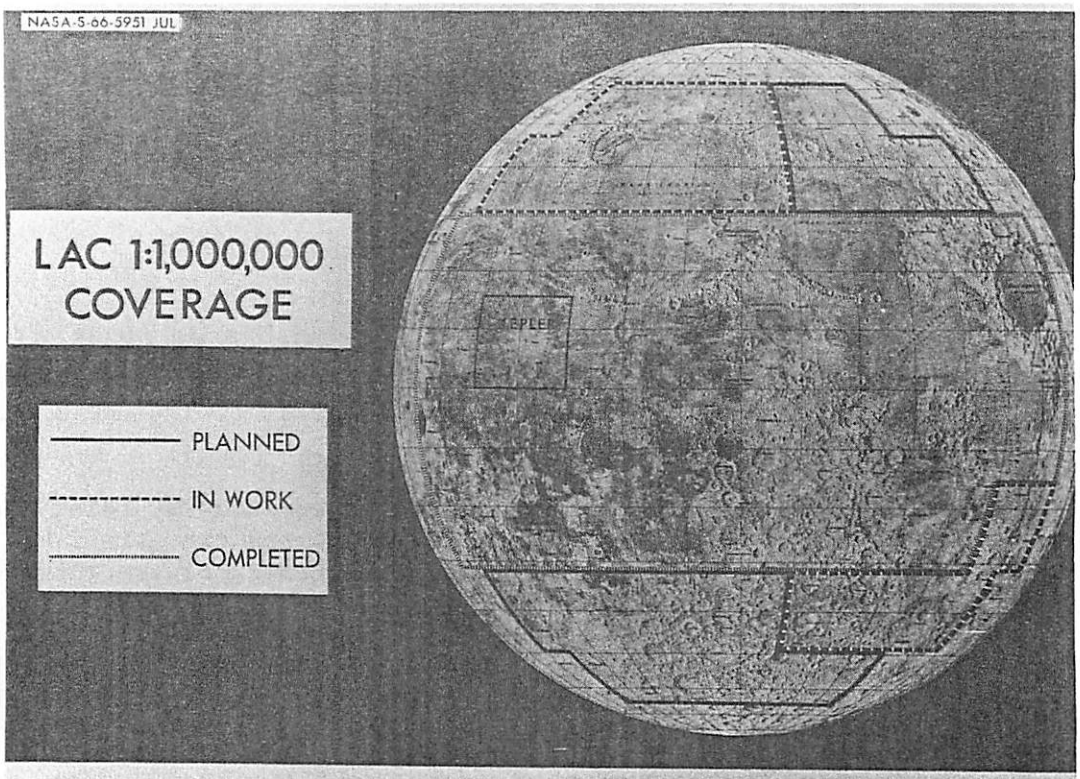
NASA-S-66-5951 JUL
LAC 1:1,000,000
COVERAGE
PLANNED
IN WORK
COMPLETED
KEPLER

Fig. 1

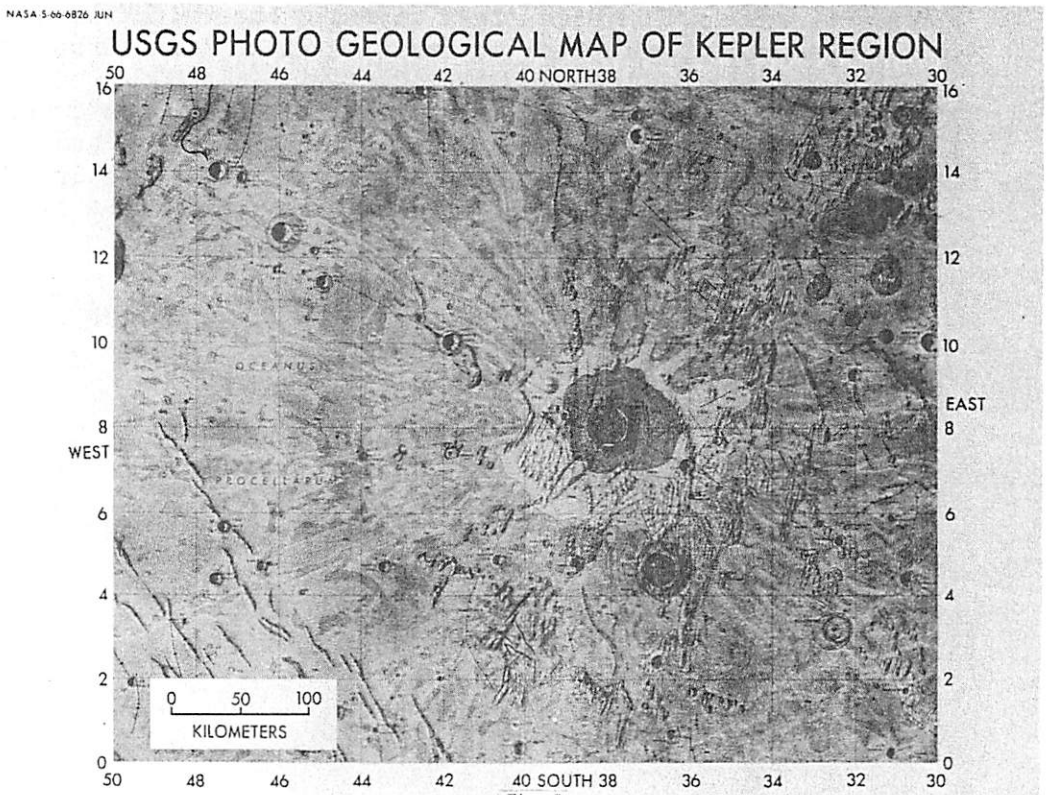
NASA-S-66-6826 JUN
USGS PHOTO GEOLOGICAL MAP OF KEPLER REGION
50 48 46 44 42 40 NORTH 38 36 34 32 30
16 14 12 10 8 6 4 2 0
WEST
EAST
OCEANUS
PROCELLARUM
0 50 100
KILOMETERS
50 48 46 44 42 40 SOUTH 38 36 34 32 30

Fig. 2

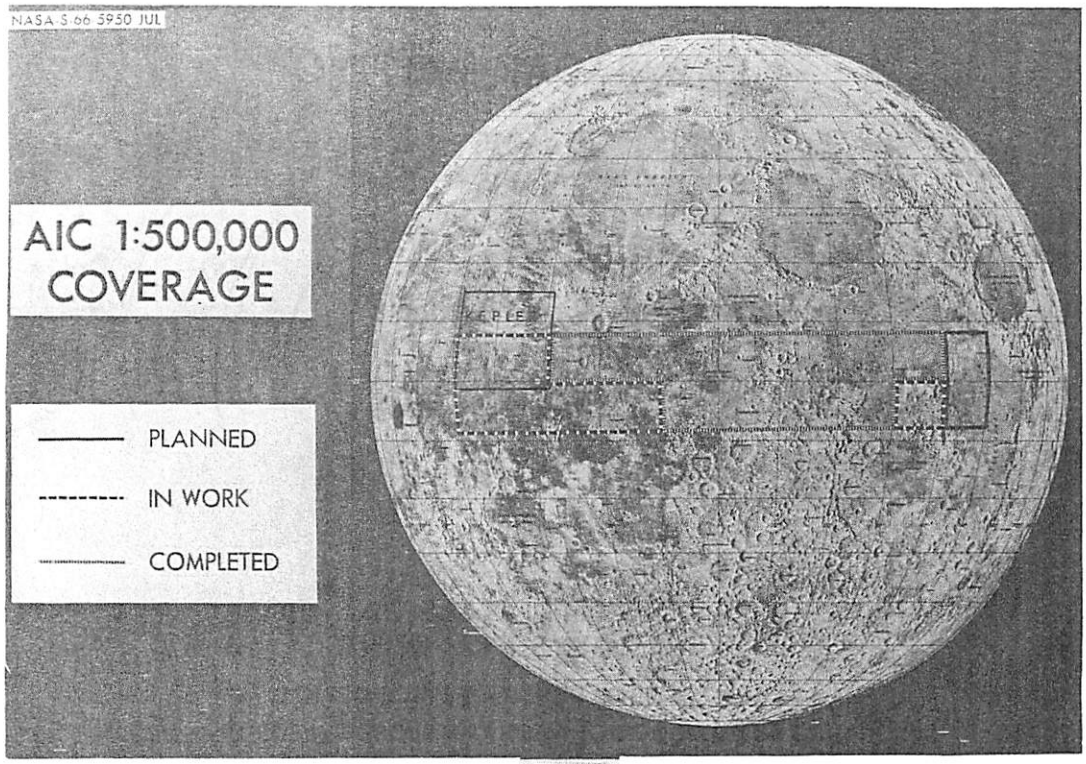

Fig. 3

NASA-S-66-6024 MAY

THERMAL ENHANCEMENTS (LINES) AND
HOT SPOTS (DOTS) NEAR THE END OF TOTALITY

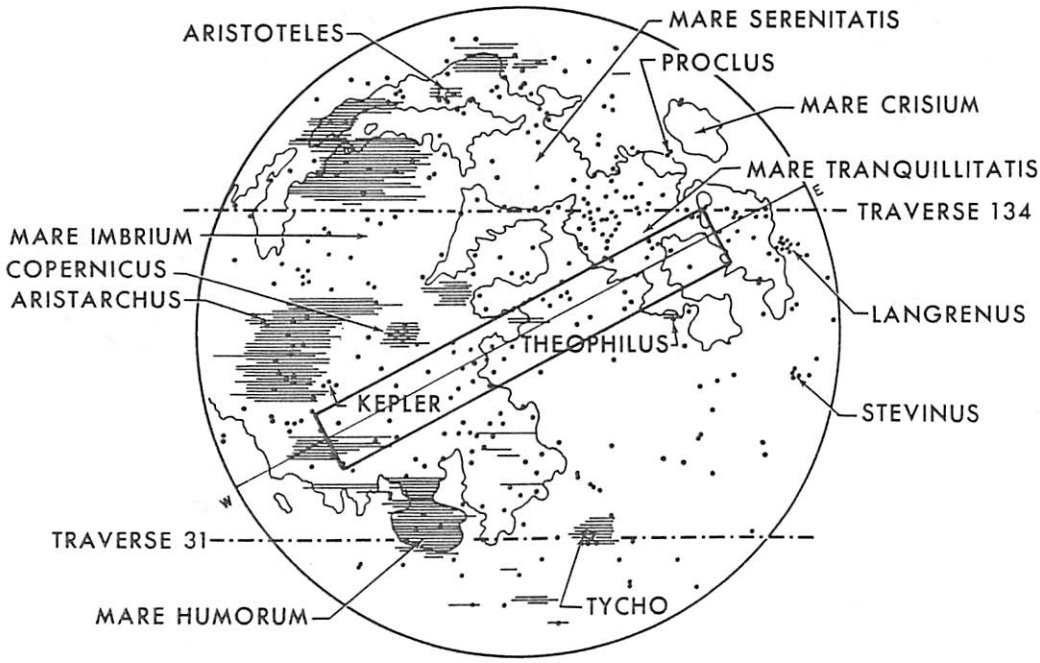

Fig. 4

NASA-S-66-6053-JUN

RADAR MAPPING

MIT LINCOLN LABS
ARECIBO (CORNELL)

0.86 CM
3.8 CM
23.0 CM
70.0 CM
7.5 M

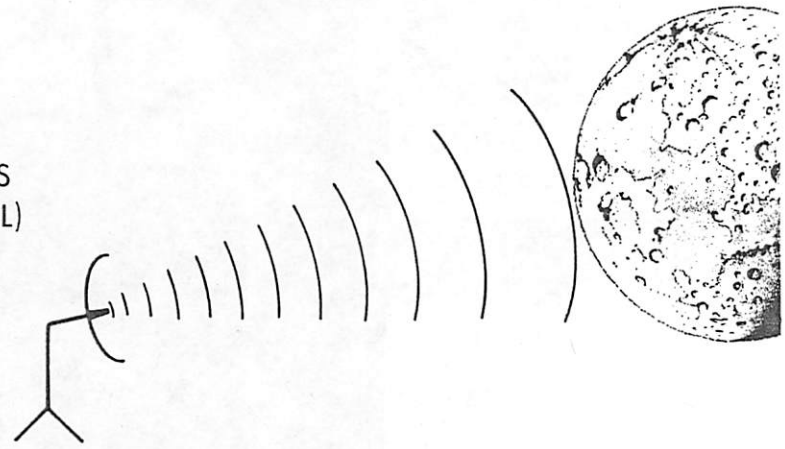

LOCALIZED AREAS ON MOON
(<10 SQ KM IN SIZE)

1. ESTIMATE BULK DENSITY VERSUS DEPTH
2. SURFACE ROUGHNESS-RMS SLOPE VERSUS SPACING

Fig. 5

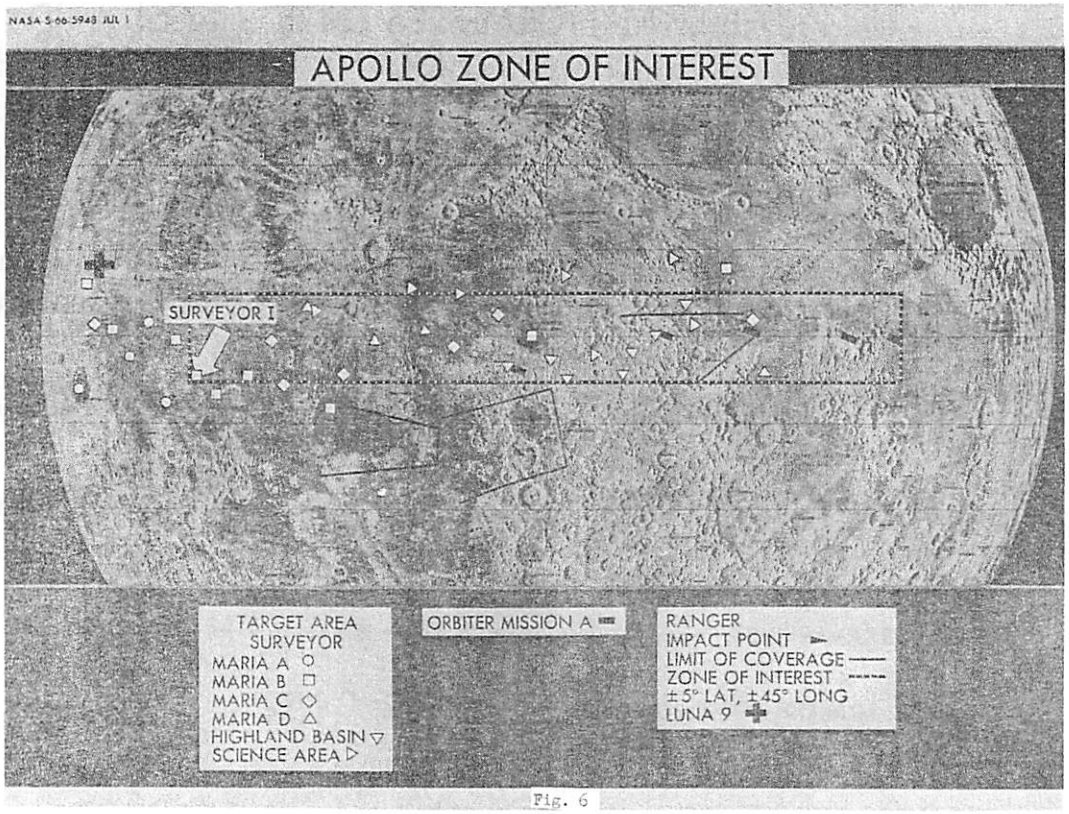

Fig. 6

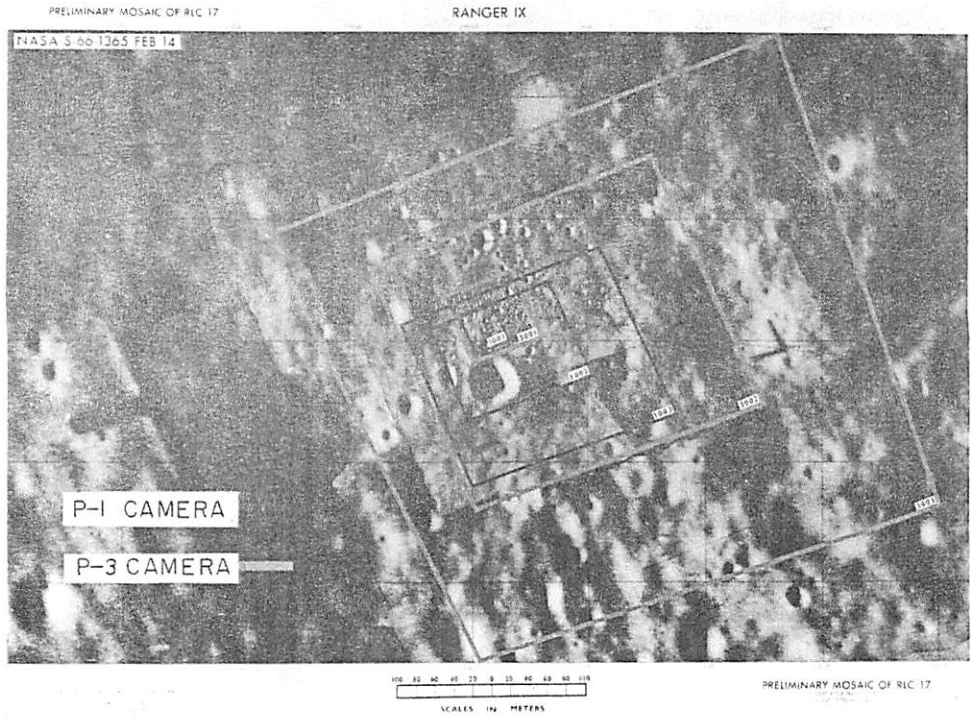
PRELIMINARY MOSAIC OF RLC 17
RANGER IX
NASA S 66 1365 FEB 14
P-I CAMERA
P-3 CAMERA
SCALES IN METERS
PRELIMINARY MOSAIC OF RLC 17

Fig. 7

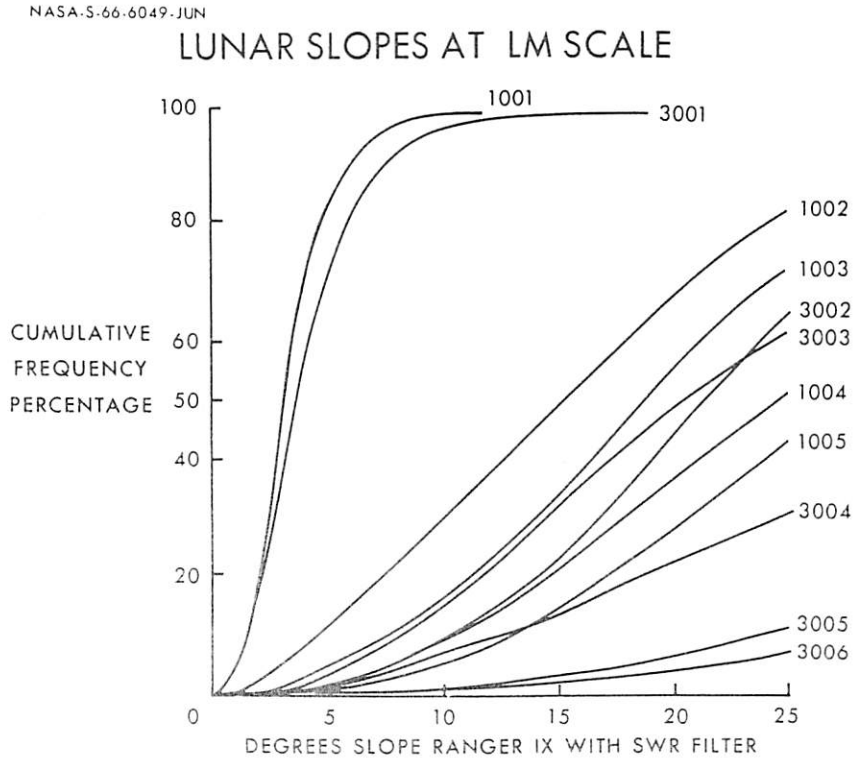
NASA-S-66-6049-JUN
LUNAR SLOPES AT LM SCALE
CUMULATIVE FREQUENCY PERCENTAGE
100
80
60
50
40
20
0
5
10
15
20
25
DEGREES SLOPE RANGER IX WITH SWR FILTER
1001
3001
1002
1003
3002
3003
1004
1005
3004
3005
3006

Fig. 8

NASA-S-66-6056 JUNE

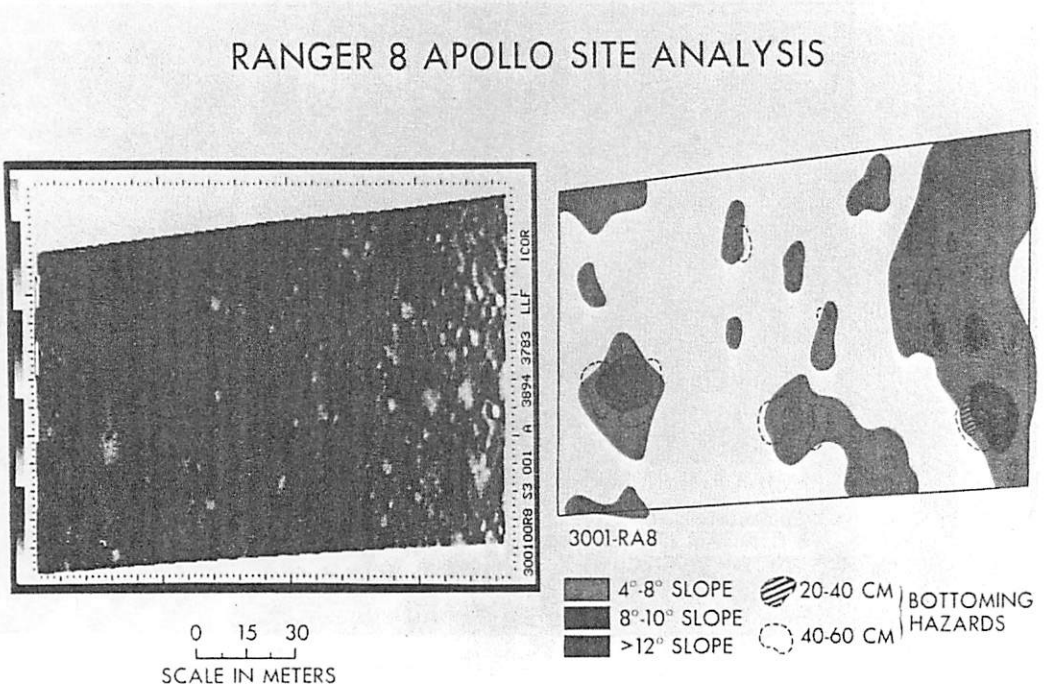

Fig. 9

NASA-S-66-6055-JUN

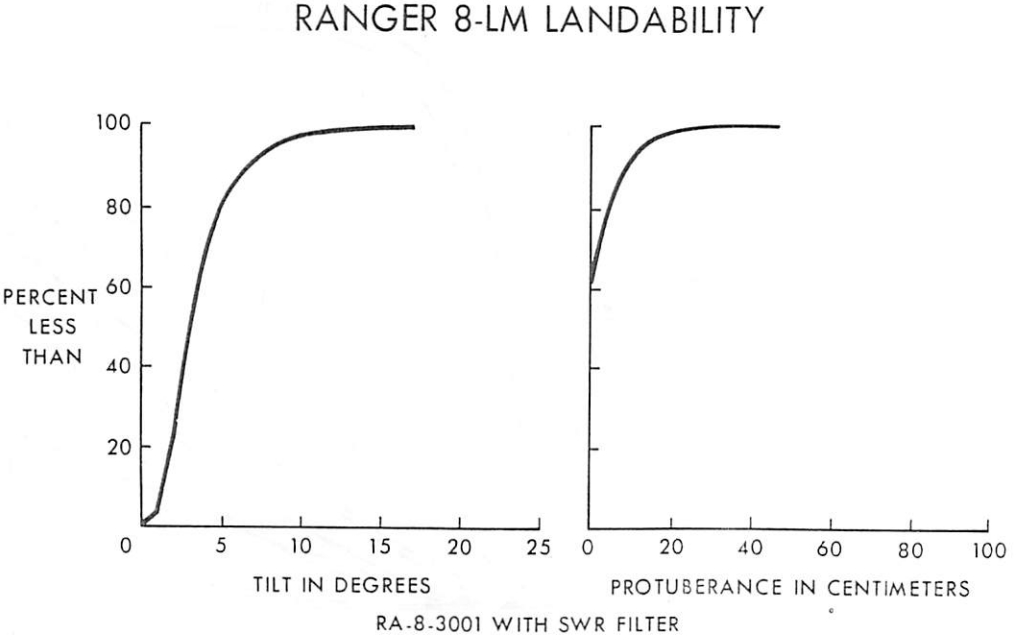

Fig. 10

RANGER IX PHOTOGRAPH OF FLOOR OF ALPHONSUS

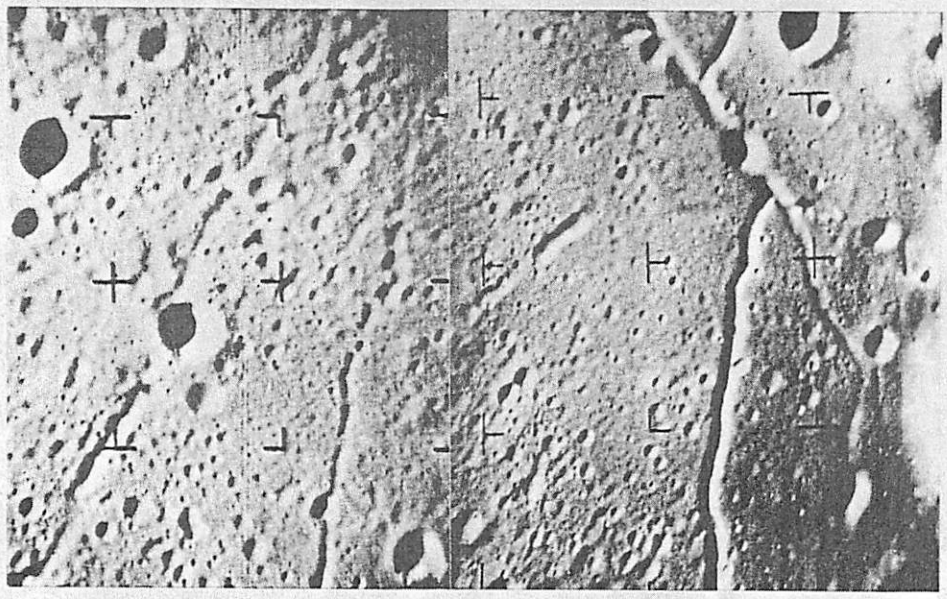

0 5 10KM
SCALE

Fig. 11

GEOLOGICAL MAP OF THE FLOOR OF THE ALPHONSUS

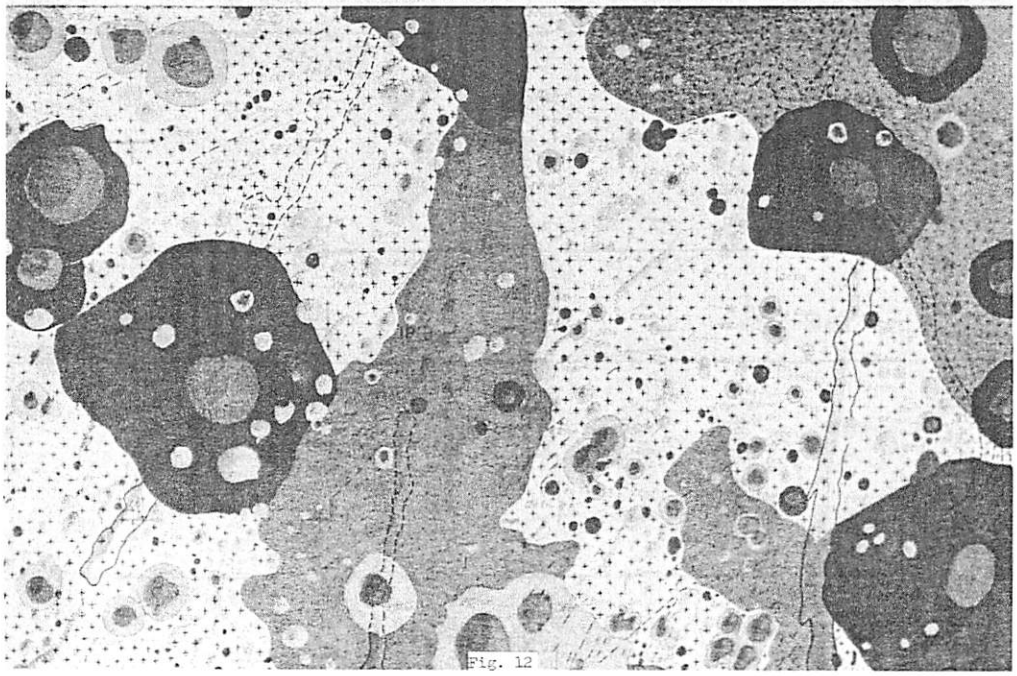

Fig. 12

NASA-S-66-5056 JUNE 1

KUIPER BEARING STRENGTH ANALYSIS

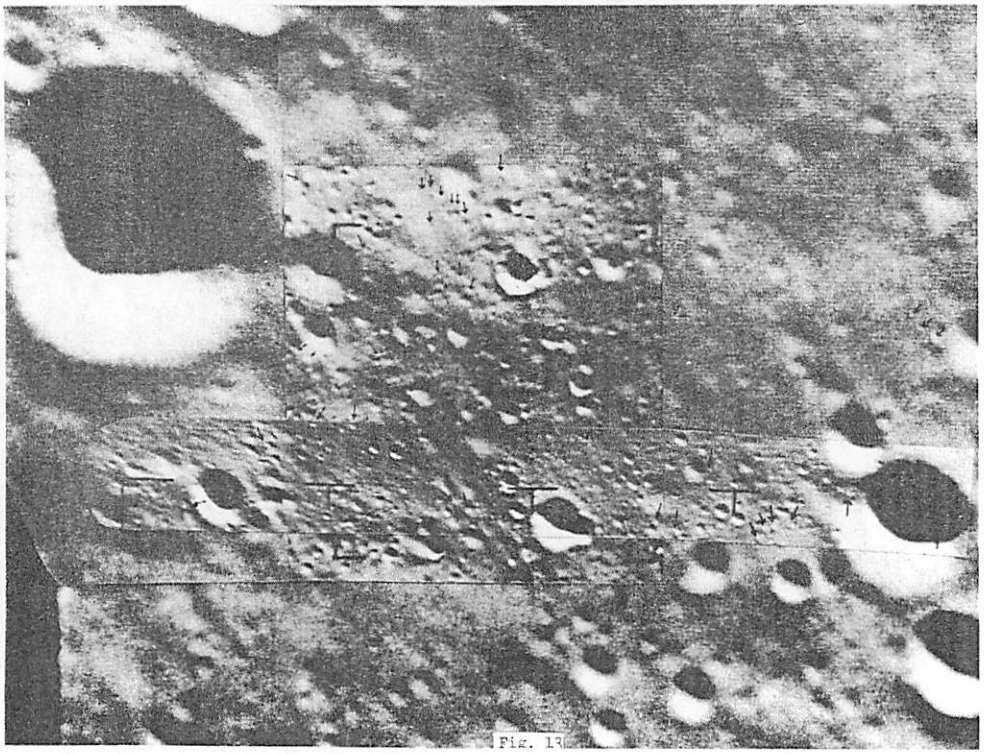

FIG. 13

NASA-S-66-5160 JUN 8

SKETCH OF PORTION OF LUNA IX PANORAMA TAKEN FEBRUARY 5, 1966 TILT 21 , SUN ELEVATION 27

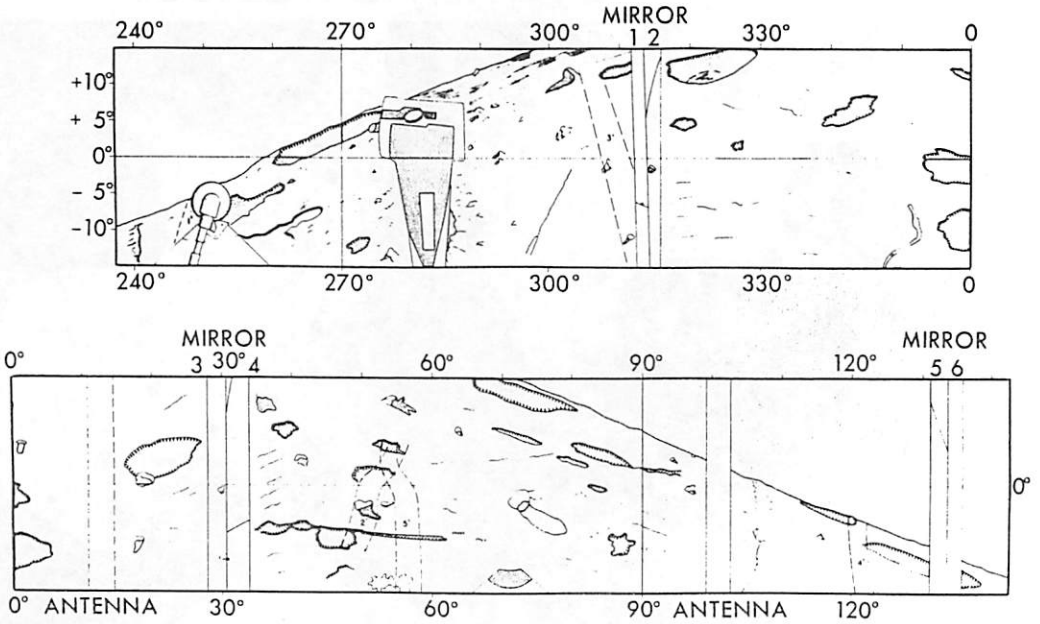

FIG. 14

LUNAR IX PHOTOGRAPHIC INTERPRETATION

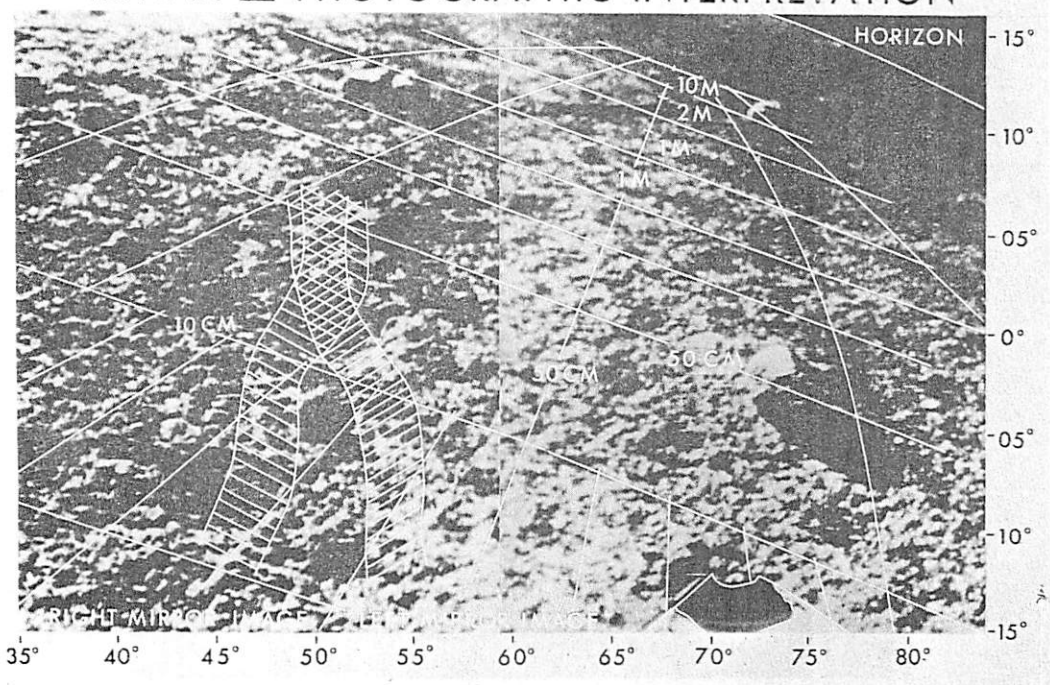

Fig. 15

SURVEYOR I

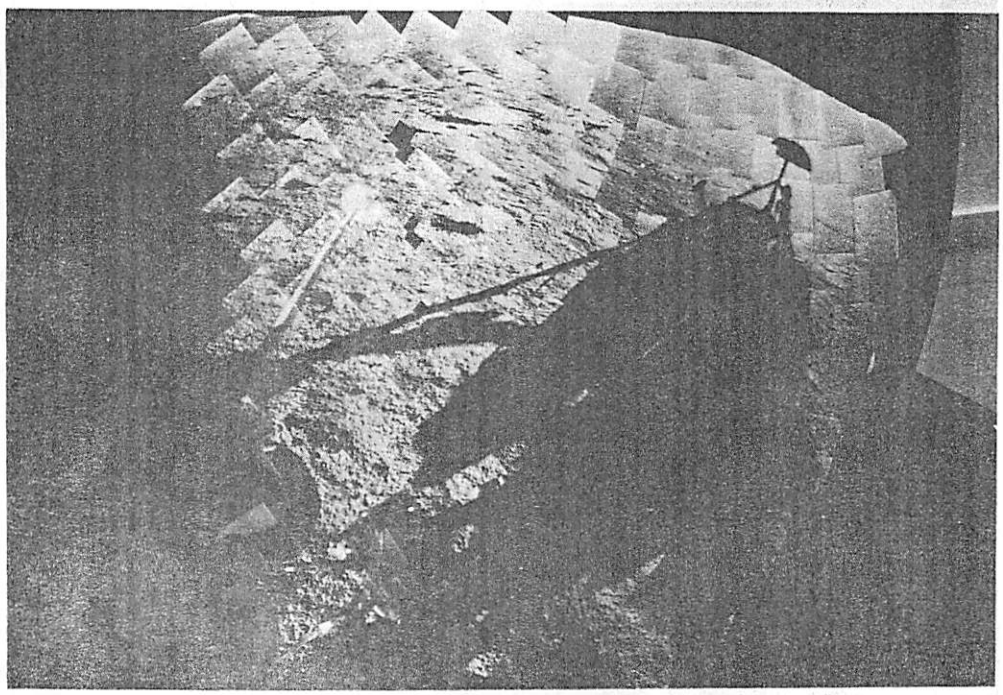

SUN ANGLE ~10°

Fig. 16

SURVEYOR I

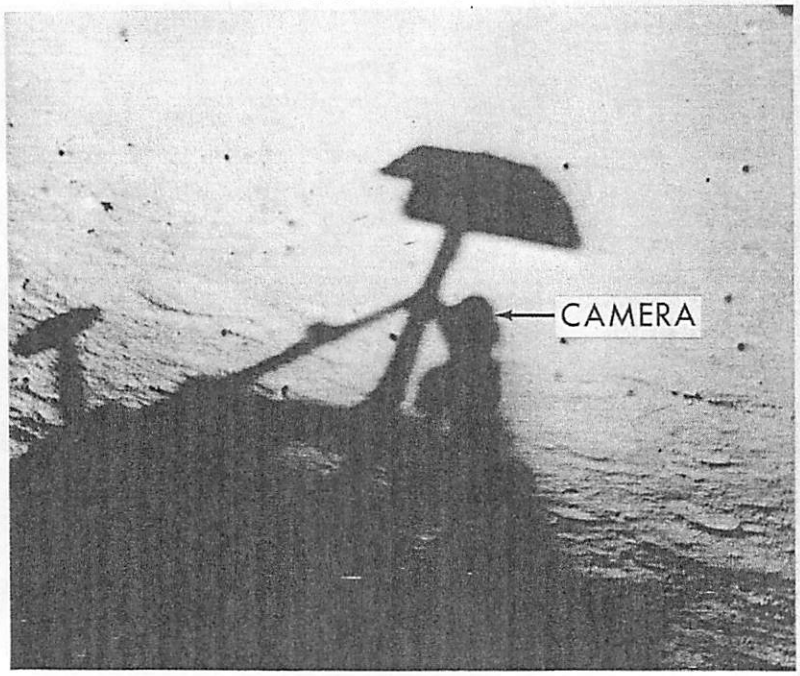

SUN ANGLE ~ 10°
FOV ~ 25°

SURVEYOR I

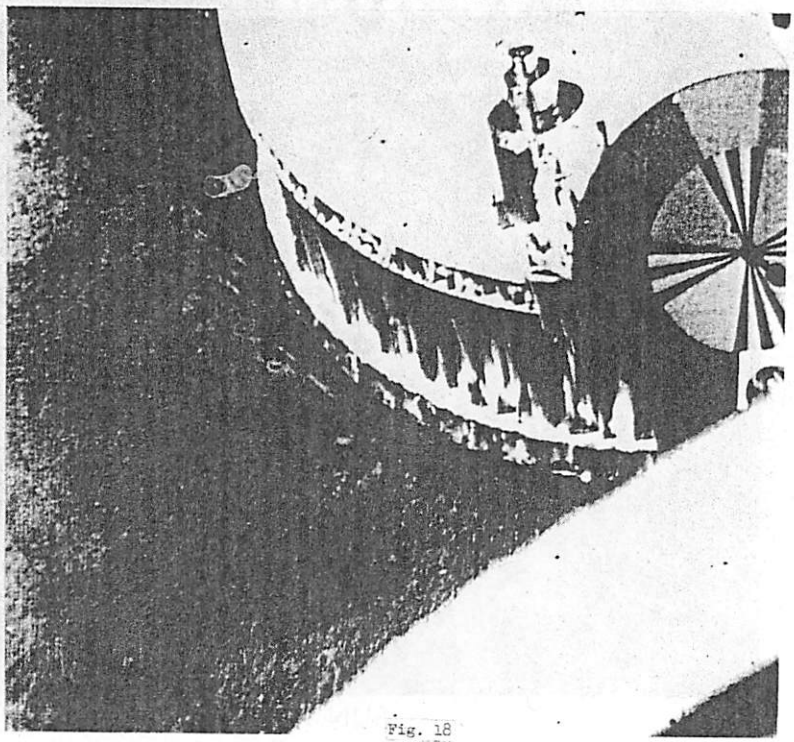

Fig. 18

SURVEYOR I

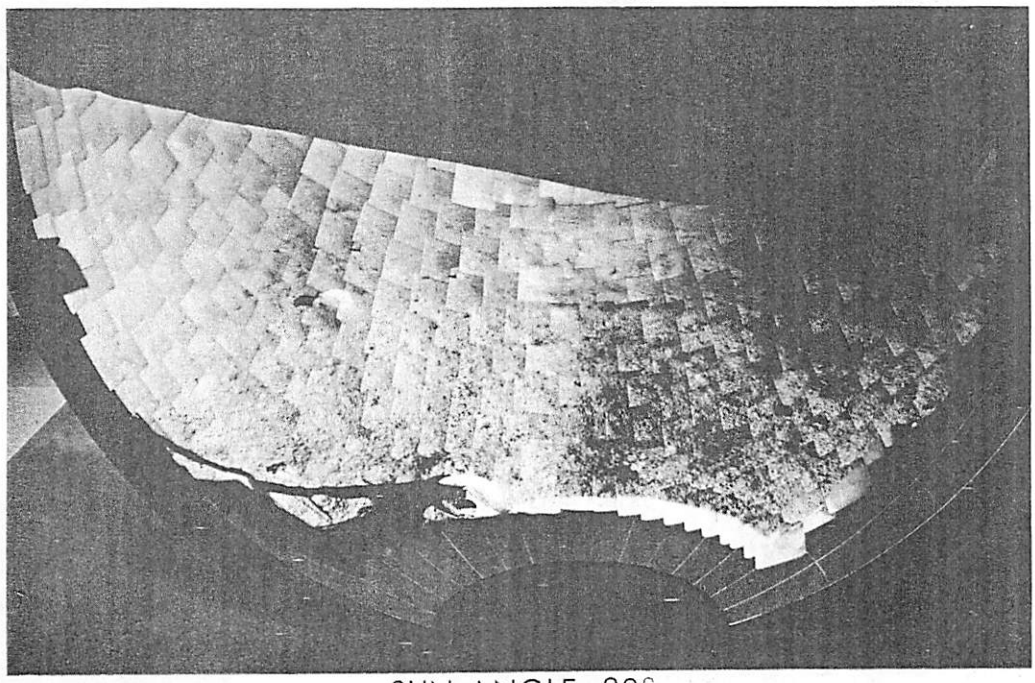

SUN ANGLE ~20°

Fig. 19

SURVEYOR I

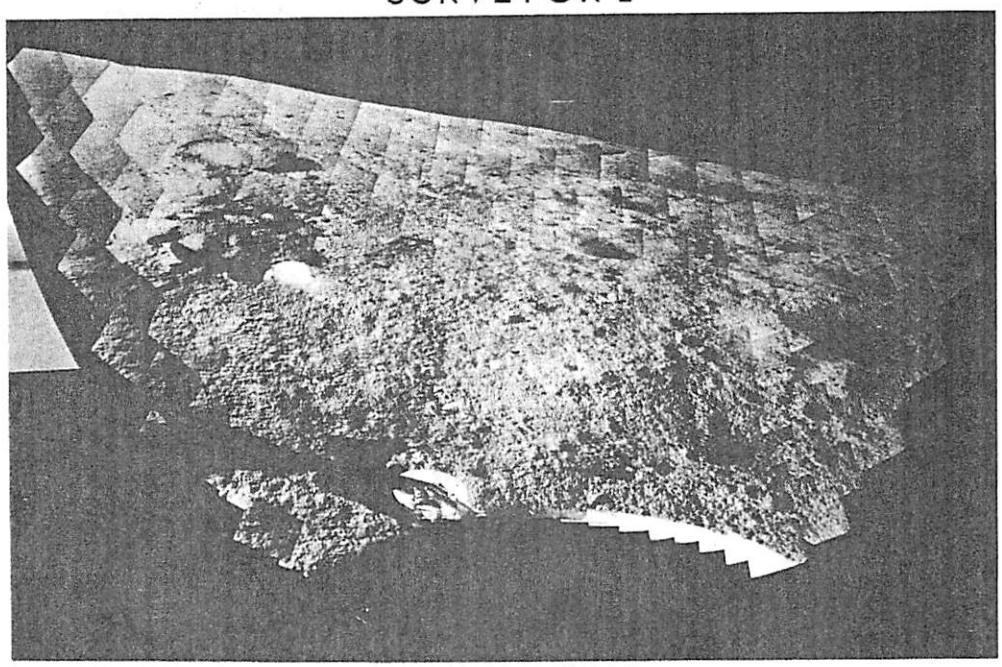

SUN ANGLE ~10°

Fig. 20

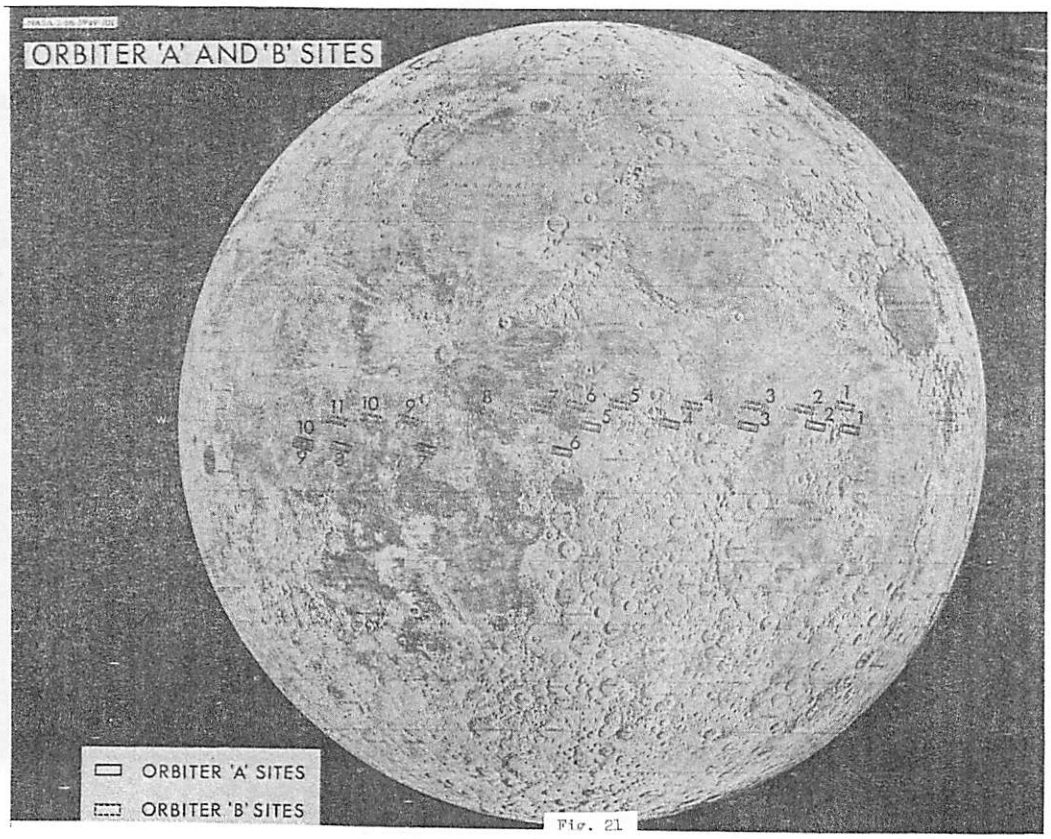

Fig. 21

NASA-S-66-6443 JUN

DETERMINATION OF POTENTIAL AREAS OF LANDING INTEREST

BASED ON CURRENT LANDING SITE SELECTION CRITERIA

↓

REJECT IN SEQUENCE

1. SLOPES > 10°
2. SLOPES 6 - 10°
3. CRATERS 0.5 - 10 KM DIA
4. AREAS TOO SMALL FOR LM 3σ DISPERSION ELLIPSE
5. UNACCEPTABLE RADAR APPROACH PATHS

↓

POTENTIAL TARGETS FOR ORBITER AND SURVEYOR

Fig. 22

ORBITER "A" MISSION-SITE NO. 5

CRATER AND SLOPE DELINIATION

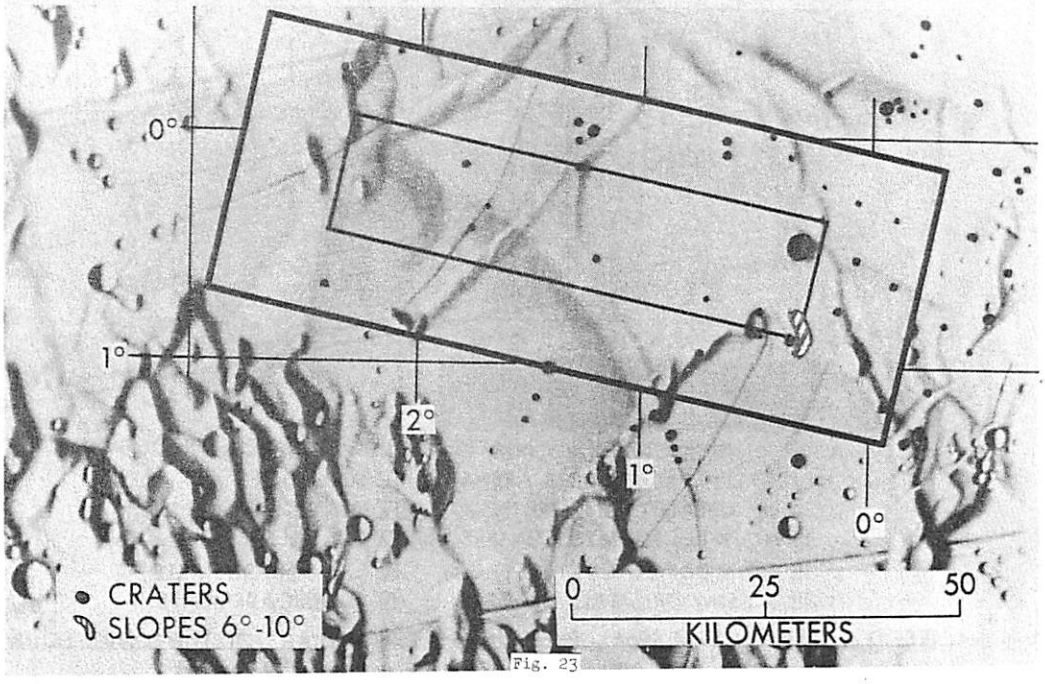

Fig. 23

ORBITER "A" MISSION-SITE NO. 5

ANALYSIS BASED ON 5.3 × 18.5 Km LANDING ELLIPSE WITH 55 Km (30 N M) RADAR APPROACH PATH

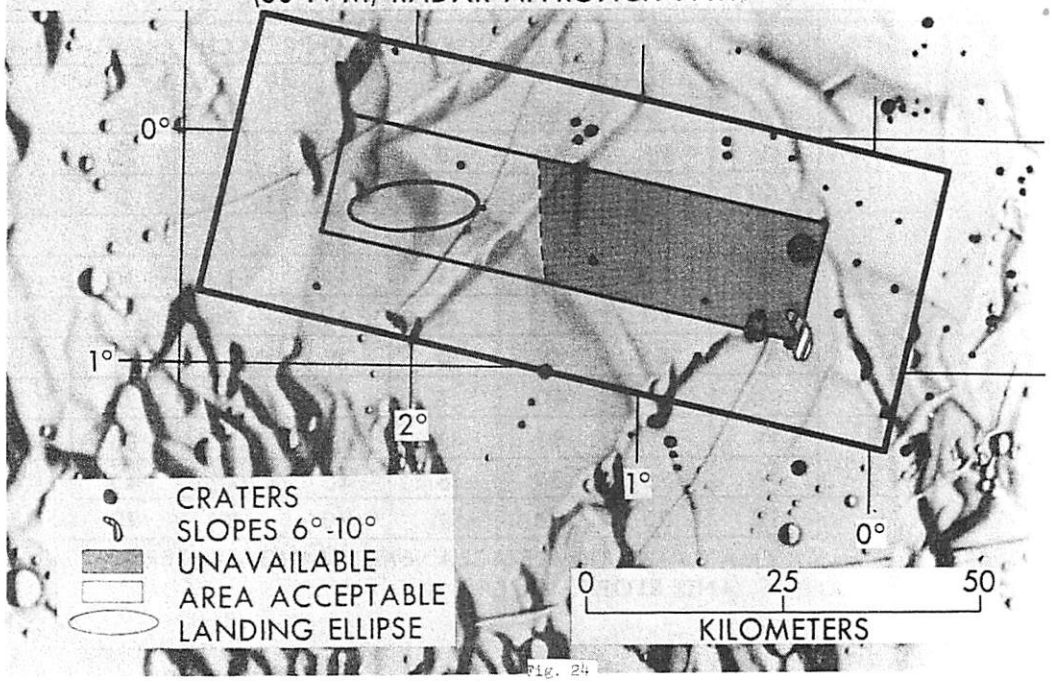

Fig. 24

NASA-S-66-3891 JUNE

ORBITER 'A' MISSION - SITE NO. 5

TERRAIN FEATURES

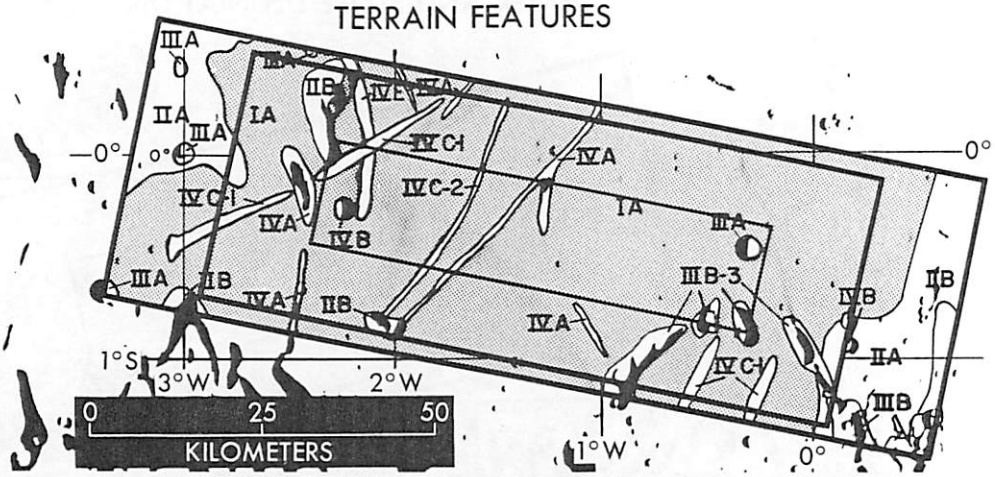

I A	MARE, UNDIFFERENTIATED	III C	CRATERS FIELDS AND CRATERS
II A	UPLAND, PLAINS AREAS	IV A	RIDGES
II B	UPLAND (SUBDUED)	IV B	DOMES
III A	WELL FORMED CRATERS	IV C-1	RILLS
III B	MODIFIED CRATERS	IV C-2	SINUOUS RILLS
III B-3	RIM OR SMALL CRATERS	IV E	ESCARPMENTS

REF D H DAHLEM ETAL 1966 - PRELIMINARY TERRAIN MAP OF THE LUNAR EQUATORIAL BELT

Fig. 25

NASA-S-66-5208 JUN

HIGH RESOLUTION AREAS

ORBITER A ELLIPSE 5.3 × 18.5 Km

SITE NO.	MAX* AREA	RADAR APPROACH PATH (N MI)					
		10		20		30	
	%	%	#	%	#	%	#
1	95	80	8	40	5	20	2
2	90	20	2	0	0	0	0
3	95	60	8	60	7	57	7
4	90	27	3	15	1	10	1
5	95	70	8	42	5	7	1
6	55	0	0	0	0	0	0
7	95	60	7	33	4	0	0
8	99	85	8	85	8	85	8
9	90	55	6	45	4	45	4
10	98	90	8	90	8	90	8

*MAX ACCEPTABLE AREA (EXCLUDING CRATERS AND SLOPES OVER 6°)

Fig. 26

NASA-S-66-5207 JUN

HIGH RESOLUTION AREAS

ORBITER B ELLIPSE 5.3×18.5 KM

SITE NO.	MAX* AREA	RADAR APPROACH PATH (N MI)					
		10		20		30	
	%	%	#	%	#	%	#
1	100	75	6	45	5	20	2
2	95	70	7	45	5	30	3
3	95	33	5	33	5	30	4
4	85	22	2	7	1	0	0
5	70	9	1	0	0	0	0
6	90	43	4	10	1	10	1
7	60	17	2	10	1	10	1
8	90	42	5	23	3	23	3
9	90	20	2	0	0	0	0
10	98	95	9	95	9	95	9
11	97	85	8	85	8	77	7

*MAX ACCEPTABLE AREA (EXCLUDING CRATER, AND SLOPES OVER 6°)

Fig. 27

NASA-S-66-5183 JUN

AVAILABLE ORBITER SITES FROM MISSION A & B

(5.3 × 18.5 KM ELLIPSE)
(30 N MI RADAR APPROACH)

DESCENDING ORDER OF SITES AVAILABLE	ORBITER SITE (NO. OF ELLIPSES)
1	B-10 (9)
2	A-8 (8)
3	B-11 (7)
4	A-3 (7)
5	A-9 (4)
6	B-3 (4)
7	B-2 (3)
8	B-8 (3)
9	B-1 (2)
10	A-1 (2)
11	B-6 (1)
12	A-5 (1)

Fig. 28

NASA-S-66-5947 JUL

AREAS FOR APOLLO LANDING SITE ANALYSIS

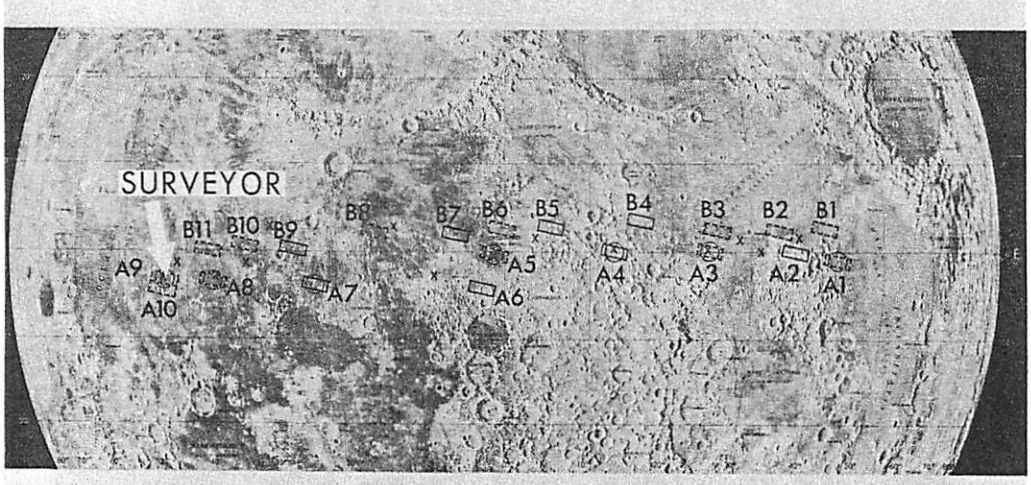

ORBITER A AND B SITES

FAVORED ORBITER A AND B SITES

SITES NOW USED IN MISSION PLANNING

X LUNAR LANDING AREA – NATURAL ENVIRONMENT AND PHYSICAL STANDARDS FOR THE APOLLO PROGRAM, APRIL 1965

Fig. 29

NASA-S-66-6052-JUN

SOURCES OF DATA FOR LANDING SITE SELECTION

DATA	SOURCE
LEM SLOPE FREQUENCY DISTRIBUTION	MSC
LEM BOTTOMING HAZARD FREQUENCY DISTRIBUTION	MSC
ANALYSIS OF TERRAIN FOR LANDING RADAR APPROACH	MSC
TOPOGRAPHIC MAPS	DOD, ACIC & AMS
PHOTO-GEOLOGIC MAPS	USGS
LUNAR SOIL MECHANICS PROPERTIES	JPL SURVEYOR– WORKING GROUPS USGS MSC
ANALYSIS OF SITES FOR SCIENTIFIC INTEREST	USGS
ORBITER DATA SCREENING	LRC, MSC & USGS

Fig. 30

CONTROL OF LUNAR SURFACE CONTAMINATION
AND
BACK CONTAMINATION

BY
RICHARD H. KOHRS

THE PURPOSE OF THIS PRESENTATION IS TO:

Show the current status of hardware design and procedures that are being developed to control or minimize lunar surface and back contamination.

Subsequent charts will show:

a. For each crew biological contamination source, the hardware or procedure being developed to minimize lunar surface contamination.

b. Preliminary contour plots showing the level and area of concentration of the descent propellant contaminants.

c. The current design criteria for the prevention of back contamination plus the spacecraft and recovery procedure postulated to meet this criteria.

d. The current design requirements and concepts of the Lunar Receiving Lab.

BIOLOGICAL LUNAR SURFACE CONTAMINATION

Figures 1, 2, and 3 summarize for each crew biological contamination source the hardware or procedure design currently being implemented. The prevention of exposure of crew biological excretions is accomplished primarily when there is still lunar surface sampling and exploration time remaining. All storable excretions are kept in the LM up to the completion of the last excursion. At this time the storage containers are offloaded onto the lunar surface and then stored in the LM descent stage by the LM crewman. Similarly, after the LM crewman enters the LM after the final excursion, certain EMU components are offloaded onto the lunar surface. Offloading of these storage containers and equipment accounts for approximately a 100 pound inert weight savings which is equivalent to approximately 200 pounds of total ascent stage launch weight.

SUPPORTING DATA

Sweat Filter	95% Effective
Cabin Air	80% Effective
LiOh Cannisters	Tests scheduled this month at Ft. Dietrich
Germicide	SETOL

NASA-S-66-5740 JUN 16

LUNAR SURFACE CONTAMINATION

BIOLOGICAL CONTAMINATION SOURCE	DISPOSITION
FECES URINE	STORED WITHIN LM UNTIL LUNAR SAMPLING AND EXPLORATION COMPLETED
LiOH CANISTERS	TRANSFERED TO THE LUNAR SURFACE AND STORED IN LM DESCENT STAGE PRIOR TO LAST EVA INGRESS
PLSS CONDENSATE	FECES, URINE, AND PLSS CONDENSATE CONTAINERS CONTAIN GERMICIDE
SWEAT	PASSED THROUGH BACTERIA FILTER PRIOR TO BEING VENTED ONTO LUNAR SURFACE
CABIN AIR	PASSES CONTINUOUSLY THROUGH LiOH CANISTER DURING CABIN DEPRESSURIZATION PASSES THROUGH FILTER INSTALLED ON CABIN VENT

Fig. 1

NASA-S-66-5133 JUN 8

LUNAR SURFACE CONTAMINATION

BIOLOGICAL CONTAMINATION SOURCE	DISPOSITION
EXTRAVEHICULAR ASTRONAUT	
FECES	DEFECATION NOT ANTICIPATED. IF REQUIRED, STORED IN SUIT UNTIL RETURN TO LM
URINE	STORED IN SUIT AND THEN DUMPED INTO STORAGE CONTAINERS UPON RETURN TO LM CABIN
LiOH CANNISTERS	REMOVED FROM BACK PACK WITHIN LM, STORED, AND THEN OFFLOADED INTO DESCENT STAGE
SWEAT	COLLECTED AS PLSS CONDENSATE. DUMPED INTO STORAGE CONTAINERS UPON RETURN TO LM
SUIT AIR	PASSES THROUGH LiOH CANNISTER IN BACK PACK. - .04 LB/HR SUIT LEAK ONTO SURFACE

Fig. 2

NASA-S-66-5134 JUN

LUNAR SURFACE CONTAMINATION

BIOLOGICAL CONTAMINATION SOURCE	DISPOSITION
EXTRAVEHICULAR MOBILITY UNIT COMPONENTS	LEFT ON LUNAR SURFACE AFTER COMPLETION OF LAST LUNAR EXPLORATION
1 PLSS	ONE PLSS RETAINED DURING LM ASCENT FOR BACKUP EXTRAVEHICULAR TRANSFER
2 PR LUNAR BOOTS	

Fig. 3

DESCENT ENGINE CONTAMINATION

Figures 4 through 7 show the amounts of the principal LM exhaust gas constituents that will be adsorbed on the lunar surface in the vicinity of the LM touchdown site. These charts are results of an initial study of GAEC and show preliminary estimates. The maps are oriented with respect to the landing trajectory so that the LM approaches the touchdown point from the top of the map. It is apparent that the most heavily contaminated regions lie along the trajectory. Maps of this type could serve as guides to locations from which lunar surface samples containing minimum amounts of contamination can be collected. They could also indicate to scientists the amounts of contamination that will exist in samples gathered at various locations with respect to the touchdown point.

Contours of constant adsorption in units of micrograms of adsorbed gas per square centimeter of lunar surface are plotted for H_2O, OH, NO, O, and O_2. CO, CO_2, H, and H_2 are also present in the exhaust; however, no appreciable amounts of these adsorbed contaminants should be found in lunar samples.

Maps of this type including information on the depth of contamination could be used as an important tool in compensating for contamination. Such maps would indicate that the astronauts need to collect samples at distances of only 1000 or less feet from the LM to insure samples that are relatively uncontaminated.

Similarly, if the location, time, and depth at which every lunar sample is collected is recorded, a comparison can be made between the amounts and distribution of actual versus predicted contaminants during postflight evaluation. This data would be useful in the development of distribution maps for subsequent flights.

SUPPORTING DATA

It is currently estimated that approximately 1/3 of exhaust by-products will be H_2O, 1/3 N_2, and 1/3 H_2, CO, CO_2, H and O.

Propellant UDMH and N_2H_4 + N_2O_4 (50/50 unsymdimethydrazine/hydrazine + nitrogen tetroxide).

NASA-S-66-6086 JUN

CONTOURS OF EQUAL ADSORPTION OF H_2O IN UNITS OF $\mu g/cm^2$

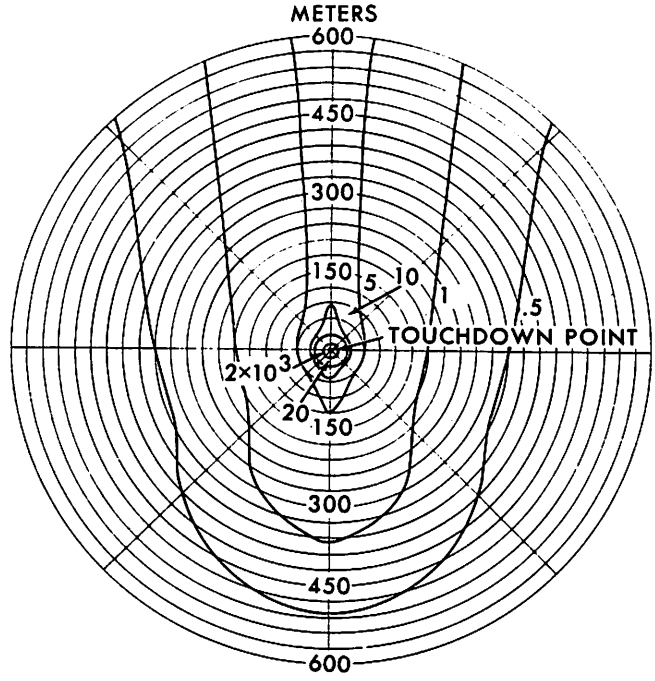

Fig. 4

NASA-S-66-6087 JUN

CONTOURS OF EQUAL ADSORPTION OF OH IN UNITS OF $\mu g/cm^2$

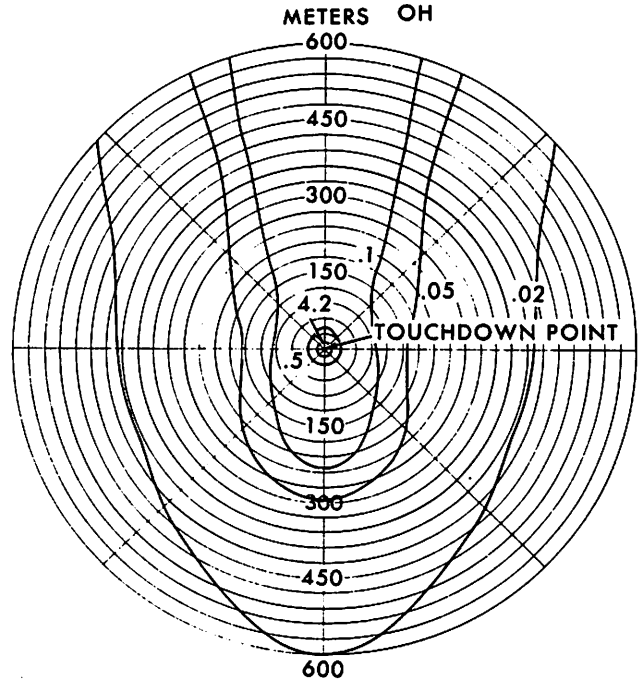

Fig. 5

NASA-S-66-6088 JUN

CONTOURS OF EQUAL ADSORPTION OF NO IN UNITS OF $\mu g/cm^2$

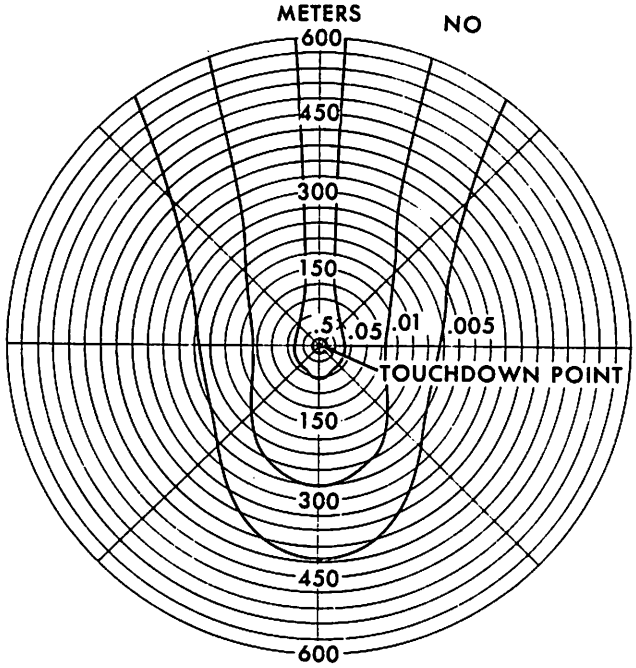

Fig. 6

NASA-S-66-6089 JUN

CONTOURS OF EQUAL ADSORPTION OF O AND O_2 IN UNITS OF $\mu g/cm^2$

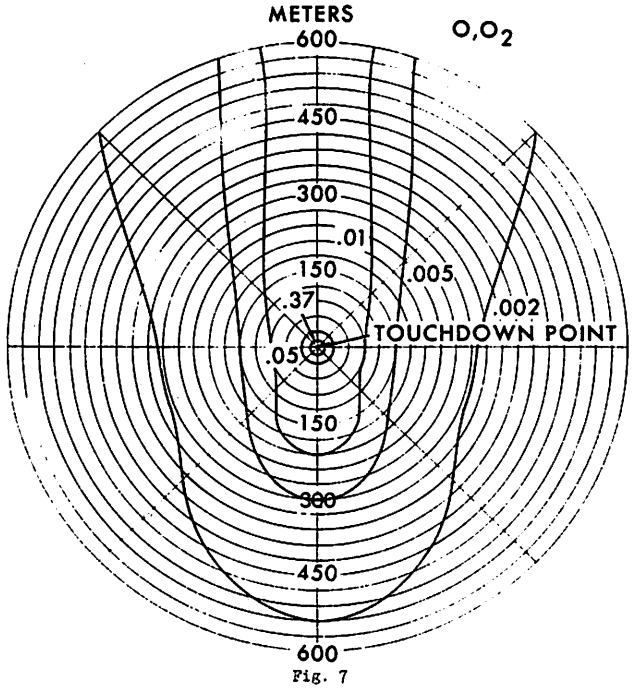

Fig. 7

BACK CONTAMINATION

The remaining charts will show the back contamination criteria, the postulated inflight and recovery procedures to meet this criteria, plus the LRL (Lunar Receiving Lab) design requirements and concepts.

Hardware and procedures to minimize back contamination can be divided into three specific phases. Namely:

a. The time from lunar landing through postearth landing recovery.

b. The time from recovery through transportation to the Lunar Receiving Lab.

c. The post mission confinement in the Lunar Receiving Lab.

Figures 8 and 9 show the spacecraft and recovery criteria recommended by the interagency committee.

Until recently no specific requirement has existed to provide hardware or develop procedures that minimize the sources of back contamination. However, the interagency committee for back contamination has recently recommended spacecraft and recovery procedures as well as approved the design requirements and functions of the Lunar Receiving Lab.

This criteria has recently been approved by NASA Headquarters and currently is under study by MSC.

This criteria was established as a result of a briefing at MSC on April 13, 1966, at which MSC outlined the spacecraft, recovery, and lab current capabilities and requirements.

The committee gave its approval to the lab requirements and recommended the spacecraft and recovery criteria shown on the next charts.

NASA-S-66-5135 JUN 8

SPACECRAFT AND RECOVERY RECOMMENDATIONS BY THE INTERAGENCY COMMITTEE

SPACECRAFT CRITERIA

- DEVISE AND PROTOTYPE TEST ANY COMBINATION OF THE LM CM RETURN PROCEDURES, ALONG WITH ANY DESIRED CONTAMINATION CONTROL EQUIPMENT, THAT WILL CUMMULATIVELY PRODUCE A DEGREE OF EARTH PROTECTION GENERALLY EQUIVALENT TO THAT ACHIEVED WITH AN EXHAUST FILTER

Fig. 8

NASA-S-66-5136 JUN 8

SPACECRAFT AND RECOVERY RECOMMENDATIONS BY THE INTERAGENCY COMMITTEE

RECOVERY CRITERIA

- MSC SHOULD PERFORM A STUDY OF ALTERNATIVES IN THE RECOVERY MODES SUCH AS SUBSTITUTING GOOD SANITATION, ISOLATION AND QUARANTINE TECHNIQUES IN PLACE OF SPECIAL ISOLATION EQUIPMENT

Fig. 9

Based on the interagency criteria the spacecraft procedures shown on figures 10 through 14 are being considered as ways of minimizing the source of back contamination.

The procedures have been subdivided into the various mission phases.

SUPPORTING DATA

a. Forward hatch open only 7% of time.

b. Helmets normally off for eating only 4% of time.

NASA-S-66-5137 JUN 8

PROCEDURES POSTULATED TO MINIMIZE SOURCES OF BACK CONTAMINATION

LUNAR SURFACE PHASE

- THE LM FORWARD HATCH WILL BE SECURED EXCEPT FOR CREW EGRESS AND INGRESS
- PRIOR TO LM INGRESS THE CREW WILL WIPE OFF EXTERNAL GARMENTS AND BOOTS
- THE CREW WILL MINIMIZE THE HELMET OFF TIME TO REDUCE DIRECT EXPOSURE TO CABIN ENVIRONMENT
- LM LiOH CANNISTERS WILL FILTER CABIN/SUIT ENVIRONMENT
- SCIENTIFIC CONTAINERS WILL BE WIPED OFF PRIOR TO LM INGRESS

Fig. 10

NASA-S-66-5138 JUN 8

PROCEDURES POSTULATED TO MINIMIZE SOURCES OF BACK CONTAMINATION

LM TO CSM TRANSFER PHASE

- AFTER HARD DOCK THE CSM WILL PRESSURIZE THE DOCKING TUNNEL, THE LM ECS WILL BE DEACTIVATED, THE LM RELIEF VALVE WILL BE MANUALLY VENTED TO CREATE A FLOW FROM CM THROUGH LM. PRESSURE HATCH REMOVED AND FLOW OF AIR WILL COME FROM CM THROUGH LM
- EXTERNAL TMG'S REMAIN IN LM ASCENT STAGE
- EQUIPMENT TRANSFERRED TO CSM WILL BE "WIPED OFF" IN THE LM PRIOR TO TRANSFER

TRANSEARTH COAST

- LiOH CANNISTERS FILTER CABIN/SUIT ENVIRONMENT

Fig. 11

NASA-S-66-5235 JUNE

PROCEDURES POSTULATED TO MINIMIZE SOURCES OF BACK CONTAMINATION

ENTRY PHASE

- LiOH CANISTERS FILTER CABIN/SUIT ENVIRONMENT
- EXTERNAL REENTRY TEMPERATURES WILL DECONTAMINATE THE EXTERNAL SURFACE OF THE SPACECRAFT

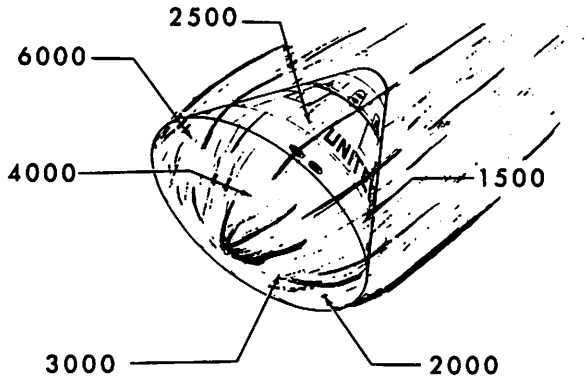

SURFACE TEMPERATURE °F

90% SURFACE LOST
600°F BOND LINE AT CHUTE DEPLOYMENT
300°F BOND LINE AT TOUCHDOWN

Fig. 12

NASA-S-66-5139 JUN 8

PROCEDURES POSTULATED TO MINIMIZE SOURCES OF BACK CONTAMINATION

POSTLANDING

- VENTILATION SYSTEM PROVIDES 100 - 150 CFM AIR CIRCULATION. STUDY CURRENTLY BEING PERFORMED TO SHOW IMPACT OF PROVIDING POSTLANDING BIOLOGICAL FILTRATION.

Fig. 13

NASA-S-66-5234 JUN

PROCEDURES POSTULATED TO MINIMIZE SOURCES OF BACK CONTAMINATION (CONT)

	PRESENT SYSTEM WITH FILTER	REDESIGNED SYSTEM		
		NEW FAN WITH FILTER	PRESENT FAN WITH FILTER PLUS WATER COOLED SUITS	NEW FAN WITH FILTER PLUS WATER COOLED SUITS
△ INERT WEIGHT	4 LBS	210 LBS	35 LBS	43 LBS
EFFECTIVE CSM WEIGHT	9 LBS	450 LBS	75 LBS	93 LBS
LIMITS	THERMAL CONTROL OF CREW INADEQUATE		THERMAL CONTROL OF CREW MARGINAL	
COST & SCHEDULE	TBD	TBD	TBD	TBD

Fig. 14

Figures 15 through 20 show the postulated recovery procedures being considered from time of initial pararescue contact through shipment to the Lunar Receiving Lab.

The procedures have been subdivided for various situations. That is, crew egress prior to retrieval: Crew in CM at ship retrieval; Crew transfer to LRL; Spacecraft transfer to LRL.

NASA-S-66-5140 JUN 8

PROCEDURES POSTULATED TO MINIMIZE SOURCES OF BACK CONTAMINATION

CREW EGRESS PRIOR TO RETRIEVAL

- PARARESCUE PERSONNEL JUMP WITH FLOTATION COLLAR AND BIOLOGICAL ISOLATION SUITS
- PARARESCUE PERSONNEL INSTALL FLOTATION COLLAR, PUT BIOLOGICAL ISOLATION SUITS IN RAFT OUTSIDE OF CM
- CREW EGRESS FROM CM, GET INTO RAFT , AND DON BIOLOGICAL ISOLATION SUITS
- PARARESCUE PERSONNEL ASSIST FLIGHT CREW ONLY IF NEEDED; OTHERWISE MOVE SOME DISTANCE AWAY UNTIL THE CREW DONS SUITS
- RECOVERY SHIP PROCEEDS TO LANDING POINT; RETRIEVES SPACECRAFT, FLIGHT CREW, AND PARARESCUE PERSONNEL

Fig. 15

NASA-S-66-5141 JUN 8

PROCEDURES POSTULATED TO MINIMIZE SOURCES OF BACK CONTAMINATION

CREW EGRESS PRIOR TO RETRIEVAL (CONTINUED)

- AFTER CM IS ABOARD SHIP, ONE MEMBER OF FLIGHT CREW REENTERS CM IN ORDER TO REMOVE LUNAR SAMPLES, FLIGHT TAPES,ETC. ITEMS ARE PLACED IN AN APPROPRIATE CONTAINER, CREW MEMBER EGRESSES, AND DONS A FRESH BIOLOGICAL ISOLATION SUIT.
- FLIGHT CREW PROCEED TO QUARANTINE QUARTERS OR FACILITY FOR MEDICAL AND MISSION DEBRIEFING. (MEDICAL PERSONNEL ARE THEN QUARANTINED ALONG WITH THE CREW.)
- FLIGHT CREW AND MEDICAL PERSONNEL STAY IN QUARANTINE UNTIL SHIP REACHES NEAREST APPROPRIATE DOCK.
- ALL WASTE PRODUCTS OF QUARANTINED PERSONNEL ARE COLLECTED AND TREATED.

Fig. 16

NASA-S-66-5142 JUN 8

PROCEDURES POSTULATED TO MINIMIZE SOURCES OF BACK CONTAMINATION

CREW IN CM AT SHIP RETRIEVAL

- PARARESCUE PERSONNEL JUMP WITH FLOTATION COLLAR, BIOLOGICAL ISOLATION SUITS, AND CABIN FILTRATION DEVICE*
- PARARESCUE PERSONNEL INSTALL FLOTATION COLLAR AND REMOVE CM HATCH AND INSTALL FILTRATION DEVICE
- PARARESCUE PERSONNEL ASSIST FLIGHT CREW ONLY IF NEEDED; OTHERWISE MOVE SOME DISTANCE AWAY
- RECOVERY SHIP PROCEEDS TO LANDING POINT; RETRIEVES SPACECRAFT/CREW, AND PARARESCUE PERSONNEL
- AFTER CM IS RETRIEVED AND PLACED ON DECK, FLIGHT CREW EGRESS WITH LUNAR SAMPLES, FLIGHT TAPES, ETC, DON BIOLOGICAL ISOLATION SUITS, AND PROCEED TO QUARANTINE QUARTERS OR FACILITY FOR MEDICAL AND MISSION DEBRIEFING

*CABIN FILTRATION DEVICE CURRENTLY UNDER STUDY. IF SPACECRAFT HAS FILTER, THIS DEVICE MAY NOT BE REQUIRED

Fig. 17

NASA-S-66-5143 JUN 8

PROCEDURES POSTULATED TO MINIMIZE SOURCES OF BACK CONTAMINATION

CREW IN CM AT SHIP RETRIEVAL (CONT)

- FLIGHT CREW PROCEED TO QUARANTINE QUARTERS OR FACILITY FOR MEDICAL AND MISSION DEBRIEFING. (MEDICAL PERSONNEL ARE THEN QUARANTINED ALONG WITH THE CREW)
- FLIGHT CREW AND MEDICAL PERSONNEL STAY IN QUARANTINE UNTIL SHIP REACHES NEAREST APPROPRIATE DOCK
- ALL WASTE PRODUCTS OF QUARANTINED PERSONNEL ARE COLLECTED AND TREATED

Fig. 18

NASA-S-66-5144 JUN 8

PROCEDURES POSTULATED TO MINIMIZE SOURCES OF BACK CONTAMINATION

CREW TRANSFER TO AIRCRAFT FOR FLIGHT TO LRL, HOUSTON

- FLIGHT CREW AND MEDICAL PERSONNEL DON BIOLOGICAL ISOLATION SUITS, LEAVE QUARANTINE QUARTERS, AND TRANSFER BY APPROPRIATE TRANSPORTATION TO AIRCRAFT. LUNAR SAMPLES, TAPES, ETC., ARE TRANSFERRED

- FLY TO ELLINGTON, TRANSFER BY APPROPRIATE TRANSPORTATION TO LRL

Fig. 19

NASA-S-66-5145 JUN 8

PROCEDURES POSTULATED TO MINIMIZE SOURCES OF BACK CONTAMINATION

QUARANTINE SPACECRAFT

- ABOARD SHIP THE HATCH IS REPLACED

- EXTERNAL SURFACES OF SPACECRAFT ARE CHEMICALLY TREATED

- AT DOCKSIDE SM/RCS IS DEACTIVATED AND THEN TRANSFERRED TO LSRL BY AIR AND SURFACE TRANSPORTATION

Fig. 20

Figure 21 shows the general flow sequence from recovery of spacecraft, crew, lunar samples, and miscellaneous equipment from the recovery ship through distribution and return of scientific samples.

NASA-S-66-5146 JUN 8

TRANSPORTATION TO AND FROM LRL

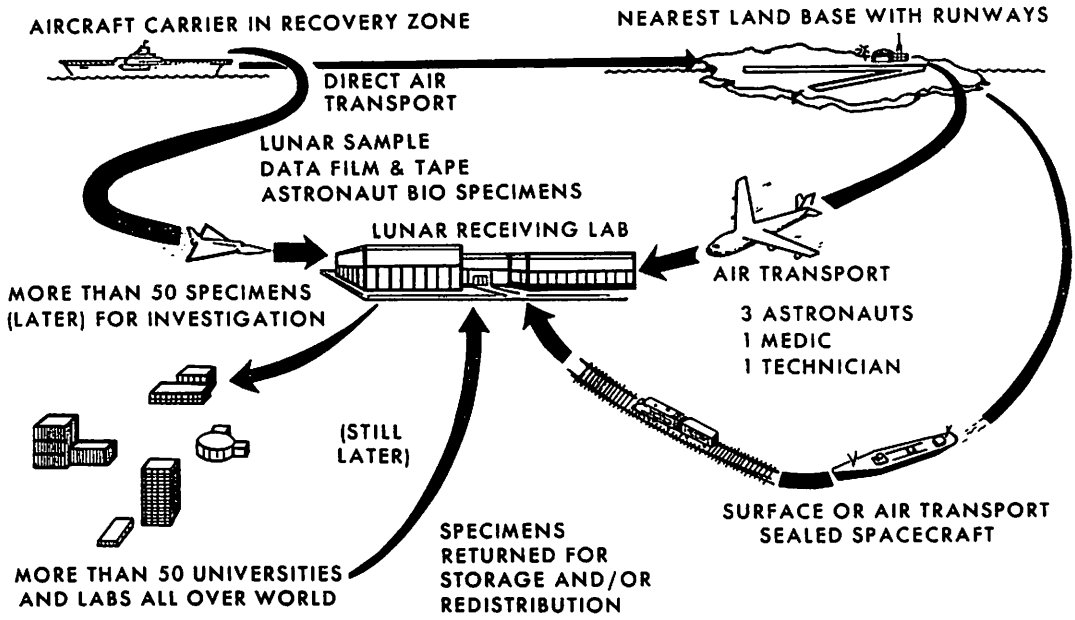

Fig. 21

Figures 22 through 26 show the Lunar Receiving Lab functions during quarantine plus the containment concepts currently planned for the spacecraft, crew, and lunar samples.

NASA-S-66-5151 JUN 8

LUNAR RECEIVING LABORATORY OPERATIONS

LUNAR RECEIVING LAB FUNCTIONS DURING QUARANTINE

- ASTRONAUT ISOLATION
  - POST FLIGHT MEDICAL EXAMINATION
  - TECHNICAL DEBRIEFING
  - PARTICIPATION IN SAMPLE IDENTIFICATION AND SCIENTIFIC DEBRIEFING
  - EXPERIENCE INPUT TO NEXT FLIGHT
- SAMPLE ISOLATION
  - OPEN CONTAINERS, IDENTIFY & CATALOG
  - REMOVE SPECIMENS FOR QUARANTINE CLEARANCE TESTS
  - PERFORM TIME DEPENDENT SCIENTIFIC EXPERIMENTS
  - PREPARE FIFTY OR MORE SPECIMENS TO BE SENT TO OUTSIDE LABS

Fig. 22

NASA-S-66-5150 JUN 8

LUNAR RECEIVING LABORATORY OPERATIONS (CONT)

LUNAR RECEIVING LAB FUNCTIONS DURING QUARANTINE

- QUARANTINE CLEARANCE TEST
  - PERFORM MINIMUM BIO-TESTS IN CONFORMANCE WITH INTERAGENCY REQUIREMENTS TO CERTIFY SAFE RELEASE OF ISOLATED PERSONNEL AND EQUIPMENT
- DATA FILM AND TAPE ISOLATION
  - PLAY TAPES THROUGH BIOLOGICAL BARRIER FOR OUTSIDE PROCESSING
  - DEVELOP FILM AND PRINT THROUGH OPTICAL PRINTER FOR OUTSIDE USE
- SPACECRAFT COMMAND MODULE ISOLATION
  - AVAILABLE FOR ESSENTIAL TECHNICAL INSPECTION
  - AVAILABLE FOR ADDITIONAL BIO-SAMPLING

Fig. 23

NASA-S-66-5149 JUN 8

LUNAR BIOLOGY PROGRAM
BASIC CONTAINMENT CONCEPTS
SPACECRAFT

- NO ENTRANCE PERMITTED TO SPACECRAFT INTERIOR
- SPACECRAFT STORED IN NON-QUARANTINE AREA
- IF REQUIRED, SPACECRAFT STORAGE AREA MAY BE INCORPORATED INTO CREW RECEPTION AREA
- POSSIBLE REQUIREMENTS INCLUDE
  - COMPONENT ANALYSIS OR REMOVAL
  - FURTHER BIOLOGIC ASSESSMENT OF SPACECRAFT
- REMAINS QUARANTINED FOR SAME PERIOD AS CREW (21 DAYS)

Fig. 24

NASA-S-66-5148 JUN 8

LUNAR BIOLOGY PROGRAM
BASIC CONTAINMENT CONCEPTS
CREW RECEPTION AREA

- FACILITY FEATURES
  - SINGLE BARRIER
  - ALL WASTE HEAT TREATED
  - ALL EFFLUENT AIR FILTERED THROUGH 'BIOLOGICAL' FILTERS
  - NEGATIVE PRESSURE MAINTAINED INSIDE FACILITY
- NO PERSONNEL CAN LEAVE FACILITY DURING QUARANTINE PERIOD
- AS REQUIRED, PERSONNEL CAN ENTER FACILITY
- POSSIBLE REQUIREMENTS INCLUDE
  - MEDICAL ASSISTANCE
  - TECHNICAL PERSONNEL TO EXAMINE SPACECRAFT
  - FACILITIES PERSONNEL TO REPAIR EQUIPMENT
- CREW REMAINS ISOLATED FOR 21 DAYS, UNLESS SAMPLE ASSAY POSITIVE

Fig. 25

NASA-S-66-5147 JUN 8

LUNAR BIOLOGY PROGRAM BASIC CONTAINMENT CONCEPTS

LUNAR SAMPLE

- FACILITY FEATURES
  - DOUBLE BARRIER CONCEPT
  - SECONDARY BARRIER - BUILDING WALLS
  - PRIMARY BARRIER - CABINET SYSTEM
  - OPTIMUM AIR PRESSURE DIFFERENTIALS MAINTAINED
  - LIQUID EFFLUENTS HEAT STERILIZED
  - EFFLUENT AIR FROM CABINET INCINERATED
  - EFFLUENT AIR FROM ROOM FH FILTERED THROUGH 'BIOLOGICAL' FILTERS
  - 100% MAKE-UP AIR
  - ALL MAKE-UP AIR FILTERED THROUGH BIOLOGICAL FILTERS
- ALL PERSONNEL ENTER AND EXIT THROUGH CHANGE ROOM - SHOWER

Fig. 26

THERMODYNAMIC CONSTRAINTS ON LUNAR MISSION CAPABILITY

by

Jerry W. Craig

THERMODYNAMIC CONSTRAINTS ON LUNAR MISSION CAPABILITY

1.0 MISSION CONCEPT FOR APOLLO THERMAL DESIGN

Thermal design of the Apollo spacecraft was initially based upon the concept of steady state worst case environmental conditions. In other words, each element of the spacecraft was to be designed to exist in the worst cold or hot condition for an indefinite time period. The primary incentive for this criteria was our desire to eliminate any potential mission constraints.

Early calculations revealed cost, complexity and weight penalties would be large if this criteria was adhered to. For instance, a cooling loop was required for maintaining temperature control of propellants for both Reaction Control System (RCS) and Service Propulsion System (SPS).

Because of this large impact, it was decided that thermal design mission conditions should be established. This criteria has been used to desigh the spacecraft thermally and establishes a certain boundary within which the spacecraft missions must be planned. Figure 1 indicates salient features of this design mission. This does not mean that we will fly this mission. Sufficient flexibility results from designing to this criteria that a large variety of mission conditions can be accommodated.

We are presently conducting parametric analysis to better define this operating envelope of the thermal design. We expect to provide mission planning with sufficient data by the end of the summer to more realistically include thermal constraints in the planning of the lunar mission.

To illustrate the sensitivity of the spacecraft to mission conditions, let us examine the response characteristics of the Command Module heat shield. Figure 2 shows the response of the heat shield to the space environment and indicates the relaxation in temperature requirements afforded by the mission constraints.

Virtually all components in the spacecraft have temperature limitations which could be exceeded under some conceivable mission condition. However, certain components are more sensitive. Figure 3 shows those components which analysis has revealed to be most sensitive.

In summary, we have designed for well defined transient mission conditions with a capability for limited steady-state (worst case) conditions, and normal communication, guidance, experimental thrusting, or contingency type mission requirements. We are actively engaged in analysis to provide parametric data to completely define the operating envelope of the thermal design of the spacecraft. Figure 4 summarizes these primary points.

2.0 THERMAL COATING CONTAMINATION DATA

The greatest uncertainty in establishing the capability of the spacecraft thermal control system to effect the required mission evolves from a lack of understanding of the effect of self-induced environments on the spacecraft thermal coating. Figure 5 shows a layout of the upper stages of the lunar vehicle. During boost, the solid propellant rocket motors for jettison of the Launch Escape System (LES) and Saturn II stage impinge directly on the spacecraft. In addition, cork located on both the Service Module and Command Module for thermal protection of the structure during boost emits ablation products which can impinge on spacecraft thermal control surfaces.

The thermal control surfaces which concern us most are also indicated on Figure 5. The effect of degraded coating performance will be discussed in greater detail a little later. However, let me briefly summarize the functions affected. The Environmental Control System (ECS) radiator heat rejection capability is reduced as the solar absorptance of the radiator surface is increased. The result is a requirement for increased water boiling. A similar reduction in Electrical Power System (EPS) radiator capability results from coating degradation. Such a reduction here means that the allowable fuel cell power level is restricted. We have already seen an indication of the response characteristics of the heat shield and how they vary with changing coating properties. The primary effect is that our original mission flexibility is further restricted.

The first information regarding the effect of the boost environment on thermal coatings was collected by the Marshall Space Flight Center (MSFC) during the SA-8, -9, and -10 missions. Several thermocouples were located on the Service Module Adapter (SMA) between the Saturn IV stage and the payload. These temperatures have been recorded for many months and correlated with the SMA coating properties. Figure 6 shows these data. Note that the α/ε ratio (ratio of solar absorptance to infrared emittance) has increased by a factor of two over the initial value.

Several calorimeters were shrouded so as to protect them from the boost environment. These measurements indicated no change in coating properties in the shrouded areas. Figure 7 shows the configuration of these vehicles compared to the Saturn V lunar vehicles.

Additional data were collected on a ground test at the Arnold Engineering Development Center (AEDC). The test setup is shown in Figure 8. The test consisted of firing a 3,500-pound thrust engine at altitude and measuring the effects for thermal coating properties. Two Apollo coatings were tested. The results of the test are shown in Figure 9. Note that the α/ϵ increase of the radiator coating is somewhat less than that experienced in the SA-8, -9, and -10 flights but is still of sufficient magnitude to significantly affect thermal performance.

The Service Module coating α&ϵ each increased, but at nearly the same rate, so that the α/ϵ ratio remained approximately constant.

Figure 10 shows results of analyses conducted to relate test data to the lunar mission design situations. This analysis consists of a prediction of particle impingement in the test environments and in the lunar mission. The analysis indicates a more severe environment for the lunar mission than the test conditions; therefore, some extrapolation is required.

A second type of test has also been conducted to further define expected degradation. An emission spectrographic analysis of deposits from the Spacecraft 009 and 002 windows and the test samples from the AEDC ground test are shown in Figure 11. Note the similarity of deposits on all three samples; they would not be expected to be exactly the same due to the slightly different environment, handling procedures, etc. Most of the metal oxides contained in the solid propellants are found on all three samples. These deposits have been laboratory synthesized and deposited on coatings in varying densities on the optical properties listed. The results of this investigation are shown on Figure 12. Preliminary indications are that this data correlated with the previous tests.

We are also concerned about the effect of these deposits on the transmittance of the spacecraft windows. Figure 13 shows the effect of the AS-201 mission environment on Spacecraft 009 window performance. Spacecraft 002 data shows a similar degradation. We are not certain about the relative effect of boost, entry, and recovery; however, we strongly suspect that most of

the degradation occurs during boost. A camera will be mounted in Spacecraft 011 to record the change in window clarity during the AS-202 boost phase.

The effect of RCS plume impingement on coatings will be determined by scaled ground tests at a simulated altitude of 300,000 feet. These tests will be completed in July and will include the effect of ablating cork.

No applicable test data is available to quantitate cork ablation biproducts effect on coating performance. No tests other than the RCS motor tests are funded to further define this uncertainty.

A test to determine coating properties of Spacecraft 012 will be conducted during mission AS-204. This test should provide reasonable substantiation of our predicted lunar constraints.

3.0 MISSION CONSTRAINTS

The mission constraints which result from the coating degradation will now be discussed in detail. Figure 14 summarizes the predicted coating properties after boost for those components which are most sensitive.

We predict the ECS radiator coating to degrade to an $\alpha_s = 0.5$, while the emittance remains 0.92. An analysis of radiator performance with and without this degradation was conducted. Power requirements, heat leaks, metabolic rates, etc., for the lunar mission were also determined. A heat load and water generation profile resulted. Combination of the above data results in the predicted radiator mission constraint as shown on Figures 15 and 16. These plots of available spacecraft water as a function of time show that the present water tankage is inadequate for abort from lunar orbit after failure of the primary cooling system. The system would be adequate if no failure occurred in the primary cooling loop or if the radiator coating were protected to prevent boost contamination.

The maximum power capability of the Electrical Power System is shown on Figure 17 as a function of radiator solar absorptance for the design condition of two fuel cell operation in lunar orbit. The predicted coating degradation will limit fuel cell power level to approximately 2,450 watts for periods greater than one hour in lunar orbit. Since our mission study indicates no requirements in excess of this level, this poses no mission constraint.